

CHARACTERIZATION AND AGING STUDIES OF SELECTIVE SOLAR C/Al₂O₃/Al
ABSORBER SURFACES

Petri Konttinen

Dissertation for the degree of Doctor of Science in Technology to be presented with due permission of the Department of Engineering Physics and Mathematics for public examination and debate in Auditorium F1 at Helsinki University of Technology (Espoo, Finland) on the 23rd of April, 2004, at 12 noon.

Helsinki University of Technology
Department of Engineering Physics and Mathematics
Laboratory of Advanced Energy Systems

Teknillinen korkeakoulu
Teknillisen fysiikan ja matematiikan osasto
Teknillinen fysiikka – energiatieteet

Distribution:
Helsinki University of Technology
Advanced Energy Systems
P.O.Box 2200
FIN-02015 HUT
Finland
Tel. +358-9-451 3198
Fax. +358-9-451 3195
Email: petri.konttinen@hut.fi
Internet: <http://www.hut.fi/Units/AES/>

Supervisor: Prof. Peter Lund
Opponent: Prof. Bo Carlsson

Number of pages: 69 + app. 89

ISBN 951-22-7002-1
ISBN 951-22-7003-X (pdf)

ISSN 1456-3320
ISSN 1459-7268 (pdf)

UDC 620.93:535.34:539.2

Copyright © 2004 Petri Konttinen

Electronic version available at:
<http://lib.hut.fi/Diss/2004/isbn951227003X/>

Otamedia Oy
Espoo, 2004

Abstract

Solar thermal collectors are mainly used for domestic water and space heating. They capture incident solar radiation, convert it to usable thermal energy, and transfer the energy into a heat transfer fluid. All of this should be accomplished economically with minimal energy loss. One of the most important components of the solar thermal collector is the solar absorber. To be effective, the absorber should exhibit wavelength selectivity, i.e. have maximum solar absorptance and minimum thermal emittance. Selective solar absorbers have been studied intensively since the 1950's. State-of-the-art sputtered selective solar absorbers have good optical properties and long lifetime. A drawback can be high manufacturing costs.

The main purpose of this thesis was the characterization and improvement of a mechanically-manufactured selective C/Al₂O₃/Al absorber surface. The manufacturing method is the only one based on solely mechanical treatment. The optical properties and microstructure of surface samples were analysed. Together with an industrial partner the manufacturing methods were refined. Comprehensive accelerated aging studies were carried out for the absorber surface.

As a result the solar absorptance and the thermal emittance were improved to 0.90 and 0.22, respectively. The microstructure of the surface is composed of microgrooves and unhomogeneous carbon, graphite or graphite/alumina clusters. Inside a glazed collector a service lifetime between 20 and 25 years can be expected. The main degradation mechanism found was hydration of Al₂O₃ if condensed water is present on the surface at an elevated temperature. For very humid climates, an additional moisture barrier would be advisable even for glazed collector applications. For non-glazed applications moisture resistance needs to be improved.

The price of the required manufacturing infrastructure for the C/Al₂O₃/Al absorber varies. It may be very low for manual manufacturing up to some tens of thousands euros for a more sophisticated mechanical workshop. Optical properties and energy yield of the C/Al₂O₃/Al absorber are in the same range as the best commercial spectrally selective paints, but lower than sputtered surfaces. Economically the C/Al₂O₃/Al absorber may compete with selective and non-selective paints in most glazed applications.

Keywords: solar energy, solar thermal absorber, accelerated aging, mechanical manufacturing

Foreword

This work has been carried out at the Laboratory of Advanced Energy Systems, Department of Engineering Physics and Mathematics at Helsinki University of Technology. It has been financed mainly by the National Technology Agency (TEKES), with additional funding from the government through the position of an assistant at the laboratory.

I would like to warmly thank my supervisor, professor Peter Lund for his high-performance guiding, endlessly motivating way of communicating, and providing me with the opportunity and facilities to do the research work and writing. I am grateful to Professor Rainer Salomaa for his encouragement and for giving me the position of an assistant, which has been very helpful in finalizing of this thesis.

The co-operation with the industry partners has been most fruitful. Especially I want to thank Mr. Risto Kilpi and Mr. Roland Hanslin from SunFin Technologies Ltd and Mr. Kari Ratala from Lahti Energia Ltd.

I wish to express my sincere thanks to the whole staff – current and previous – of the laboratory. Dr. Pertti Aarnio has been a unique source of the most fascinating discussions. Dr. Eero Vartiainen, Dr. Markku Hagström and Dr. Kimmo Peippo have shown good examples to me how to reach the goal. Ms. Satu Isokoski and Ms. Auli Kajatie have been the secretarial backbone of the laboratory. Mr. Seppo Wulff has taught me a lot of practical high-quality measurement of variables. From my younger colleagues especially Mr. Janne Halme, Mr. Thomas Carlsson, Mr. Jukka Paatero and Mr. Matti Noponen have provided me with many good advices.

I thank Mr. Michael Ross for grammar checking of the dissertation, and my sister-in-law, Ms. Katja Arola for grammar checking of some of the articles.

I am grateful to my wife Sini, my mother Paula, my father Esko and my sister Meri for their love and support. This dissertation is devoted to my daughter Lilja, who is two-and-a-half years old at the moment I am writing this foreword. I hope this work will inspire her to follow her dreams and ambitions in the future without bowing to the dead weight of tradition. She will have to make her own decisions, as I have made mine.

Espoo, December 2003

Petri Konttinen

To
Lilja

Table of contents

ABSTRACT	3
FOREWORD	4
TABLE OF CONTENTS	7
LIST OF PUBLICATIONS [A-G]	8
BRIEF DESCRIPTION OF THE PUBLICATIONS	9
AUTHOR'S CONTRIBUTION	10
SYMBOLS AND ABBREVIATIONS	11
1 INTRODUCTION	13
1.1 GENERAL	13
1.2 OBJECTIVES AND SCOPE OF THE STUDY	15
2 THEORETICAL BACKGROUND	16
2.1 OPERATING PRINCIPLES OF FLAT PLATE SOLAR COLLECTORS	16
2.2 SOLAR AND THERMAL RADIATIVE ENERGY	17
2.3 SOLAR ABSORPTANCE AND THERMAL EMITTANCE	19
2.4 SPECTRALLY SELECTIVE ABSORBER SURFACES	21
2.5 STATE OF THE ART SELECTIVE ABSORBER DESIGN	26
2.6 C/AL ₂ O ₃ /AL ABSORBER SURFACES	27
2.7 MATHEMATICAL MODELLING	28
3 EXPERIMENTAL METHODS	29
3.1 OPTICAL CHARACTERIZATION	29
3.2 MICROSTRUCTURAL CHARACTERIZATION	33
4 ACCELERATED AGING	36
4.1 AGING FACTORS	36
4.2 TESTING PROCEDURE, STANDARD TESTS	36
4.3 EQUIPMENT USED AT HUT	39
4.4 ADDITIONAL AGING TESTS, THERMAL CYCLING AND IRRADIATION	39
4.5 ADDITIONAL AGING TESTS, TOTAL-IMMERSION SIMULATED ACID AND NEUTRAL RAIN	41
5 RESULTS	42
5.1 OPTICAL AND MICROSTRUCTURAL CHARACTERIZATION	42
5.2 ACCELERATED AGING	51
5.3 OPTICAL PERFORMANCE AND COLLECTOR ENERGY YIELD	58
6 DISCUSSION AND CONCLUSIONS	59
REFERENCE LIST	61

PUBLICATIONS

List of publications [A-G]

- A. P. Konttinen, P.D. Lund, R.J. Kilpi (2003), *Mechanically manufactured selective solar absorber surfaces*, Sol. Energy Mater. Sol. Cells **79**, 273-283
- B. P. Konttinen, R. Kilpi, P.D. Lund (2003), *Microstructural analysis of selective C/Al₂O₃/Al solar absorber surfaces*, Thin Solid Films **425**, 24-30
- C. P. Konttinen, P.D. Lund (2002), *Characterization of selective absorbers prepared through a mechanical treatment*, invited lecture, in Proceedings of World Renewable Energy Congress VII, Cologne, Germany, 29 June - 5 July, 2002
- D. P. Konttinen, P.D. Lund, *Thermal stability and moisture resistance of C/Al₂O₃/Al solar absorber surfaces*, Sol. Energy Mater. Sol. Cells, in press
- E. P. Konttinen, P.D. Lund (2004), *Microstructural optimization and extended durability studies of low-cost rough graphite-aluminium solar absorber surfaces*, Renewable Energy **29**, 823-839
- F. P. Konttinen, P.D. Lund, *Physical interpretation of impacts from a low cost manufacturing process on the surface microstructure of a novel solar absorber*, Sol. Energy Mater. Sol. Cells, accepted for publication, 3 December, 2003
- G. P. Konttinen, T. Salo, P.D. Lund, *Corrosion of unglazed rough graphite-aluminium solar absorber surfaces in simulated acid and neutral rain*, submitted to Solar Energy, 3 December, 2003

Publications by the author not included in this dissertation:

- P. Konttinen, P.D. Lund, *Thermal and optical analysis of low-cost coloured metal sheets for solar collector*, in Proceedings of Eurosun 2000, Copenhagen, Denmark, 19 – 22 June, 2000
- P. Konttinen, P.D. Lund, *Novel low cost selective C/Al₂O₃/Al solar absorbers for easy industrial manufacturing*, in Proceedings of ISES Solar World Congress 2003, Göteborg, Sweden, 14 – 19 June, 2003

Brief description of the publications

Publication A: Development of manufacturing processes for the mechanically manufactured C/Al₂O₃/Al surface and its basic characterization are described. The composition and structure of the surface was characterized by scanning electron microscopy and electron microprobe analysis. Spectroradiometry and FTIR-spectrometry were used for optical characterization. The surface was found to consist mainly of Al₂O₃ and a carbon matrix organized as a heterogeneous groove structure. A solar absorptance $\alpha = 0.90$ and a thermal emittance $\varepsilon = 0.25$ were achieved. Comparison to a state-of-the-art sputtered surface show some 17 per cent lower annual energy yield and 11 per cent lower solar fraction.

Publication B: The elemental composition and geometrical structure of the C/Al₂O₃/Al surface was characterized by x-ray photoelectron spectroscopy (XPS), scanning electron microscopy, energy dispersive x-ray spectroscopy and optical microscopy. The XPS analyses revealed that the surface contains Al₂O₃ and C most likely in graphite form. Optical microscopy suggested that graphite may form heterogeneous agglomerated clusters on the surface. The thickness of the possible clusters varies, the maximum estimated thickness being in the range of 300 nm. Emittance was improved from 0.25 to 0.22 without decreasing the solar absorptance. Theoretically increasing the incomplete graphite coverage and decreasing the maximum graphite cluster thickness might increase α to 0.94 and lower ε . This might be achieved by altering the composition and the structure of the grinding pad used and by finding suitable manufacturing parameters for the advanced pad.

Publication C: Additional information is presented about the surface manufacturing development and microstructure to that already published in Publications A and B. Possible interpretations of energy dispersive x-ray spectroscopy results are discussed.

Publication D: C/Al₂O₃/Al surfaces were exposed to thermal stability and moisture resistance tests following the IEA Solar Heating and Cooling Programme recommendations (draft ISO/DIS 12592). The main degradation mechanism found was hydration of aluminium oxide to pseudoboehmite and boehmite. The estimated service lifetime with an optical performance better than 95% of its initial of the absorber surface was based on two literature references, where time of wetness frequency distribution of a nickel pigmented anodized absorber solar collector microclimate was measured. The estimated service lifetime in normal use is 20 or 25 years, depending significantly on the time of wetness frequency distribution of the surface. The estimate of 25 years can be regarded more accurate, as it is based on measurements of adequately insulated collectors, whereas the other data set is based on collectors that may have been subjected to stronger than normal wind and rain loads.

Publication E: Based on a literature review, a lower thermal emittance could theoretically be achievable by optimizing the graphite layer thickness, groove depth and surface profile periodicity. It may be possible that a more arbitrary form of roughening could produce values of α and ε closer to those of a sinusoidal profile. Manufacturing parameters, i.e. the composition of silicon carbide grinding pad and the corresponding grinding pattern, need to be enhanced to achieve optical improvements. The commercially available grinding pads used so far have not yielded optimal results. A low cost colloidal silica dipping antireflection (AR) coating could theoretically improve $\alpha > 0.90$.

Absorber samples were subjected to 383 days of temperature and irradiance cycling. In total, the samples were exposed to ultraviolet (UV) irradiation equivalent to 5 – 15 years of normal

outdoor use. The results show that the samples are not sensitive to natural levels of UV irradiation or temperature cycling induced degradation of optical properties. A clear improvement in absorptance was observed after the first 50 days of cycling. The elevated temperature of 130°C is the probable cause for the increase. Reference samples indicated similar aging behaviour both after four years of natural exposure and after relatively short constant temperature tests at 120°C and 180°C.

Publication F: Different interpretations of the surface microstructure are discussed. Atomic force microscopy indicates that the surface has microgrooves with variable sharpness and a depth of approximately 80-160 nm. Dynamic collector testing results show some 5 per cent lower energy yield compared to a similar collector containing nickel pigmented anodized absorber surface.

Publication G: Total-immersion aerated and deaerated tests in simulated acid and neutral rain showed that the absorbers are very durable at a pH level of 3.5. At pH 4.5 and 5.5 aluminium oxide (Al_2O_3 , alumina) on the surface hydrates significantly in most cases. Therefore the surfaces can not be recommended for use in non-glazed applications if they are exposed to rain with pH exceeding ~ 3.5 . The total-immersion test needs to be developed further as the test results exhibited weak dependency on temperature and time. The results indicate that unglazed solar absorber surfaces based on aluminium substrate need to be well protected against rain diffusion onto the substrate in order to prevent degradation caused by hydration of aluminium oxide.

Author's contribution

The author has written publications A-G and is responsible for their contents. The author conducted all the optical characterizations and aging tests at Helsinki University of Technology (HUT). Mr. R. Hanslin and Mr. R.J. Kilpi from SunFin Technologies Ltd. originally invented the manufacturing principle, manufactured all absorber samples and used the author's optical and microstructural results to improve the manufacturing methods. Prof. P.D. Lund suggested many of the subjects for the articles, supervised, tutored and reviewed all the work and calculated annual energy gains and solar fractions for Publication A. Mr. T. Salo has given valuable input into Publication G as an electrochemical corrosion expert by helping to interpret the results and by manufacturing the simulated rain.

Dr. T. Tesfamichael from Uppsala University performed optical reference measurements needed for calibration of HUT's equipment. Ms. P. Raivio, Dr. U. Tapper and Mr. T.E. Gustafsson from Technical Research Centre of Finland (VTT) performed the scanning electron microscopy (SEM) and energy dispersive x-ray spectroscopy (EDS) analyses and Mr. M. Kolari from VTT manufactured the crosscut samples. Dr. J. Lahtinen and Mr. E. Harju from HUT conducted the x-ray photoelectron spectroscopy (XPS) and atomic force microscopy (AFM) analyses, respectively. The author is responsible for the interpretation of the results of the above-mentioned non-optical analyses presented in publications A-G.

Symbols and abbreviations

a_n	Arrhenius acceleration factor [-]
A_c	collector area [m ²]
b_0	experimental incidence angle constant [-]
C_1	first Planck's radiation constant [m ² W]
C_2	second Planck's radiation constant [mK]
E_b	total hemispherical energy emitted by a blackbody [J m ⁻²]
E_T	Arrhenius activation energy [J mol ⁻¹]
$E_{\lambda b}$	monochromatic hemispherical energy emitted by a blackbody [J m ⁻²]
F_R	collector heat removal factor [-]
G_{λ}	monochromatic solar normal irradiance for air mass 1.5 [W m ⁻² K ⁻¹]
G_{sc}	extraterrestrial solar constant [W m ⁻²]
I	total irradiance onto the collector plane [W m ⁻²]
$I_{\lambda,i}$	monochromatic incident irradiance [W m ⁻²]
$I_{\lambda b}$	monochromatic black body irradiance [W m ⁻²]
$K_{ia}(\theta)$	incidence angle modifier [-]
k	extinction coefficient [-]
$(mC)_e$	effective thermal capacitance [J m ⁻² K ⁻¹]
n	refractive index [-]
n_{eff}	effective refractive index [-]
$N(E)$	kinetic energy distribution [-]
PC	performance criterion function [-]
Q_u	collector array thermal output [W m ⁻²]
R	ideal gas constant = 8.3143 [J mol ⁻¹ K ⁻¹]
T	absolute temperature [K]
T_a	ambient air temperature near the collector [K]
T_f	average fluid temperature in collector ($= \frac{T_i + T_o}{2}$) [K]
T_i	fluid inlet temperature [K]
T_n	reference temperature [K]
T_o	fluid outlet temperature [K]
T_{ref}	measured time of wetness temperature [K]
U_L	collector overall heat loss coefficient [W m ⁻² K ⁻¹]

Greek

α	absorptance, hemispherical absorptance [-]
$\alpha(\mu, \phi)$	directional absorptance [-]
α_{λ}	monochromatic hemispherical absorptance [-]
$\alpha_{\lambda}(\mu, \phi)$	monochromatic directional absorptance [-]
α_1	first order (flow) heat loss coefficient [W m ⁻² K ⁻¹]
α_2	second order (flow) heat loss coefficient [W m ⁻² K ⁻²]
Δ	change in variant [-]
ε	emittance, hemispherical emittance [-]
$\varepsilon(\mu, \phi)$	directional emittance [-]
ε_{λ}	monochromatic hemispherical emittance [-]
$\varepsilon_{\lambda}(\mu, \phi)$	monochromatic directional emittance [-]
ϕ	azimuthal angle, latitude [rad], activation energy [J mol ⁻¹]
η	efficiency [-]
η_0	zero loss efficiency for total irradiance [-]

μ	cosine of polar angle [-]
θ	polar angle (angle between surface normal and incident irradiance) [rad]
ρ	reflectance, hemispherical reflectance [-]
ρ_λ	monochromatic hemispherical reflectance [-]
σ	Stefan-Boltzmann constant [$\text{W m}^{-2} \text{K}^{-4}$]
τ	transmittance [-]

Subscripts

a	absorbed, absorber
b	black body, beam irradiance
i	incident
λ	monochromatic
0	zero

Abbreviations

AES	Auger electron spectroscopy
AFM	atomic force microscopy
Alumina	aluminium oxide (Al_2O_3)
AM	air mass
AR	antireflection
Cermet	ceramic-metallic
CCD	charge coupled device
CRT	cathode ray tube
DC	direct current
DHW	domestic hot water
EDS	energy dispersive x-ray spectroscopy
ERDA	elastic recoil detection analysis
FESEM	field emission scanning electron microscopy
FTIR	Fourier transform infrared
HUT	Helsinki University of Technology
IEA SHC	International Energy Agency Solar Heating and Cooling Programme
IR	infrared
ISO	International Organisation for Standardisation
MSTC	IEA SHC Working Group “Materials in Solar Thermal Collectors”
NIR	near infrared
pH	hydrogen ion concentration (pondus hydrogenii)
PTFE	polytetrafluoroethylene
PV	photovoltaic
PVD	physical vapour deposition
r.h.	relative humidity
SEM	scanning electron microscopy
SS	stainless steel
TEKES	National Technology Agency
TG	thermogravimetry
TSSS	thickness-sensitive spectrally-selective
UV	ultraviolet
Vis.	visible
VTT	Technical Research Centre of Finland
XPS	x-ray photoelectron spectroscopy

1 Introduction

1.1 General

The direct use of solar energy may make significant contributions to mankind's future energy supply. It is abundantly available over the whole globe and it is a sustainable energy source. Political agreements, such as the Kyoto Protocol on greenhouse gas emission reduction, will likely give some edge to renewable energy – including solar – over more polluting technologies. However, the power density of solar energy is low, and the seasonal variation is large, especially at high latitudes, which creates special technical and economic demands for the solar energy utilization systems.

Earth receives a steady 170,000 TW of solar radiation. 30% of it is directly reflected back to space and the remaining 120,000 TW is converted to heat in the air, earth and oceans (47% of total), to potential energy in the hydrological cycle (23%), and to mechanical energy in winds and waves (<1%) and to chemical energy in photosynthesis (<1%). In total this corresponds to 15,000 times the human use of fossil and nuclear fuels and hydro power (Boyle, 1998). Unlike fossil and nuclear fuels, which will be depleted in the foreseeable future, solar radiation will be available for millions of years. Solar radiation can be converted into a usable form of energy as heat or electricity, either by photothermal conversion or by photovoltaic (PV) conversion, respectively. The focus of this work is on photothermal conversion and solar heating related issues.

The role of solar heating in the overall energy supply is still small. In OECD countries, solar heat utilization corresponds to about 4 Mtoe/year and reduces CO₂ emissions by 11 million tons of CO₂ per year (Weiss and Faninger, 2002). The solar collector market grows rapidly. For example in Europe it expands by about 10-15% a year. The potential market for solar heating in Europe is 1,400 million m² of collectors (ESTIF, 2003a), corresponding to approximately 45 Mtoe/year. The EU target set in the White Paper on Renewables (European Commission, 1997) is 100 million m² by the year 2010 compared to 12.3 million m² installed by 2002 (ESTIF, 2003a). The largest market area and growth is found in China where some 10 million m² of collectors were installed in 2002 (Yin Zhiqiang, 2003) and the market grows by 30% a year.

Photothermal utilization of solar energy typically involves a solar heating system that produces hot water or space heat for domestic use. The heart of the solar heating system is the solar collector. In order to enable effective solar energy utilization, absorption of incident solar radiation should be maximized and thermal losses from the collector minimized. The solar absorbing surface is one of the key components of a solar collector, and its optical properties and quality influence both the heat losses and gains. The main focus of this thesis is the solar absorber.

There are several ways to produce a solar absorber surface, ranging from simple black painted surfaces to sophisticated optical systems. A comparison of optical properties of different absorber surfaces is presented on page 24. High absorptance and low emittance accompanied with economical manufacturing cost, large production volumes and long-term durability are often the key driving factors of the R&D and industrial development work on solar absorbers. A large number of different selective solar absorber manufacturing methods has been developed, but only a few have succeeded commercially. To get an overview of the subject, the reader is referred to recent literature, e.g. (Gordon, 2001). The practical use of selective solar absorbers was introduced in 1955, when Tabor (Tabor, 1955a; Tabor, 1955b) and Gier

and Dunkle (Gier and Dunkle, 1955) presented their work in the first Solar Energy Conference held in Tucson, Arizona.

Nowadays, the most common type of spectrally selective absorber is an absorber-reflector tandem consisting of a combination of two surfaces: one being highly absorbing in the solar spectrum and the other highly reflective in the infrared wavelengths. Common techniques to produce such a surface are generally divided into wet-chemical and vacuum deposition techniques (Teschmichal, 2000). Commercial vacuum deposition products can be manufactured by reactive dc magnetron sputtering (Interpane in Germany and Sunstrip in Sweden) or activated reactive evaporation method (Tinox GmbH, Germany). Wet chemical products include black chrome (MTI Inc., USA, Energie Solaire AS, Switzerland and Batec A/S, Denmark), nickel-pigmented aluminium oxide (Sweden and Japan) and MAXORB (UK). In addition, at least two selective paints are available on the market, namely Solarect-Z™ (Slovenia) and SolkoteHI/SORB-II™ (USA).

In Germany, which has the largest solar thermal market in the EU, the sputtered absorber coatings have had the highest market share since the year 2000 (ESTIF, 2003b). The second largest EU market is in Greece, where the absorber surfaces vary from black paint to selective surfaces (ESTIF, 2003b). In China, over 84% of the annual installations in 2002 were of spectrally selective evacuated tubular collectors (Yin Zhiqiang, 2003). According to these statistics, there seems to be a strong demand for both high-end (e.g. sputtered) absorbers as well as low-cost options. In addition, there is a market interest towards developing lower cost environmentally friendly manufacturing methods with optical properties equal to current sputtered surfaces (Schreiber, 2002).

Current research topics of solar absorbers include further improvement of the microstructure, modelling and manufacturing of the sputtered surfaces (Schuler and Oelhafen, 2001; Gordo et al. 2002; Teixeira et al. 2002; Farooq and Hutchins, 2002a; Farooq and Hutchins, 2002b; Farooq and Lee, 2003; Yue et al. 2003). Another topical issue is lowering the cost of the selective surface, e.g. by improving selective paints (Orel and Gunde, 2001; Orel et al. 2001; Vince et al. 2003; Smith et al. 2003). New manufacturing methods are being studied as well, including surface W-grating geometry (Sai et al. 2003), nanomaterials (Nishimura and Ishiguro, 2002; Mastai et al. 2002) and carbon nanotubes (Cao et al. 2002). A potential low-cost approach is to use nickel nanoparticle based paint combined with an antireflection coating (Boström et al. 2003a; Boström et al. 2003b).

The typical price of a high performance flat-plate solar collector is about 200 – 250 Euro per m² of which the high quality spectrally selective absorber is about 15 – 20 %. High efficiency selective absorbers give maximum performance when covered with a high transmittance glass and are well insulated and capsulated. If operating at a lower temperature, it may be considerably cheaper to utilize a low cost absorber such as non-selective black paint, selective paint or C/Al₂O₃/Al. Further price reductions may be achieved by e.g. using cheaper window glass, insulation and capsulation.

In addition, the differences in the absorber and collector prices counts only for a part of the solar thermal system price, as can be seen by comparing system cost in Germany and Greece: a typical solar domestic hot water system installed in a one family residential unit in Germany costs around 4500 Euro (forced-circulation system, 4–6 m² flat plate collector, 300 litre tank), whereas in Greece a typical system for the same purpose costs 700 Euro inclusive of VAT and installation (thermosiphon system, 2.4 m² collector, 150 litre tank) (ESTIF, 2003a).

Therefore, for collector manufacturers and end customers, the choice of the absorber type is largely a choice of the solar heating system price range. High performance absorbers and collectors compete predominantly among themselves within their market sector (e.g. in Germany and Austria). Similarly lower performance absorbers and collectors address a different market (e.g. in Greece).

1.2 Objectives and scope of the study

This thesis deals with a novel mechanically manufactured selective C/Al₂O₃/Al solar absorber surface. The manufacturing method is the only one based on solely mechanical treatment known to the author. It was originally invented in the mid 1990s by a Finnish industrial partner with a focus on developing a low cost manufacturing method for solar absorbers. At that time there was no clear understanding of the physics of the surface or interrelationship between surface structure and its optical properties. The aim of this thesis has been to understand and improve the optical and microstructural properties and elemental composition of the C/Al₂O₃/Al solar absorber. Another important objective of this thesis has been to investigate the durability of the absorber surface and possible degradation mechanisms in different operational conditions.

The work was done in a close co-operation with Sunfin Technologies Ltd. They invented the original method of chemical/mechanical manufacturing (Publication A) and manufactured all the C/Al₂O₃/Al absorber samples. The mechanical manufacturing method used does not allow exact layer-by-layer construction of the surface as e.g. sputtering does. A great deal of the emphasis has been put on optimizing the optical properties of the surfaces without sacrificing the simplicity of the manufacturing method.

This dissertation is divided into six chapters. Chapter one introduces the subject and objectives of the work. Chapter two communicates the theoretical background of utilizing solar thermal energy, including solar and thermal radiation and operation principles of a solar collector and a selective absorber surface. Some generally used absorber design principles are briefly described. Chapter three explains experimental methods, including sample manufacturing and optical spectrometric characterization used in this thesis. Non-optical characterization used includes scanning electron microscopy, electron microprobe analysis, x-ray photoelectron spectroscopy and atomic force microscopy. Optical microscopy has been used to support other measurements. Accelerated aging test methods are described in Chapter four. Chapter five contains the main results for all the characterization and aging tests. Needs for future development based on these results are discussed in short. Chapter six contains discussion and conclusions.

2 Theoretical background

2.1 Operating principles of flat plate solar collectors

A well-designed single- or double-glazed flat plate solar collector is designed to maximize the capture of the incoming solar radiation with minimum heat losses. It then delivers as much as possible of the captured energy to the user, usually by using a working fluid (Fig. 2.1).

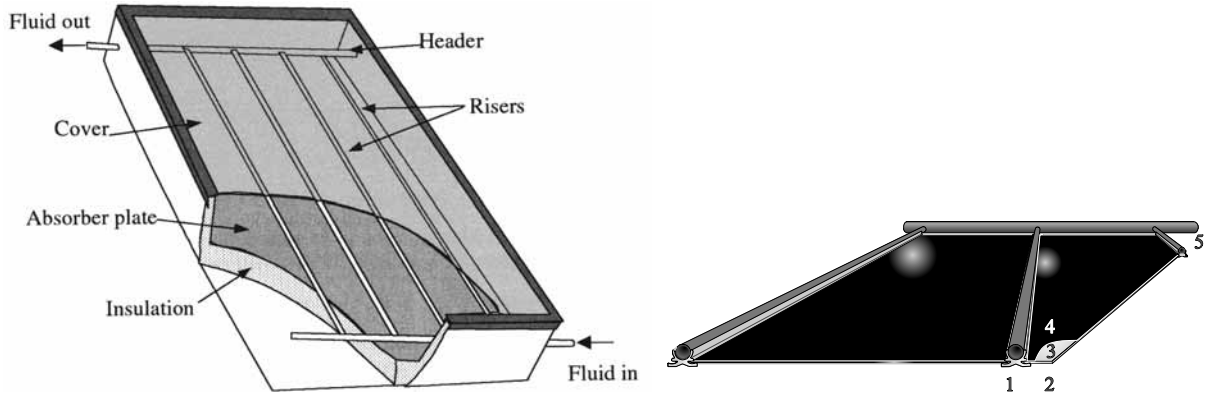


Figure 2.1. A single-glazed flat plate solar collector (left, adapted from Gordon (2001)) and a detailed cross section of the C/Al₂O₃/Al absorber plate with header and risers (right, drawing ©Lasse Kilpi, parts numbered). Collector surface area is ca. 2 – 2.5 m².

The conversion efficiency of a solar collector is limited by the thermal losses from the heated absorber due to radiation, convection and conduction. The flat plate collector non-constant efficiency η is defined as:

$$\eta = \frac{Q_u}{IA_c} = \frac{F_R [(\tau\alpha)I - U_L (T_i - T_a)]}{I}, \quad (2-1)$$

where Q_u is the collector thermal output, I is the total irradiance onto the collector plane, A_c is the collector area, F_R is the collector heat removal factor, $\tau\alpha$ is the optical transmittance-absorptance product including the angular dependency of the collector, U_L is the collector overall heat loss coefficient, T_i is the fluid inlet temperature and T_a is the ambient temperature. Eq. (2-1) yields the instantaneous collector thermal output Q_u that is delivered by the collector (Duffie and Beckman, 1991).

As can be seen in Eq. 2-1, the collector efficiency is directly proportional to the solar absorptance, α , of the absorber. The collector overall heat loss coefficient U_L includes radiative, convective and conductive heat losses. Thermal emittance, ε , of a surface is a first-order factor related to the radiative heat losses. Therefore it is desirable to maximize the solar absorptance and to minimize the thermal emittance of an absorber.

Collector efficiency measurements (Eq. 2-1) have been further developed by Perers (Perers, 1995) with improvements made to take into account thermal capacitance effects, incidence angle effects and the temperature, and the wind and sky temperature dependency of the heat loss coefficient. We have used a simplified version of the Perers' model to dynamically measure different solar collectors (Publication F) (Eq. 2-2):

$$Q_u = \eta_0 K_{\tau\alpha}(\theta) I - \alpha_1 (T_i - T_a) - \alpha_2 (T_i - T_a)^2 - (mC)_e \frac{dT_f}{dt}, \quad (2-2)$$

where η_0 is the zero loss efficiency for total irradiance, α_1 and α_2 are the first and second order flow heat loss coefficients, respectively, and $(mC)_e$ is the effective thermal capacitance of the collector. An incidence angle modifier $K_{\tau\alpha}(\theta)$ is typically used for estimating the dependency of a collector on the angle of incidence of impinging radiation (Duffie and Beckman, 1991):

$$K_{\tau\alpha}(\theta) = \frac{(\tau\alpha)}{(\tau\alpha)_n} = 1 + b_0 \left(\frac{1}{\cos \theta} - 1 \right) \quad (2-3)$$

where n is the surface normal (zero angle of incidence), θ is the angle between surface normal and incident irradiance and b_0 is the experimental incidence angle constant. Experimental dynamic solar collector performance test results including $K_{\tau\alpha}(\theta)$ for a C/Al₂O₃/Al surface and a glass assembly have been reported in a Lic. Sc. Thesis by Konttinen (2000).

The collector efficiency η should be as high as possible for optimal performance. This can be obtained by increasing absorbed solar energy – α as close to unity as possible – and by decreasing emitted thermal losses. Conductive and convective heat losses can be minimized with proper collector design and sufficient insulation or a vacuum. A prestressed low-iron glass with high solar transmittance is typically used as a cover material and the sides and the back of a collector are insulated with suitable material, e.g. rock or glass wool. An anti-reflection coating may be added on the glass in order to improve solar transmittance. This does not affect the thermal emittance since glass is opaque in the infrared.

Reducing thermal radiant heat losses to a minimum in a flat plate collector requires the use of a spectrally selective surface. According to Haitjema (1989), at a high collector temperature the emittance determines the collector efficiency, while at a low collector temperature absorptance is the decisive factor with regard to the efficiency. For low temperature applications, such as non-glazed swimming pool solar heater, a non-selective surface can be effective as well.

2.2 Solar and thermal radiative energy

The sun is ultimately the provider of all energy on the earth except nuclear and tidal. It is a continuous fusion reactor with an estimated total electromagnetic radiative power of about $3.8 \cdot 10^{27}$ W. The value of extraterrestrial solar radiation (G_{sc}) just outside the earth's atmosphere is almost constant: $1367 \pm 3\%$ W m⁻² (Duffie and Beckman, 1991), being divided into ultraviolet (8% of total), visible (46%) and near infrared (46%).

Like the sun, all objects above absolute zero temperature emit thermal radiation whose wavelength and intensity depends on the optical characteristics and the temperature of the body. Theoretically an ideal surface is a blackbody, which absorbs all wavelengths of the incident radiation and emits the maximum amount of energy according to Planck's law (Richtmyer and Kennard, 1947). The spectral blackbody radiation $E_{\lambda b}$ is calculated as:

$$E_{\lambda b} = \frac{C_1}{\lambda^5 [\exp(C_2 / \lambda T) - 1]}, \quad (2-4)$$

where C_1 and C_2 are the first and second Planck's radiation constants, respectively ($C_1 = 3.7405 \cdot 10^{-16} \text{ m}^2 \text{ W}$, $C_2 = 0.0143879 \text{ m K}$) and T is the temperature of the blackbody in Kelvin. The Stefan-Boltzmann law gives the hemispherical total emitted energy for a blackbody as:

$$E_b = \sigma T^4, \quad (2-5)$$

where σ is the Stefan-Boltzmann constant ($\sigma = 5.6696 \cdot 10^{-8} \text{ Wm}^{-2} \text{ K}^{-4}$).

The sun has an effective blackbody temperature of approximately 5800 K. The temperature in the central inner regions is significantly higher, variously estimated at $8 \cdot 10^6 \text{ K}$ to $40 \cdot 10^6 \text{ K}$ (Duffie and Beckman, 1991). The extraterrestrial spectrum and the blackbody spectrum of the sun differ from each other slightly.

Differences between the extraterrestrial and terrestrial solar spectrum are caused by absorption and scattering of the solar radiation in the ionosphere, the ozone layer or the atmosphere mainly by O_2 , O_3 , H_2O and CO_2 . Each of the atmospheric compounds absorbs certain wavelengths causing absorption holes in the terrestrial solar spectrum as shown in Fig. 2.2. Rayleigh scattering (Rayleigh, 1871) refers to the scattering of light off the molecules of the air, and can be extended to scattering from particles up to about a tenth of the wavelength of the light. Rayleigh scattering is symmetric in forward and backward directions, and is more effective at short wavelengths ($\propto 1/\lambda^4$), hence being responsible for the blue colour of the sky.

Apart from scattering and absorption, the path of the beam that traverse the atmosphere (i.e. the air mass or AM) affect the amount of the terrestrial solar irradiation available. Air mass is defined as the ratio of optical mass at an oblique path to that of the vertical path. When the sun is directly overhead, i.e. its rays are normal to the horizontal surface of the earth, the air mass has a value of 1. At high latitudes (e.g. Finland) the value of the air mass is typically 1.5 – 2. An air mass of 1.5 as defined by ISO (ISO, 1992) is used for solar energy calculations throughout this work. The variation in the solar irradiance intensity due to the change of air mass is considerable as can be seen by comparing the peak values of AM1 and AM1.5 in Fig. 2.2 and Fig. 2.3, respectively.

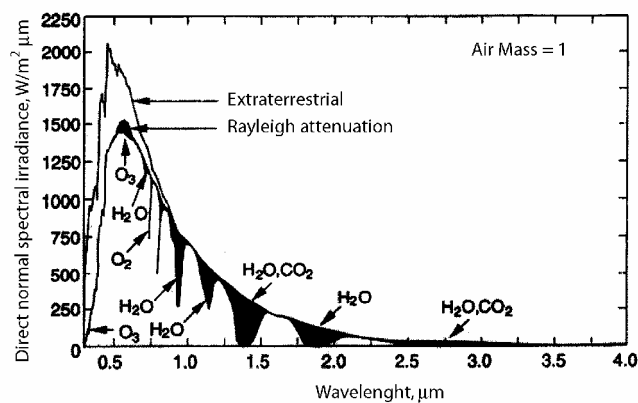


Figure 2.2. An example of the effects of atmospheric absorption and Rayleigh scattering on the spectral distribution of solar irradiance. Adapted from (Iqbal, 1983).

For solar thermal applications the most important radiation wavelength ranges are incident solar radiation between 0.3 and 2.5 μm covering ultraviolet-visible-near infrared (UV – Vis. –

NIR) and emitted thermal radiation between 2 and 50 μm . These two ranges overlap only marginally at temperatures below approximately 200°C (Fig. 2.3), which makes possible the effective operation of a spectrally selective solar absorber (see Section 2.4). Above 200°C, some energy losses are unavoidable.

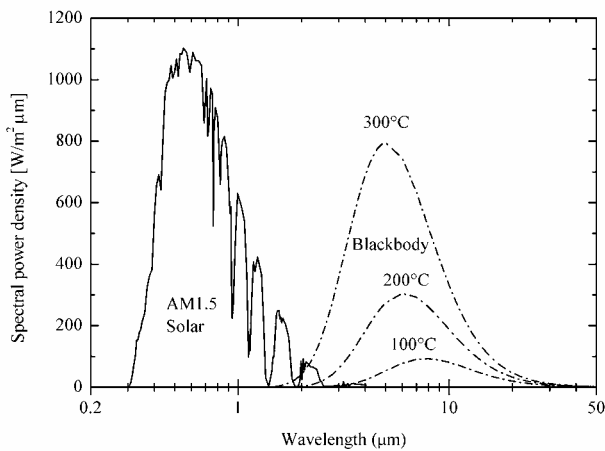


Figure 2.3. Solar hemispherical spectral irradiance for air mass 1.5 (ISO, 1992) and blackbody spectral emittance at 100°C, 200°C and 300°C.

When the temperature of the blackbody rises (see Fig. 2.3) the amount of the emitted energy increases and the location of peak power density shifts towards shorter wavelengths. The peak wavelength can be determined with the Wien's displacement law:

$$\lambda_{max}T = 2897.8 \mu\text{mK} \quad (2-6)$$

2.3 Solar absorptance and thermal emittance

For many solar absorber energy calculations only two of the surface's quantities are required: the solar absorptance, α , and the infrared thermal emittance, ε . However, these quantities can be expressed in several ways, which differ from each other significantly. The monochromatic directional absorptance $\alpha_{\lambda}(\mu, \phi)$ ¹, the directional absorptance $\alpha(\mu, \phi)$, the monochromatic hemispherical absorptance α_{λ} , and the hemispherical absorptance α are all different quantities. Exact definitions for these and equivalent four emittance cases are given in (Duffie and Beckman, 1991). It is important to distinguish the difference between one characteristic and another. For example, $\alpha_{\lambda}(\mu, \phi)$ is a property of a surface, whereas $\alpha(\mu, \phi)$ is not a property in that it depends upon the wavelength distribution of the incoming radiation.

This work is confined to the commonly used hemispherical optical properties obtained from our measuring equipment. The C/Al₂O₃/Al surfaces are rough in composition which makes them well fit for hemispherical reflectance measurements (see next Section). Some monochromatic directional emittance measurements of C/Al₂O₃/Al surfaces have been reported by Kontinen (2000). These have not been verified by reference measurements.

The monochromatic hemispherical absorptance, α_{λ} , is defined as the fraction of incident solar radiation of wavelength λ over the enclosing hemisphere that is absorbed, and the hemispherical absorptance α can be obtained by integrating over all wavelengths (Eq. 2-7):

¹ where μ is the cosine of the polar angle θ and ϕ is the azimuthal angle

$$\alpha = \frac{\int_0^{\infty} \int_0^{2\pi} \int_0^1 \alpha_{\lambda}(\mu, \phi) I_{\lambda, i}(\mu, \phi) \mu d\mu d\phi d\lambda}{\int_0^{\infty} \int_0^{2\pi} \int_0^1 I_{\lambda, i}(\mu, \phi) \mu d\mu d\phi d\lambda} \quad (2-7)$$

where $I_{\lambda, i}$ is the incident monochromatic radiant energy. If $\alpha_{\lambda}(\mu, \phi)$ is independent of direction, (i.e. $\alpha_{\lambda}(\mu, \phi) = \alpha_{\lambda}$), then Eq. 2-7 can be simplified by integrating over the hemisphere to yield

$$\alpha = \frac{\int_0^{\infty} \alpha_{\lambda} I_{\lambda, i} d\lambda}{\int_0^{\infty} I_{\lambda, i} d\lambda} \quad (2-8)$$

If the incident radiation in either Eq. 2-7 or 2-8 is solar radiation, then the calculated α is called the solar absorptance.

The monochromatic hemispherical emittance, ε_{λ} , is defined as the ratio of the monochromatic intensity emitted by a surface over the enclosing hemisphere to the monochromatic intensity that would be emitted by a blackbody at the same temperature. The hemispherical emittance ε can be obtained by integrating over all wavelengths (Eq. 2-9):

$$\varepsilon = \frac{\int_0^{\infty} \int_0^{2\pi} \int_0^1 \varepsilon_{\lambda}(\mu, \phi) I_{\lambda b}(\mu, \phi) \mu d\mu d\phi d\lambda}{\int_0^{\infty} \int_0^{2\pi} \int_0^1 I_{\lambda b}(\mu, \phi) \mu d\mu d\phi d\lambda} \quad (2-9)$$

where $I_{\lambda b}$ is the monochromatic blackbody irradiance. If $\varepsilon_{\lambda}(\mu, \phi)$ is independent of direction, then Eq. 2-9 can be simplified by integrating over the hemisphere to yield

$$\varepsilon = \frac{\int_0^{\infty} \varepsilon_{\lambda} E_{\lambda b} d\lambda}{\sigma T^4} \quad (2-10)$$

2.3.1 Reflectance of surfaces

For determining the absorptance or the emittance of a material, it is usually most convenient to measure the reflectance, ρ , and to calculate α and ε from it. When radiation strikes a body, a part of it is reflected, a part is absorbed, and if the material is transparent, a part is transmitted. For an opaque surface which does not exhibit a dependence on the azimuthal angle ϕ , and cosine of the polar angle μ , energy from all directions is either absorbed or reflected (Duffie and Beckman, 1991). Kirchoff's law states that at a given wavelength the absorptance is equal to the emittance for matter in thermodynamical equilibrium. By combining these rules we have:

$$\varepsilon_{\lambda} = \alpha_{\lambda} = 1 - \rho_{\lambda} \quad (2-11)$$

Thus, the monochromatic hemispherical emittance and the monochromatic hemispherical absorptance can both be calculated from knowledge of the monochromatic hemispherical

reflectance. If dependencies on ϕ and μ exist, then the Eq. 2-11 must be written in form of Eq. 2-12:

$$\varepsilon_{\lambda}(\mu, \phi) = \alpha_{\lambda}(\mu, \phi) = 1 - \rho_{\lambda}(\mu, \phi) \quad (2-12)$$

The spatial distribution of radiation reflected by an opaque surface can be divided into specular and diffuse. Specular reflection is mirror-like, that is, the incident polar angle is equal to the reflected polar angle and the azimuthal angles differ by 180° . A diffuse reflection obliterates all directional characteristics of the incident radiation by distributing the radiation uniformly in all directions. In practice, the reflection from a surface is neither all specular nor all diffuse, but a highly polished surface approaches specular reflection, whereas a rough surface reflects diffusely. Fig. 2.4 illustrates ideal specular reflection, ideal diffuse (Lambertian) reflection and reflection from a real opaque surface.

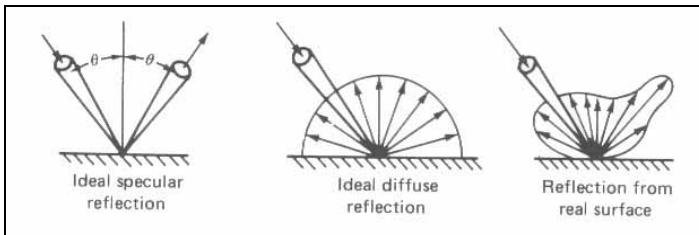


Figure 2.4. Reflection from ideal and real opaque surfaces (Duffie and Beckman, 1991).

2.4 Spectrally selective absorber surfaces

A spectrally selective absorber has different spectral reflectance at different wavelengths. The ideal spectrally selective surface operating at below approximately 100°C has as zero reflectance (i.e. unity solar absorptance) between 0.3 and $3 \mu\text{m}$ and a unity reflectance (i.e. zero thermal emittance) between 3 and $50 \mu\text{m}$. Unfortunately, an ideal surface does not exist in nature, nor can it be manufactured because no known combination of materials exhibits ideal behaviour in the reflectance transition wavelength range (Buhrman, 1986) (see Figs. 2.3 and 2.6).

Selective solar absorber surfaces have been studied quite thoroughly since the 1950's. Developed systems include intrinsic absorbers, optical trapping absorbers, coating/metal tandems, semiconductor/metal tandems, particulate coatings, multilayer thin films, transparent heat reflector/absorber tandems and transparent, heat reflecting and conducting coatings (Haitjema, 1989). Fig. 2.5 shows six examples of different absorber design possibilities.

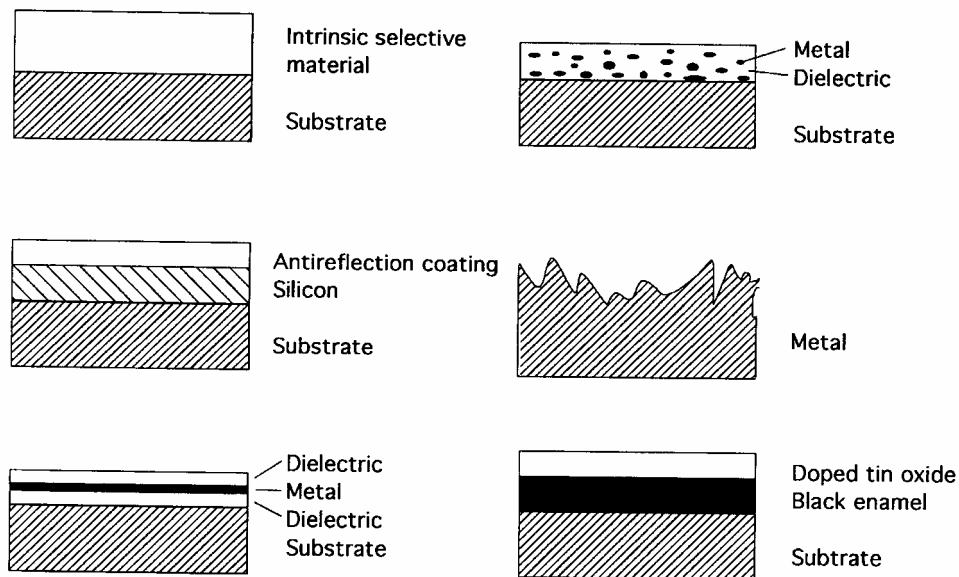


Figure 2.5. Cross-sectional schematic designs of six types of different coatings and surface treatments for selective absorption of solar energy. Adapted from (Gordon, 2001).

Of the six designs shown in Fig. 2.5 intrinsic selective material would obviously be the most straightforward approach, but this approach has generally not been very fruitful due to lack of suitable materials. In practise, useful absorbers are based on two (or more) layers with different optical properties, and are called absorber-reflector tandems. A dielectric or semiconducting coating with high solar absorptance and high infrared transmittance on top of a non-selective highly reflecting metal constitutes the tandem. Absorber-reflector tandems are also most common commercially available selective absorber types (Buhrman, 1986; Tesfamichael, 2000; Gordon, 2001). Surfaces consisting of small particles embedded in a dielectric matrix deposited on a highly infrared reflecting metal substrate are generally called ceramic-metallic or cermet surfaces (Tesfamichael, 2000). The metal particle – dielectric embedding -concept offers a high degree of flexibility and gives the designer optimization possibilities with regard to the choice of constituents, coating thickness, particle concentration, shape and orientation of particles (Gordon, 2001).

The number of selective absorber surface manufacturing methods reported in literature is very large. An annotated bibliography by Niklasson and Granqvist (Niklasson and Granqvist, 1983) covers 565 scientific papers including studies of almost 280 different coatings or surface treatments developed from 1955 until 1981. A review by Chaudhuri et al. (Chaudhuri et al. 1997) contains additional though incomplete information up to 1996. More details can also be found in (Lampert, 1979; Koltun, 1981; Agnihotri and Gupta, 1981; Inal and Scherer, 1986; Tabor, 1999).

A great deal of the early work on selective absorbers was concentrated on development of absorber-reflector metal tandems (Tabor, 1955a; Tabor, 1955b; Lampert, 1979; Agnihotri and Gupta, 1981), such as “black chrome“ which is a complex graded Cr-Cr₂O₃ composite (see Fig. 2.6) produced by electroplating (McDonald, 1975). In the 1970’s a number of advanced multilayer coatings prepared by vacuum deposition techniques had been designed and utilized for satellite temperature control within the space programmes of the USA and the Soviet Union (Niklasson and Granqvist, 1983). These coatings were found to be useful for terrestrial applications such as solar heating as well, and have been studied and developed further in

great detail. The reader can get a general picture about the key issues and the developments of selectively solar-absorbing coatings during the 1990's from e.g. (Gordon, 2001).

Currently state-of-the-art commercial selective absorbers manufactured by vacuum deposition are taking over the market from black chrome in many countries (Tesfamichael, 2000; Gordon, 2001; ESTIF, 2003b). These include sputter deposited graded chrome nitride - chrome oxide ($\text{CrN-Cr}_x\text{O}_y$) coating on copper by Interpane in Germany, reactive DC magnetron sputtered nickel-nickel oxide (Ni-NiO) coated aluminium absorber by Sunstrip in Sweden and activated reactive evaporation method coated cermet of TiN_xO_y on copper by Tinox GmbH in Germany. Sputtered stainless steel carbide (SS-C) cermet absorbers have been produced by Shiroki in Japan since the 1980s. All-glass vacuum tubes for concentrating collectors with a selective graded Al-N coating on aluminium are mass produced in China (Gordon, 2001).

With the best coatings, it is possible to achieve $0.90 \leq \alpha \leq 0.97$ and $0.03 \leq \varepsilon \leq 0.10$. Fig. 2.6 and Table 2.1 shows the solar absorptance and the thermal emittance of some commercial and laboratory-scale absorbers. Commercial coatings e.g. from Interpane, Tinox and Sunstrip have very good optical properties. The choice between manufacturers of the best coatings can be based on other factors such as price, absorber surface aesthetics and delivery time.

A low-cost selective solar absorber surface can be manufactured by using selective paints (Orel et al. 1992; Orel and Orel, 1995; Orel et al. 1996; Gunde et al. 1996; Orel et al. 1997; Orel, 1999; Orel and Gunde, 2000; Orel et al. 2001; Orel and Gunde, 2001; Smith et al. 2003). This type of absorber can be classified as the tandem type, with absorbing particles uniformly distributed in a matrix deposited on a metal substrate (Tesfamichael, 2000). The optical performance of selective paint type absorber is determined by intrinsic optical constants and particle size-dependent scattering and absorption. The commercial Solarect-Z™ thickness-sensitive spectrally-selective paint (TSSS) is prepared from an organically modified siloxane resin and an inorganic pigment of FeMnCuOx-P320 (Orel, 1999) with a pigment volume fraction of about 0.2. TSSS implies that low emittance is achieved by using thin layers (2-3 μm thick) (Gunde et al. 1996). Another commercial TSSS paint is SolkoteHI/SORB-II™, and it contains a binder of 100% silicone polymer. The optical properties of this TSSS paint depend significantly on the substrate and coating thickness (see Fig. 2.6). A potential novel approach is to use nickel nanoparticle based paint combined with an antireflection coating (Boström et al. 2003b). For a small laboratory scale sample values of optical properties equivalent to the commercial sputtered absorbers have been reported (Boström et al. 2003a). However, long-term durability of the nickel nanoparticle paint has not yet been demonstrated.

In its current state of development the optical performance of the mechanically manufactured $\text{C/Al}_2\text{O}_3/\text{Al}$ absorber (J in Fig. 2.6) surface competes with the two commercial TSSS paints. The absorptance is slightly lower and the emittance slightly higher compared to Solarect-Z™. Compared to SolkoteHI/SORB-II™, $\text{C/Al}_2\text{O}_3/\text{Al}$ absorber has slightly better optical properties. Both $\text{C/Al}_2\text{O}_3/\text{Al}$ and TSSS absorbers offer a viable alternative to non-selective black paint in cases where their better overall performance is preferred to the moderately lower cost of black paint.

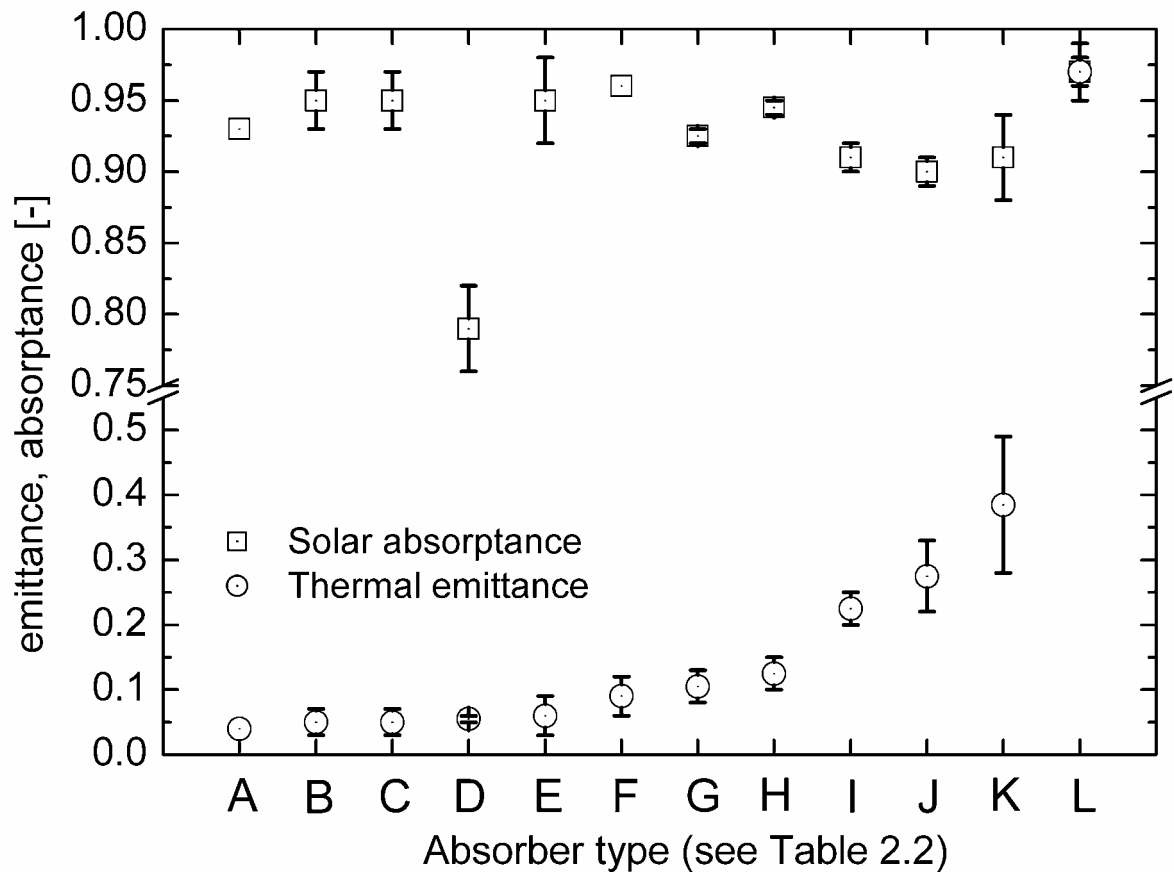


Figure 2.6. Solar absorptance and thermal emittance of some commercial and newly developed solar absorber surfaces from the lowest to the highest emittance. Table 2.1. shows the details of the surfaces.

Table 2.1. Manufacturers, manufacturing method and state of development of absorbers presented in Figure 2.6.

Denoted in Fig. 2.6	Manufacturer (M) or researchers (R)	Manufacturing method	State of development
A	Boström et al. (2003a, 2003b) (R)	Nano-particle paint	Laboratory
B	Interpane (Germany) (M)	Sputtering	Commercial
C	Tinox (Germany) (M)	Evaporation	Commercial
D	Sai et al. (2003) (R)	W-grating geometry	Laboratory
E	Sunstrip (Sweden) (M)	Sputtering	Commercial
F	Farooq and Hutchins (2002b) (R)	4-layer sputtering	Laboratory
G	Mastai et al. (2002) (R)	Silica-carbon nanocomposites	Laboratory
H	MTI (USA) (M) Energie Solaire (Switzerland) (M) Batec (Denmark) (M)	Wet-chemical black chrome	Commercial
I	Solarect-Z™ (Slovenia) (M)	TSSS paint	Commercial
J	Konttinen et al. (Publications A-G) (R)	Mechanical	Laboratory/ commercial
K	SolkoteHI/SORB-II™ (USA) (M)	TSSS paint	Commercial
	Multiple manufacturers all over the world (M)	Black paint	Commercial

Examples of the spectral reflectance and microstructural composition of two absorber-reflector tandems, namely electroplated black chrome and sputtered Ni-NiO are shown in Fig. 2.7. More detailed microstructure of two selective absorber surfaces is shown in Fig. 2.8. On the left is the theoretical depth profile of a nickel-pigmented anodized aluminium absorber coating (Andersson et al. 1980). The coating is produced by first dc-anodizing aluminium sheets in a phosphoric acid solution to generate a layer of aluminium oxide on the substrate surface. This layer acts as a matrix for small metallic nickel particles to precipitate in the pores of the Al_2O_3 layer in a subsequent process of electrochemical reduction of nickel from a solution containing NiSO_4 . The surface on the right consists of a selective cermet graded $\text{Cr-Cr}_2\text{O}_3$ film which has been produced by a reactive DC magnetron sputtering (Teixeira et al. 2001). The cermet has a thickness of approximately 300 nm and it is based on metallic chromium in a matrix of a chromium oxide with a gradient in oxygen composition. The AFM micrograph naturally shows an approximation of the surface topology, and does not provide any information about the internal structure of the graded $\text{Cr-Cr}_2\text{O}_3$ film.

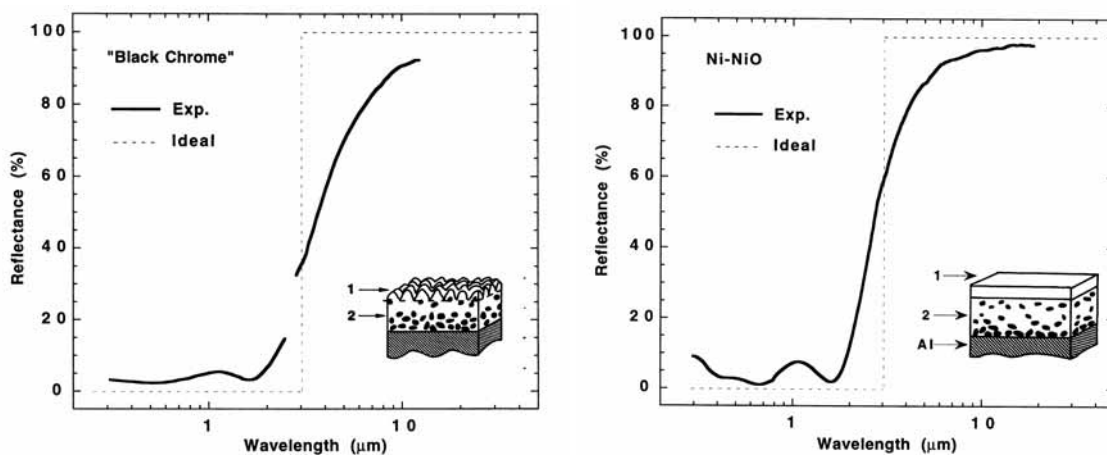


Figure 2.7. Spectral reflectance of ideal, electroplated black chrome and sputtered Ni-NiO selective solar absorber surfaces. Black chrome on the left, the inset indicates a microstructure with a graded cermet layer (2), having Cr particles dispersed in a Cr_2O_3 matrix, and a rough surface layer (1) of Cr_2O_3 . Ni-NiO absorber on the right, the inset shows an Al substrate, graded Ni-NiO (2) and an antireflection coating (1). Adapted from (Gordon, 2001).

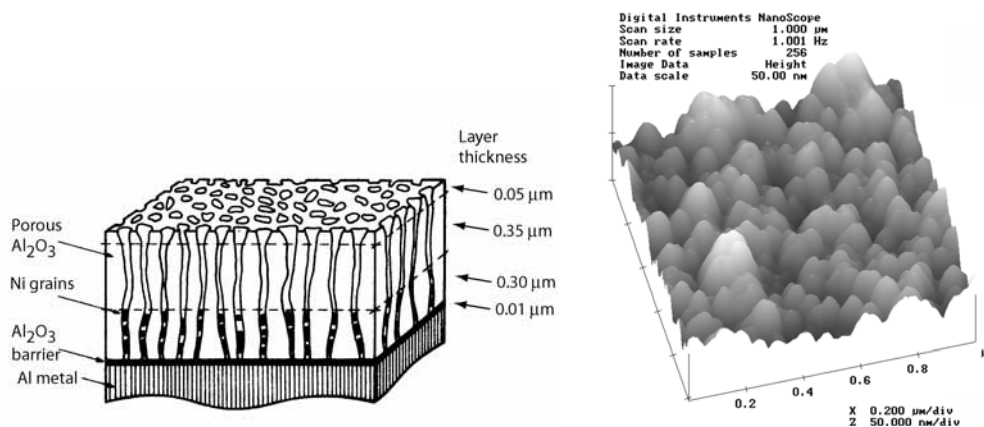


Figure 2.8. Microstructure of two solar absorber coating profiles: a) depth profile of a nickel-pigmented anodized aluminium absorber coating (Andersson et al. 1980) (left) and b) AFM micrograph of a graded $\text{Cr-Cr}_2\text{O}_3$ absorber coating (Teixeira et al. 2001) made by sputtering (right).

2.5 State of the art selective absorber design

A state-of-the-art selective absorber normally consist of thin films, sandwiched between the antireflection (AR) layer and a metallic substrate (Fig. 2.9), selectively absorbing in the solar spectrum and reflecting in the thermal spectrum: “a dark mirror”. The optical performance of dark mirror absorbers depends on the thin film design, thickness, surface roughness and optical constants of the constituents. The highest solar absorption is achieved if the film is a metal/dielectric graded composite (Farooq and Lee, 2003). An introduction to the theory of graded-index solar selective coatings can be found in (Buhrman, 1986).

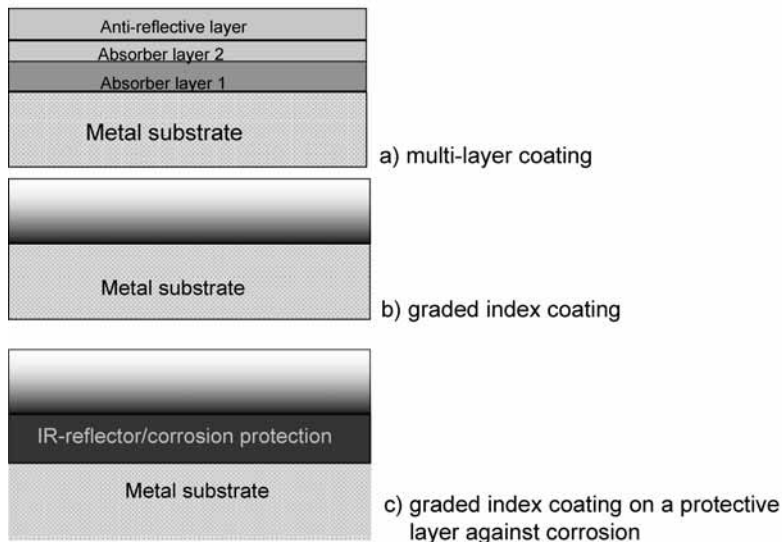


Figure 2.9. Depth profile design possibilities of solar absorber coatings. Adapted from (Czanderna, 2002).

The graded composition as shown in Fig. 2.9 should be designed with a continuously decreasing refractive index and an extinction coefficient from the substrate to the antireflection coating surface (Farooq and Lee, 2003). The ideal case is to have a refractive index $n = 1$ and extinction coefficient, $k = 0$ at the front surface in order to avoid refraction mismatch between air and the top coating. For graded surfaces, small particle composites tend to have large n values, and relatively high metal fraction composites are usually required in order to permit the utilization of the interference effect to obtain a relatively sharp absorptance edge (Buhrman, 1986). Thus an antireflection coating is necessary for reducing the front surface reflectance.

To be effective an antireflection coating must have a refractive index approximately midway between that of air ($n = 1$) and the underlying metallic selective absorber ($n \approx 2.3$). This range of n is well covered by common dielectrics and therefore it is quite easy to find an AR material compatible with any particular selective absorber (Buhrman, 1986). An example of a suitable antireflection material is approximately 80 nm thick Al_2O_3 coating (Buhrman, 1986; Farooq and Lee, 2003). More detailed description of design and use of AR coatings can be found in e.g. (Yoshida, 1979; Gombert et al. 2000; Chen, 2001).

The lowest thermal emissivity is achieved when the coating has non-metallic properties, i.e. k does not increase with wavelength, but preferably the opposite. Metallic properties within the base of the absorbing film will cause reduced infrared reflectance, i.e., increased thermal emittance.

In reality, a graded multilayer (2-5 layer) composite can produce over 95% absorptance with a very low emittance. By proper choice of layer thicknesses and refractive indices, the thin film destructive interference effect is in most cases used to enhance the solar absorptance. However, unity absorptance is almost impossible to attain in practice. For real absorbers the absorptance edge can not be completely step-like (see Fig. 2.7). Secondly, destructive interference affects reflectance throughout the solar spectrum. In addition, due to the wavelength-independency of the refractive index of the AR coating, mismatch at some wavelength range can increase spectral reflectance.

2.6 C/Al₂O₃/Al absorber surfaces

The manufacturing of the C/Al₂O₃/Al surfaces studied in this work started with experiments based on well-known methods of aluminium dyeing (Wernick et al. 1987). The first chemically/mechanically manufactured surfaces analysed at our laboratory in 1997 showed a solar absorptance of ~0.6 and a thermal emittance of ~0.4. In the beginning, there was no clear understanding of the physical properties of the experimental surfaces. The development steps of the manufacturing processes until the current low-cost novel mechanically driven abrasive method are described in Publication A. At present stage as a result of this thesis work, the understanding of the surface structure has increased significantly and also the optical properties have been clearly improved. These will be described in further sections in more detail.

The latest versions of the surfaces were manufactured on Al-substrate sheets by mechanically operated grinding. The dimensions of the 99.5% pure Al-substrate sheets are: length 2 meters, width 0.12 meters and thickness 0.5 mm. The mechanical grinding method implements a non-correlating classical random noise signal, which generates the control voltage for the X/Y – electromagnetic control units of the grinding unit. The grinding unit drives a grinding pad attached to a wheel head (Fig. 2.10). Very hard grinding particles, e.g. silicon carbide are attached in the pad thus forming a 3-dimensional matrix. The size of the particles varies and is typically between 300 nm – 2 μm. While the pad wears, new particles come into touch with the surface of the absorber substrate, increasing the uniformity of the process. The Al-substrate sheet moves back and forth under the grinding unit in a relatively slow motion, typically less than 1 m s⁻¹. In addition, the grinding unit moves the grinding pad across the substrate 2-dimensionally with variable speed (from zero to 20 m s⁻¹) and direction.

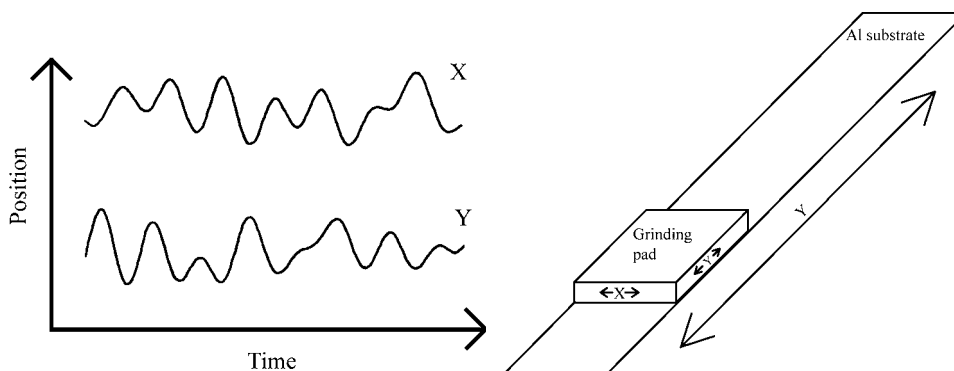


Figure 2.10. The non-correlating classical random noise used for moving the grinding pad in X/Y -directions across the substrate (left and right). The substrate moves back and forth slowly in Y-dimension (right, not to scale).

During the grinding process the grinding pad is saturated with carbon dust, which is bound to the pad by static electricity. Carbon dust reacts with the surface being scratched (containing

Al₂O₃ and unoxidized Al) and atmospheric oxygen forming a matrix structure on the final surface. This structure contains mainly the elements Al, O and C, and it covers the surface as a blackish or dark grey layer. Changing the size of grinding pressure, speed and time has a strong effect on the optical properties of the surface formed (Publications A-B). As a result of all the analyses, we assume that the carbon coverage and thickness mainly determine the solar absorptance of the surface with a possible small additional effect of optical trapping by surface roughness. The emittance is assumed to be determined by the carbon layer thickness as well, but surface roughness may contribute to it significantly.

The effect of the alumina layer on both α and ε of the C/Al₂O₃/Al absorber is unknown as there is not certainty of its thickness and structural composition. Alumina is used as an antireflection layer (see Section 2.5), but it can contribute to the thermal emittance of C/Al₂O₃/Al surface as well, depending on the thickness of the alumina.

Although a great number of absorber surfaces have been developed since the 1950s, the C/Al₂O₃/Al surface is unique in the following aspects: First, it combines a rough surface with a thin graphite-alumina absorption layer in a single phase manual or mechanical manufacturing process. Secondly, the manufacturing method is probably among the lowest capital cost methods available for achieving equally good optical properties and durability without environmentally harmful waste products. Virtually no infrastructure is required for manual manufacturing and the price of equipment for mechanical manufacturing may be some tens of thousands euros (Kilpi, 2003). The manufacturing infrastructure costs of the C/Al₂O₃/Al surface are approximately in the same range with the currently available commercial TSSS paints. For comparison, sputtering requires relatively large vacuum chambers and black chrome manufacturing requires large electrolyte tanks, which make both these technologies significantly more expensive.

Previous studies of combining a graphite layer and a rough surface to form a solar absorber have been done by (Botten and Ritchie, 1977) and (Golomb, 1978). An early work about using mechanical grinding to increase the selectivity of surfaces prior to deposition of multi-layer interference coating has been reported by Kudryashova (Kudryashova, 1969). The surface manufacturing method described in this dissertation differs from these in that it utilizes mechanical grinding for adding a graphite layer on a metal substrate and thus forms the selective surface without further treatments.

2.7 Mathematical modelling

Mathematical modelling and performance simulation of the C/Al₂O₃/Al surfaces are out of the scope of this work. An introduction to modelling can be found in (Gordon, 2001). Effective medium theories can be used to derive the dielectric permeabilities of the heterogeneous layers of metal-dielectric absorbers (see Section 2.4 for more details about absorber design). The optical properties can then be calculated by standard methods (Gordon, 2001). Methods used for modelling include two-flux simulation such as Kubelka-Munk theory (Gunde et al. 1996), four-flux simulation (Tesfamichael et al. 1998), N-flux simulation (Nitz et al. 1998) and Monte Carlo simulation (Nitz et al. 1998; Arancibia-Bulnes and Ruiz-Suarez, 1998). In the case of the C/Al₂O₃/Al absorber, more precise knowledge of the microstructure of the surface would first be needed to enable even crude modelling.

3 Experimental methods

3.1 Optical characterization

3.1.1 Measurement of absorptance and emittance

Spectrophotometers equipped with integrating spheres are typically used for the measurement of the hemispherical reflectance of absorber surfaces. UV-Vis.-NIR spectrophotometers measure the solar spectrum range and IR spectrometers cover the infrared range. The interior walls of the integrating spheres are coated with almost perfectly diffusing and highly reflecting materials, typically BaSO₄ for the solar spectrum range and gold for IR wavelengths. The theory and design of integrating spheres, their use for spectral measurements, analyses of the results, error sources and error correction methods have been extensively reported in the literature (Gindele et al. 1985; Roos and Ribbing, 1988; Roos et al. 1988; Roos, 1991; Roos, 1993; Nostell et al. 1999b; Roos et al. 2000).

The equipment used for solar absorptance measurements at the AES laboratory consists of a LI-COR LI-1800 portable spectroradiometer with an external integrating sphere attached via a quartz fibre optic probe. The inner walls of the integrating sphere are coated with BaSO₄ and a BaSO₄ plate is used as a reference (Fig. 3.1). The incident angle of reflectance is 10° (not indicated in Fig. 3.1, left).

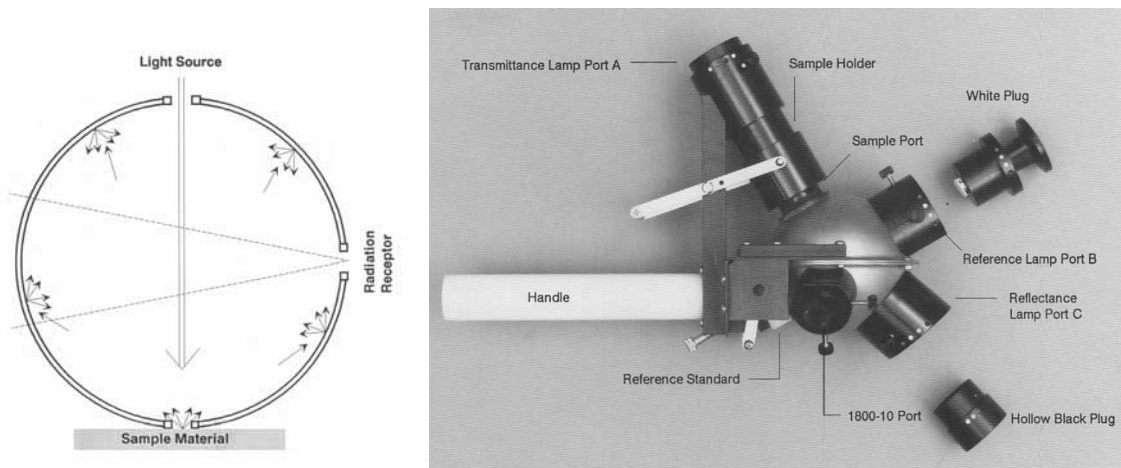


Figure 3.1. Li-cor integrating sphere operational schematic diagram. Internal (left) and external (right) view.

The solar hemispherical absorptance, α , was determined by measuring the monochromatic hemispherical reflectance ρ_λ from 0.39 to 1.1 μm , and α was calculated (based on Eq. 2-8 and 2-11).

$$\alpha = \frac{\int_{0.39\mu\text{m}}^{1.1\mu\text{m}} G_\lambda \cdot (1 - \rho_\lambda) d\lambda}{\int_{0.39\mu\text{m}}^{1.1\mu\text{m}} G_\lambda d\lambda}, \quad (3-1)$$

where G_λ is the monochromatic solar normal irradiance for air mass 1.5 (ISO, 1992).

A MIDAC Prospect IR FTIR-spectrometer is used for emittance measurements between 2.5 - 20 μm . The system consists of a main unit and a DRIFT accessory for partially spherical measurement as it was not possible to install an integrating sphere for the MIDAC system. More details of the emittance measurements are given in Section 3.1.4 “Error estimates of emittance measurement”.

The infrared (semi)hemispherical emittance, ε , was determined by measuring the monochromatic (semi)hemispherical reflectance ρ_λ from 2.5 to 20 μm , and ε was calculated (based on Eq. 2-9 – 2-11):

$$\varepsilon = \frac{\int_{2.5\mu\text{m}}^{20\mu\text{m}} E_{\lambda b} \cdot (1 - \rho_\lambda) d\lambda}{\int_{2.5\mu\text{m}}^{20\mu\text{m}} E_{\lambda b} d\lambda}, \quad (3-2)$$

where $E_{\lambda b}$ is the monochromatic Planck blackbody emittance at 100 °C.

3.1.2 Reference measurements

Not having an IR-spectrometer equipped with a proper integrating sphere, reference measurements were required in order to calibrate our system to give reliable results. Additionally, it was not possible to measure between 0.3 – 0.39 μm and 1.1 – 2.5 μm with our equipment. With reference measurements we could measure the whole UV–Vis.–IR spectrum between 0.3 – 20 μm and verify the results of our measurements (see Publications A-D for more details).

In total about one thousand C/Al₂O₃/Al samples have been optically characterized with the LI-COR LI-1800 spectroradiometer and the MIDAC Prospect IR FTIR -spectrometer. Reference measurements for 11 C/Al₂O₃/Al samples and one sputtered reference sample were conducted by Dr. Tuquabo Tesfamichael at the Ångström laboratory of Uppsala University, Sweden. The equipment included a Beckman spectrophotometer UV 5240 with integrating sphere and a Bomem Michelson 110 FTIR spectrometer with integrating sphere (see (Tesfamichael, 2000) for more details about the equipment).

The hemispherical absorptance measurements done at HUT comply within one percentage point for eight C/Al₂O₃/Al samples out of 11 with the Uppsala results. Results were within 1.5 per cent for two samples and 3 per cent for one sample. There are two main reasons for the differences: First, the Li-cor device used at HUT can not measure wavelength ranges of 0.3 – 0.39 μm (UV) and 1.1 – 2.5 μm (NIR). α_λ of C/Al₂O₃/Al surfaces is typically smaller in the far end of NIR spectrum compared to Vis. – near NIR spectrum (Fig. 3.2, sample A). This increases the integrated α measured at the HUT compared to the Uppsala results. Secondly, spectral values of α_λ are typically about 1-2 percentage points lower for all the HUT measurements (Fig. 3.2). Possible causes for lower spectral values are differences in the quality of the reference sample, quality of the inner BaSO₄ coating of the integrating sphere and optics of the measurement equipment.

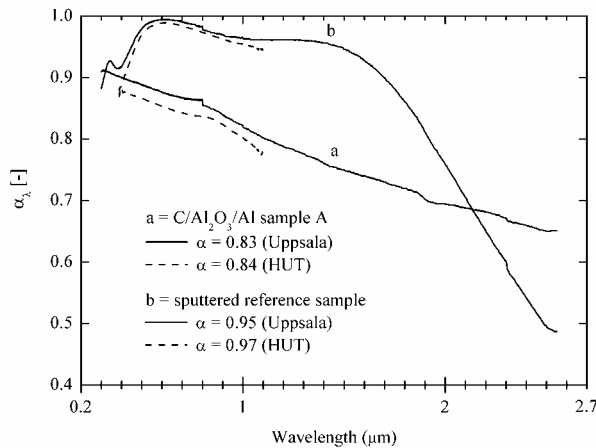


Figure 3.2. Typical monochromatic hemispherical absorptance measurement results (HUT) and reference measurement results from Uppsala.

The hemispherical emittance measurement results between Uppsala and HUT varied from -4 to +10 percentage points¹ for all the C/Al₂O₃/Al samples and +11 percentage points for the sputtered reference sample before calibrating the MIDAC Spectrometer. After calibration the absolute differences in ε between HUT and Uppsala measurements were within 1-2 percentage points for all samples (see Section ‘3.1.4 Error estimates of emittance measurement’).

3.1.3 Error estimates of absorptance measurements

The accuracy of measurement is affected by the physical properties of all the equipment in the path of light: the illuminator, the integrating sphere, the quartz fibre optic probe, the filter, the monochromator and the detector. Therefore an absolute calibration spectrum is needed. When using the external integrating sphere, a calibration spectrum of a reference sample of BaSO₄ is measured before each new sample is measured. This minimises the effect of changes in environmental factors. However, according to Roos and Ribbing (Roos and Ribbing, 1988) for strongly diffusing samples a PTFE reference would be preferred and a BaSO₄ reference is better suited for specular samples. In addition, measurement of the calibration spectrum can cause some systematic error to the following absorptance measurement.

The manufacturer calibrates the LI-1800 at approximately 25 °C. The temperature of the room where we measure is usually between 22 – 27 °C. Error caused by a change of temperature varies from 0 up to 6 per cent, depending on the wavelength. According to the manufacturer, the temperature dependence is not a problem as long as measurements are taken at about the calibrating temperature.

As mentioned earlier, the monochromatic hemispherical reflectance is measured at wavelengths between 390 and 1100 nm. 300 – 390 nm could be measured with the spectroradiometer as well, but data below 390 nm have proven to be inaccurate since the quartz fibre cable of the integrating sphere transmits little UV radiation. The “worst case” absorptance measurement error between 350 – 1100 nm is about ±5 percentage points (Myers, 2003). However, repeated measurements of any optically homogeneous sample give quite similar results, the standard deviation typically being below 0.005.

¹ Being above 4 per cent only for the samples that suffered intensive damage in the accelerated aging tests

3.1.4 Error estimates of emittance measurement

Error in the emittance measurements is caused by the properties of the MIDAC spectrometer, the DRIFT accessory and the combination of these two. The DRIFT accessory is not specifically designed to be used with the MIDAC spectrometer. Halme (Halme, 2000) has studied the previously unknown error sources of the MIDAC-DRIFT assembly. After receiving the reference emittance results we calibrated the assembly accordingly to correspond with the results.

Anomalies in the emittance spectrum measured with the HUT equipment between 5.5 – 10 μm (Fig. 3.3) are most likely due to non-unity spectral reflectance of the mirror used as a reference (Halme, 2000). To verify this, diffusely reflective KBr powder (Graseby Specac Ltd, 2000) was used as a reference instead of a specularly reflecting mirror and the resulting monochromatic hemispherical emittance was scaled to the same level (Fig. 3.4). The results show that the anomalies disappear almost completely, which support the theory of non-unity mirror reflectance.

The reason for using a mirror as a reference is based on the geometry of the DRIFT accessory and the corresponding beam path (Halme, 2000). In order to use any diffusely reflecting reference material we would need to know the angular distribution of its spectral reflectance. As this is not known for the KBr powder, a mirror with assumed unity angular spectral reflectance is used. The error in ε caused by non-unity spectral reflectance between 5.5 – 10 μm is in the range of one percentage point in most cases.

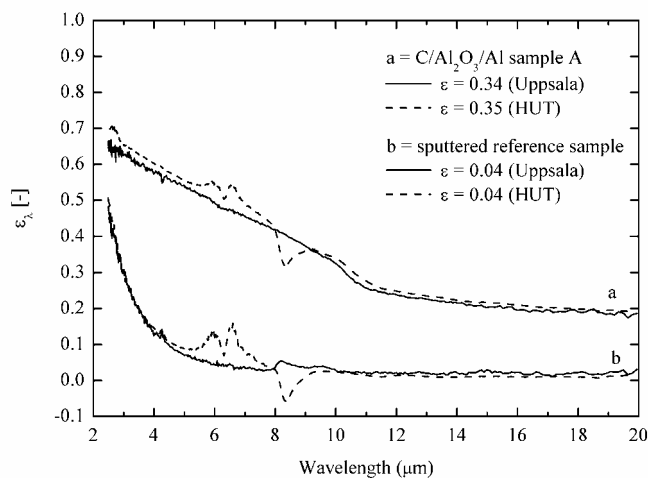


Figure 3.3. Typical monochromatic hemispherical emittance measurement results (HUT) and reference measurement results from Uppsala. A mirror has been used as a reference for HUT measurements.

As a result of the calibrating process of the LI-COR spectroradiometer and the MIDAC spectrometer, both the solar absorptance and thermal emittance of absorber samples can be measured with reasonable accuracy and good repeatability. A typical accuracy for C/Al₂O₃/Al samples is within $\pm 1 - 2$ percentage units compared to the measurements performed at Uppsala University.

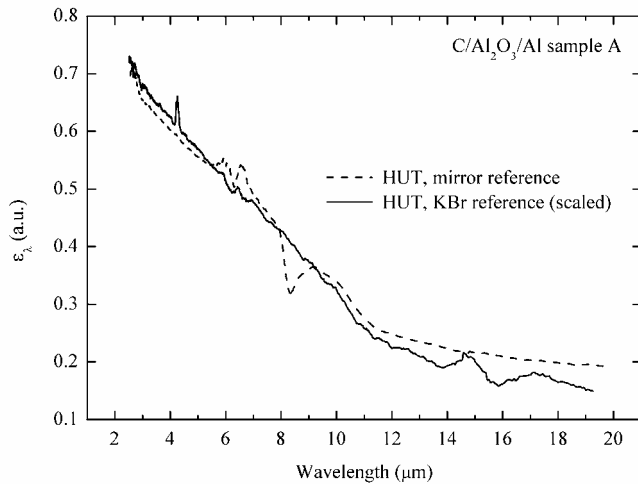


Figure 3.4. Typical monochromatic hemispherical emittance measurements for a mirror reference and a KBr reference (HUT). Results scaled to the same level (Y-axis only).

The measurement error estimate of an integrating sphere (and the DRIFT accessory) depends on the homogeneity of the sample as well. If the reflection of a sample is strongly angle-dependent, the results can vary more than 50 per cent when a round sample is turned 60° between measurements with an integrating sphere (Roos et al. 1988). Results for the C/Al₂O₃/Al samples show no angle-dependent behaviour (Publication A).

After calibrating the MIDAC-DRIFT assembly, the absolute differences in ε between HUT and Uppsala measurements were within 1-2 percentage points for all samples (Fig. 3.3). The same samples were measured in both places, but the exact measured area varied slightly.

However, the DRIFT accessory can not be recommended for this kind of analysis due to the fact that the sample size is restricted to a disk with a 10 mm diameter. This requires cutting a new disk from the sample after every absorptance measurement. The disk can not be utilized in further tests, as it is too small in diameter to be measured with the LI-COR spectroradiometer. Therefore the number of emittance and absorptance measurements possible for each sample is quite restricted, especially if the samples are 50 x 50 mm or smaller in size. In addition, quality variation in production caused 1-3 per cent variation in optical properties of many C/Al₂O₃/Al samples. This caused a lot of extra work in determining the actual changes in the α and ε due to aging tests: after initial measuring of α and ε of any given spot, no subsequent measurements of α of the same spot could be made. Therefore extra care had to be taken in selecting samples with uniform optical properties over an area large enough for several measurements.

3.2 Microstructural characterization

Microstructural characterisation of C/Al₂O₃/Al absorber samples was performed with scanning electron microscopy (SEM) (model JEOL JSM-820), field emission scanning electron microscopy (FESEM) (model DSM 982 Gemini), energy dispersive x-ray spectroscopy (EDS) (model JEOL JSM-820 with a PGT IMIX and model DSM 982 Gemini with a Noran Pioneer Si(Li) x-ray detector), x-ray photoelectron spectroscopy (XPS) (model Surface Science Instruments SSX-100), optical microscopy (Nikon type 104 equipped with a JVC 3-CCD colour video camera, model KY-F55B) and atomic force microscopy (AFM) (model DME Rasterscope 4000).

In the literature, a variety of other methods have been used for microstructural characterization of solar absorber surfaces. Examples of these are Auger electron spectroscopy (AES) (Shanker and Holloway, 1985; Pavlovic and Ignatiev, 1987; Vuletin et al. 1989; Taixin et al. 1993; Kaltenbach et al. 1998; Szzer et al. 1998) and elastic recoil detection analysis (ERDA) (Assmann et al. 1996; Eisenhammer et al. 1998).

3.2.1 Scanning electron microscopy and energy dispersive x-ray spectroscopy

A scanning electron microscope functions by scanning a focused beam of high energy electrons across a sample surface. The beam-specimen interaction produces a number of signals including secondary electrons, back-scattered electrons and x-rays (Fig. 3.5). The image is formed by using a detector, an amplifier and a cathode ray tube (CRT) display. The back-scattered electrons provide an image with atomic number contrast. x-rays are produced by the interaction of the electron beam with atoms in the specimen. These x-rays are characteristic of the elements present and they may be separated in an energy spectrum to identify the elemental composition of the specimen. This method is called energy dispersive x-ray spectroscopy (EDS). A detailed description of operation principle of SEM and EDS can be found in e.g. (Goldstein et al. 1992). Field emission SEM (FESEM) is similar to SEM, except that it is equipped with a field-emission cathode in the electron gun. It provides narrower probing beams at low as well as high electron energy, resulting in both improved spatial resolution and minimized sample charging and damage compared to SEM.

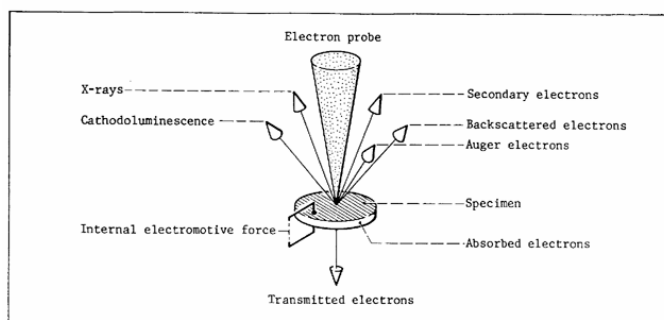


Figure 3.5. Primary electron beam and the corresponding signals generated by the sample (Jeol Ltd.)

3.2.2 x-ray photoelectron spectroscopy

In x-ray photoelectron spectroscopy, a sample is illuminated with x-rays which excite photoelectrons from the surface (Christie, 1989). A major advantage of the technique is that the photoelectron energy is dependent on the precise chemical configuration of the surface atoms and pronounced chemical shifts are produced in the position of the peaks in the XPS spectrum. The photoemission of the sample is observed by measuring the energy spectrum of the emitted photoelectrons. Since the energy levels are quantised (Christie, 1989, pp. 129-131), the photoelectrons have a kinetic energy distribution, $N(E)$, consisting of a series of discrete bands that essentially reflects the “shell” form of electronic structure of the atoms in the sample. The experimental determination of $N(E)$ by a kinetic energy analysis of the photoelectrons produced by exposure to x-rays is termed x-ray photoelectron spectroscopy.

3.2.3 Optical microscopy

An optical microscope was used for imaging the absorber samples at lower magnifications. With this model solid samples can be illuminated from the top thus providing a clear image of the object. A charge coupled device (CCD) camera was used for digital imaging of the samples. A limiting factor of using light microscopy for characterization of solar absorber

surfaces is its resolution, which is estimated to be approximately 1 – 2 times the wavelength of the incident light for 10x – 40x magnifications used. However, optical microscopy was useful for gaining additional information on C/Al₂O₃/Al samples due to their relatively gross microstructural nature (see Section 5.1.3 Optical microscopy analyses).

3.2.4 Atomic force microscopy

Atomic force microscopy (AFM) (Binnig et al. 1986) is in principle a scanning probe microscope. Unlike optical and electron microscopes which 'look' at the sample, the probe microscope form image by 'feeling' the structure of the sample. In the AFM, the probe is mounted on a spring, and is brought into contact with a surface such that it experiences a very small interaction force, usually of the order of nano-newtons. The probe is then raster scanned across the surface, while maintaining a constant force between the tip and the sample (Figure 3.6). These deflections of the cantilever, which are caused by changes in surface stiffness or topography, allow the AFM to record topographic contours of a surface.

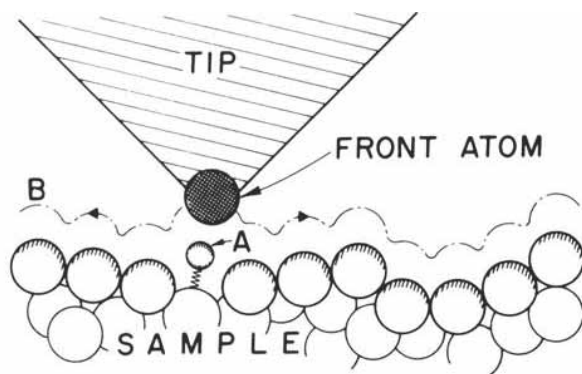


Figure 3.6. Description of the operation of an AFM. A tip follows contour B to maintain constant force between the tip and a sample. The force can come from an AC voltage on the tip, or from an externally applied magnetic field for adatoms with a magnetic moment. Adapted from (Binnig et al. 1986)

4 Accelerated aging

Accelerated aging tests are used to estimate the service lifetime of solar absorber surfaces. A minimum service lifetime of 25 years is a commonly used target when designing new absorbers. The maximum service lifetime of an absorber coating is reached if the annual solar fraction of a domestic hot water system is decreased by 5% due to deterioration of its optical properties caused by degradation. Accelerated aging tests are typically conducted under three different conditions: a) high temperatures and low humidity, b) service temperatures under condensation conditions and c) service temperatures and high humidity air containing sulphur dioxide (Carlsson et al. 1994; Brunold et al. 2000a; Brunold et al. 2000b; Carlsson et al. 2000a; Carlsson et al. 2000b; Köhl, 2001).

IEA Solar Heating and Cooling Programme (IEA SHC) Working Group “Materials in Solar Thermal Collectors” (MSTC) has proposed an accelerated aging test procedure as a standard to the ISO TC 180 ‘Solar Energy’ (draft ISO/DIS 12592) (Brunold et al. 2000a; Brunold et al. 2000b). Further IEA SHC work concerning accelerated aging of solar absorber materials will be published in (Czanderna, 2002). Earlier IEA SHC accelerated aging studies include (Lampert, 1989; Hollands et al. 1990; Carlsson et al. 1994).

Additional information about accelerated aging of solar absorber surfaces can be found in the following publications: (Pettit, 1983; Mabon and Inal, 1984; Moore, 1986; Köhl et al. 1989; Roos and Georgeson, 1991; Taixin et al. 1993; Lee et al. 1993; Schön et al. 1994; Gampp et al. 1994; Orel and Orel, 1995; Chaudhuri et al. 1997; Kaltenbach et al. 1998; Gampp et al. 1998; Konttinen, 2000; Schuler et al. 2000; Kaluza et al. 2001; Köhl, 2001; Schuler et al. 2001; Ghodsi et al. 2001)

4.1 Aging factors

According to the IEA SHC Task X and the working group MSTC results, (Carlsson et al. 1994; Brunold et al. 2000b) the main degradation mechanisms contributing to the degradation of solar energy absorber surfaces are:

- Degradation due to thermal load (oxidation)
- Degradation due to high humidity or condensation of water on the absorber surface (hydration and hydrolysis)
- Degradation due to air pollutants such as sulphur dioxide (atmospheric corrosion)

The standard tests (draft ISO/DIS 12592) were originally designed for the qualification of electroplated and sputtered selective absorber coatings. According to (Carlsson et al. 2000b), if a surface consists of an organic coating, the effect of UV-degradation on the optical performance should be considered as well. Other possible degradation factors are described by Lampert (Lampert, 1989). These include physical stress, abrasives and dirt.

4.2 Testing procedure, standard tests

The testing procedure of the draft ISO/DIS 12592 document consists of temperature tests, condensation tests and sulphur dioxide tests. A detailed description of the testing procedure can be found in, e.g., (Carlsson et al. 2000b). A brief introduction is given below.

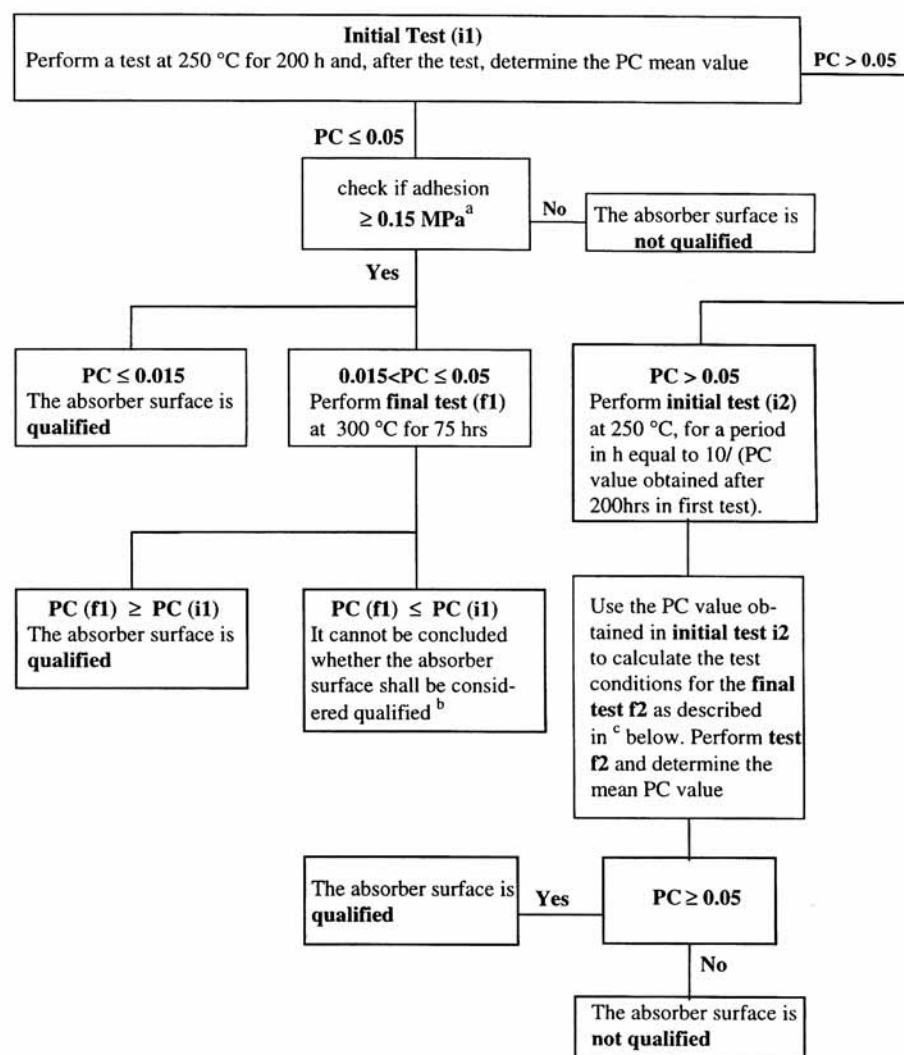
For estimating the acceptable service life of an absorber coating, the IEA SHC Task X (Carlsson et al. 1994) has defined a performance criterion function, PC :

$$PC = -\Delta\alpha + 0.25\Delta\varepsilon \leq 0.05 \quad (4-1)$$

When the value of the *PC* function has been increased to 0.05, the solar fraction of a domestic hot water (DHW) system has been reduced by around 5 per cent in a relative sense for a low-fraction flat plate collector solar DHW system (Carlsson et al. 2000b). The absorber surface should consequently be considered to have failed, due to degradation in the optical performance.

The thermal stability test consists of an initial test at 250°C for 200h followed by an adhesion test (Carlsson et al. 2000b). The absorber panel size is 50 mm x 50 mm for all tests, and three samples are tested simultaneously. Additional tests may be required at different temperatures and/or for different test duration, depending on the results of the initial test (see Table 4.1). The adhesion of the coating prior to and after each test can be assessed by a procedure standardised in ISO 4624 or by a simple tape test.

Table 4.1. Testing procedure for qualification of the thermal stability of absorber surfaces (Carlsson et al, 2000b).



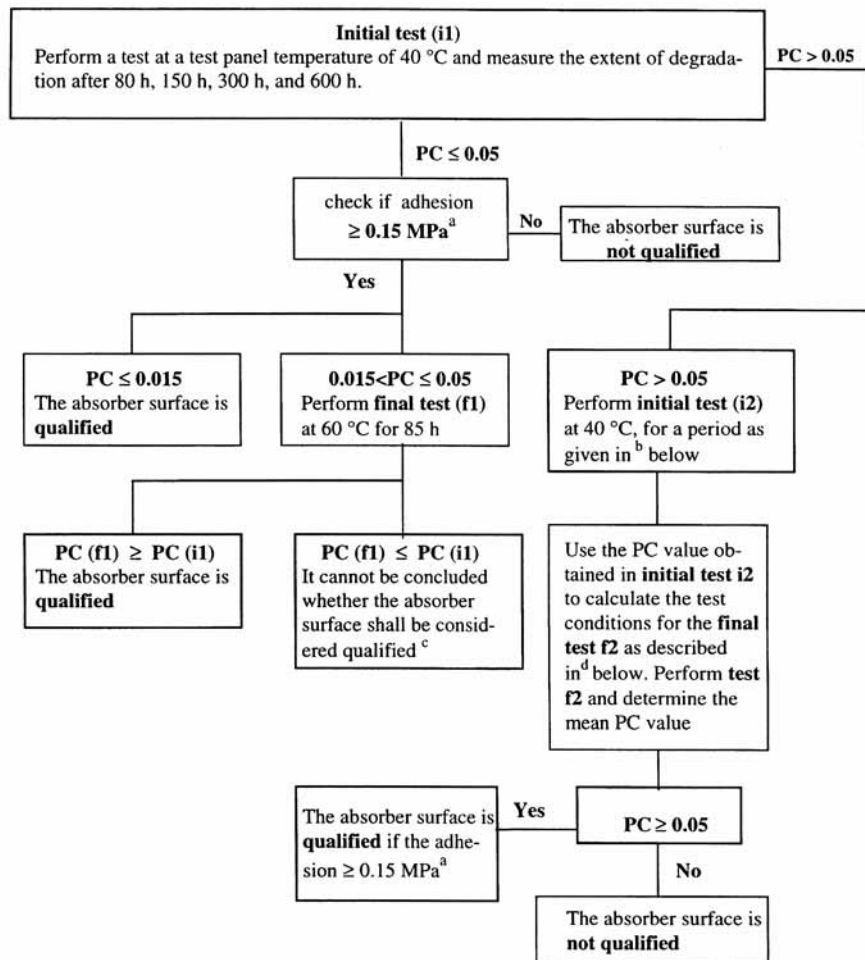
^a If a tape test is used check the adhesion between the coating and the substrate, the adhesion between the tape and the coating should be better than 0.15 MPa.

^b A more comprehensive investigation of the thermal stability is recommended.

^c Estimate by interpolation, the testing time, that would correspond to $PC = 0.05$. Determine the lowest acceptable activation energy on the 250°C curve in Fig 3. in (Carlsson et al, 2000b) and also the corresponding failure time in a test at 200°C and perform that test for a period corresponding to that time. Determine after the test PC and if relevant also the adhesion of the coating.

Moisture tests consist of initial tests at an absorber panel temperature of 40°C for 80 - 600h (Carlsson et al. 2000b). Absorber samples are cooled to 5°C below the chamber temperature thus causing continuous condensation on the surfaces. Subsequent tests, if needed, depend on the initial test results (Table 4.2).

Table 4.2. Testing procedure for qualification of the resistance to moisture of absorber surface (Carlsson et al, 2000b)



^a If a tape test is used check the adhesion between the coating and the substrate, the adhesion between the tape and the coating should be better than 0.15 MPa.

^b If $PC > 0.05$ after 80 h of testing, perform a new test at 40°C for 40 h. If $PC > 0.05$ after 150 h of testing, 300 h of testing, and 600 h of testing, perform new tests at 40°C for 115 h, 225 h, and 450 h, respectively. Perform test i2 without any interruptions for measurements until after complete test.

^c A more comprehensive investigation of the resistance to moisture is recommended.

^d Estimate by interpolation, the testing time, which should correspond to $PC = 0.05$. Determine the lowest acceptable activation energy on the 40°C curve in Fig. 5 in (Carlsson et al, 2000b) and also the corresponding testing time for a test f2 at 30°C.

Atmospheric corrosion resistance testing is determined by exposing absorber samples to circulating air of a relative humidity of 95 per cent, temperature of 20°C, and with a concentration of sulphur dioxide of 1 ppm. According to Carlsson et al. (2000b), the test is essentially performed as described in ISO 10062 ‘Corrosion tests in artificial atmosphere at very low concentrations of polluting gases’.

The results of each test are analysed separately, and the dominant aging factors are determined for the absorber being tested.

4.3 Equipment used at HUT

A high temperature air-circulating oven was utilized for thermal stability testing (Publication D). The oven meets the IEA SHC testing equipment requirements (Carlsson et al. 2000b) for assessing the thermal stability of an absorber surface, except for the cooling rate requirement. Therefore the test panels were removed from the oven immediately after the specified testing time was reached, as recommended by Carlsson et al. (Carlsson et al. 2000b).

A climate chamber (Fig. 4.1) was used for moisture and condensation testing (Publication D). The climate chamber meets the IEA SHC testing equipment requirements for assessing the resistance of the absorber surface to moisture (Carlsson et al. 2000b). An exception was that due to technical restrictions cooling fluid flow was less than recommended 90 l min^{-1} thus increasing the temperature difference between the three samples. To minimize the effect of this we accepted results only for the two samples adjacent to the sample temperature sensor (see Fig. 4.1) if the result of the third sample deviated from these significantly.

4.4 Additional aging tests, thermal cycling and irradiation

In addition to standard accelerated aging testing, additional temperature and irradiance cycling tests were performed in three phases (Publication E). The test method and equipment are described in detail in (Kontinen, 2000). Fig. 4.2 shows an overview of the inner chamber of the climate chamber together with the UV lamps and sample holder used for phase 3 testing. Phase 2 was otherwise similar except that the lamps were oriented vertically and the samples horizontally. For phase 1 an external solar simulator was used and the samples were oriented vertically.

The purpose of the cycling test was to simulate and accelerate the temperature and irradiance conditions that the absorber surfaces are exposed to in normal outdoor use. The upper temperature limit of the chamber was a restrictive factor as the maximum selective $\text{C}/\text{Al}_2\text{O}_3/\text{Al}$ absorber surface stagnation temperatures inside a flat plate solar collector can rise up to 180°C . Therefore additional tests were performed at 120°C and 180°C for determining the effect of constant temperature alone on the optical properties.

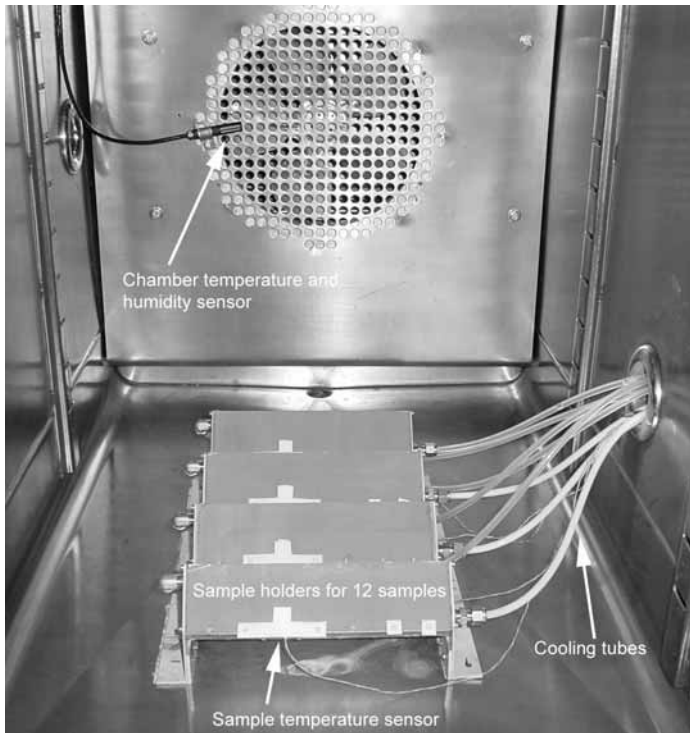


Figure 4.1. A view of the climate chamber used at HUT for moisture and condensation tests. Inner chamber dimensions 0.59 x 0.8 x 0.75 m, volume 354 litres.

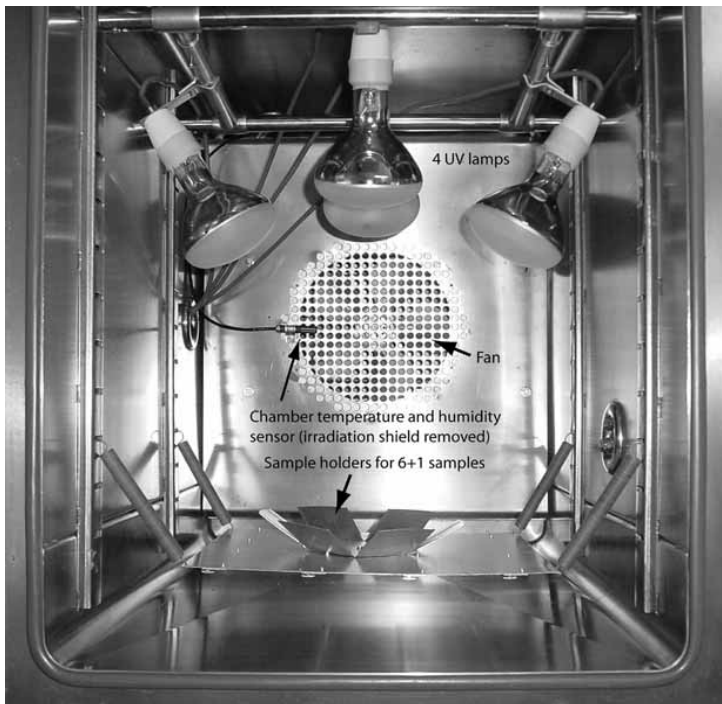


Figure 4.2. A view of the climate chamber used for phase 3 UV exposure and temperature cycling testing (reconstructed). Six samples (7 cm x 7 cm) can be tested simultaneously at 30° slope inclination. One sample can be tested in the middle of the sample holder with approximately 75% higher irradiance.

4.5 Additional aging tests, total-immersion simulated acid and neutral rain

Degradation mechanisms of unglazed C/Al₂O₃/Al solar absorber surfaces based on aluminium substrate were studied. Unglazed solar absorbers are subject to ambient conditions, such as rain, wind and deposits, more severe than absorber surfaces inside covered collectors. The complexity of the possible degradation mechanisms and their interactions make it difficult to estimate the effect of different ambient factors on the lifetime of an unglazed absorber. However, the effect of individual factors can be examined in laboratory conditions in order to provide a picture of their influence on the behaviour of the absorber in the corrosive medium. This will aid in deciding whether the operating conditions are favourable or unfavourable to the corrosion resistance of the absorber.

Surface samples were immersed (Fig. 4.3) to O₂-aerated or zero-aerated (with N₂) simulated acid rain with pH 3.5 and pH 4.5, and simulated neutral rain with pH 5.5, at temperatures of 60, 80 and 99 °C (Publication G). Temperature levels were chosen based on calculated stagnation temperature levels in Helsinki. Samples were analysed optically with LI-COR and MIDAC spectrometers. Thermogravimetry (TA, Mettler TA thermal analysis system) was used to determine the mass changes of some of the samples exposed to simulated rain tests. EDS was used to study the elemental composition changes.

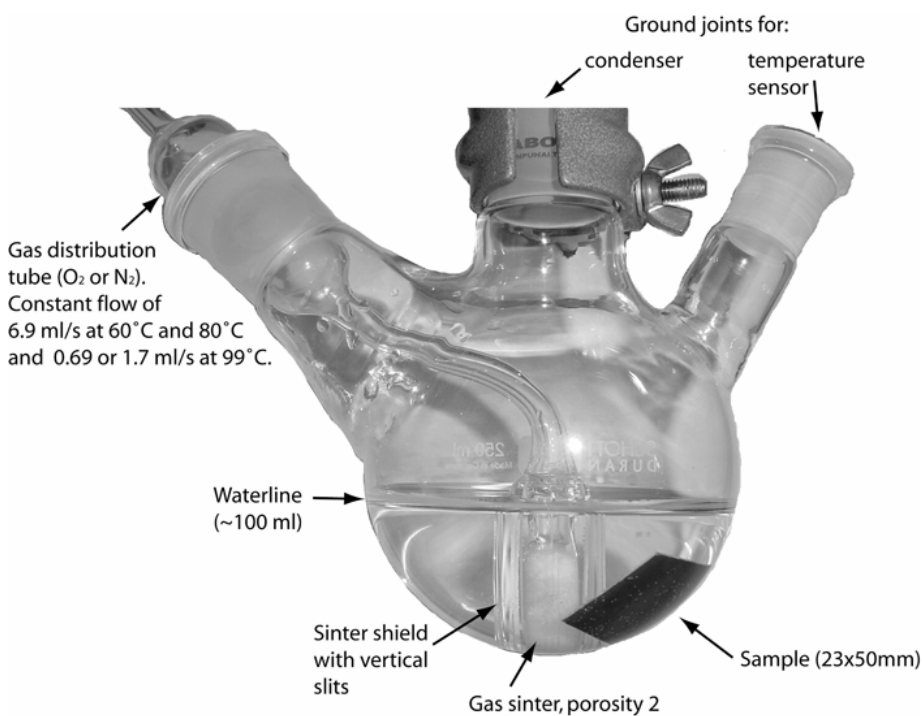


Figure 4.3. Photograph of the simulated rain total-immersion setup including a three-necked flask (250 ml volume), 100 ml of simulated rain, a C/Al₂O₃/Al absorber sample (23 x 50 mm in size) and a gas distribution tube. Heating system consisting of paraffin oil bath, heater and temperature controller is not shown.

5 Results

5.1 Optical and microstructural characterization

5.1.1 SEM and EDS analyses

The C/Al₂O₃/Al surfaces were first characterized by SEM (model JEOL JSM-820) and EDS (model PGT IMIX). At that time there was no clear understanding of the physics of the surface or interrelationship between surface microstructure and its optical properties. The microstructure of the surface as seen by SEM (Fig 5.1) is that of small grooves, organized in a heterogeneous two-dimensional (and partly three-dimensional) groove matrix (Publication A). The width of the grooves varies, and is typically between 1 and 2 μm. Due to continuous grinding process, some of the grooves are deeper and/or have sharper edges than the others. The probable cause for this is that during grinding the grooves formed earlier are ground over multiple times with grains of different size and shape, causing only the latest formed grooves to appear very clear and sharp-edged.

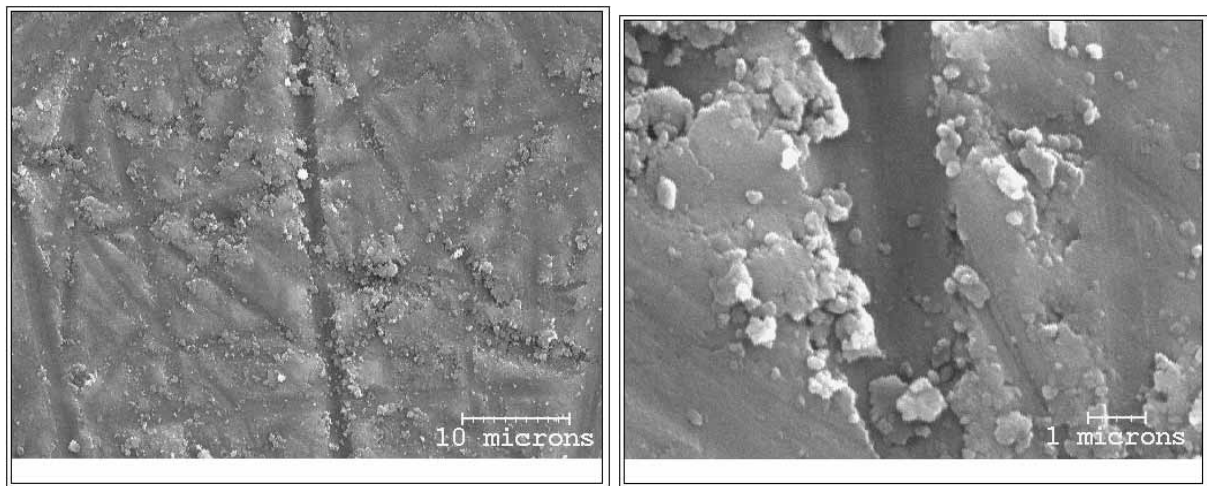


Figure 5.1. SEM micrograph of a typical C/Al₂O₃/Al surface (denoted as A in Publications A and B) (left) and magnification the vertical microgroove in the middle (right).

For determining the elemental composition of the surface concurrent EDS analyses were conducted. Very small traces of Si, Mn, Fe and Cu were detected. EDS showed a tiny amount of carbon as well but this was expected as the samples shown in Fig. 5.1 were coated with a thin layer of carbon prior to the analyses! According to the Al-sheet manufacturer, the sheet can contain small amount of Si, Fe, Cu, Mn, Mg, Zn and Ti (Table 5.1).

Table 5.1. Elemental composition of the Al substrate sheet according to the Al manufacturer. Specifications: 99.5% purity, EN AW 1050A, hardness number 14.

	Si	Fe	Cu	Mn	Mg	Zn	Ti	Al
Min	0.00	0.00	0.00	0.00	0.00	0.00	0.00	99.50
Max	0.25	0.40	0.05	0.05	0.05	0.07	0.05	-

In further SEM and EDS analyses, gold was used as the coating material instead of carbon. By analysing both the active surface side and the backside of a gold-coated sample we could determine the existence of the carbon layer formed during the manufacturing process (Fig. 5.2). Further XPS analyses have verified these results (Publication C).

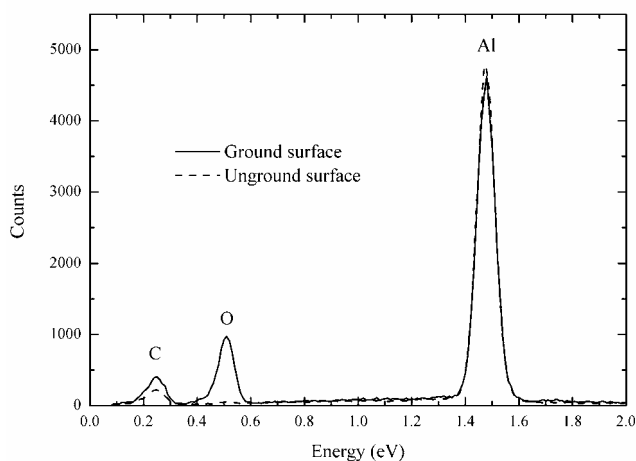


Figure 5.2. EDS -analysis of a typical C/Al₂O₃/Al surface, ground manually for 15 minutes. Untreated aluminium backside of the same sheet shown as a reference.

The EDS analyses show that there is a significant difference in oxygen content between a typical C/Al₂O₃/Al surface and its untreated aluminium backside. In addition, there is some difference in carbon content and virtually no difference in aluminium content. Therefore, during grinding some of the elemental components of the Al surface are strongly oxidized and some carbon is added on the surface. Some of the carbon measured from the backside may be due to carbon dust contamination during the grinding process, although the surface was cleaned, probably with ethanol, prior to the analysis.

5.1.2 XPS analyses

In order to verify the chemical composition of the added oxygen and carbon compound on the surface, two samples of a typical C/Al₂O₃/Al surface were analysed by XPS (Publication B). The results are shown in Fig. 5.3, the two samples are denoted as 1 and 2. The XPS result for the oxygen compound is Al₂O₃, likely to be formed in the grinding process of Al-sheet in air. The Al₂O₃ -related peak intensities of the binding energies are 74.3 eV (Paparazzo, 1988) and 74.35 eV (Nefedov, 1982) as well as O1s with 531.52 eV (Wagner et al. 1982). The C1s compound corresponding to the peak binding energy of 284.8 eV may be carbon in graphite form (Bachman and Vasile, 1989). Some other potential C1s matches such as HC=O, CO, (CH₂)_n, CHO, not marked in Fig. 5.3 with smaller binding energy intensities could have been formed.

In addition, the backside of a sample was analysed (Publication B), denoted as "back" in Fig. 5.3. Due to the nature of the manufacturing method containing carbon dust, the backside of the substrate is contaminated with carbon compounds while attached to the grinding bed. As the front and back surfaces of the C/Al₂O₃/Al samples contain a large amount of carbon, XPS alone cannot be regarded as an absolutely reliable method for determining the chemical composition of the surface. The energy scale was fixed to Al2p for all samples assuming Al₂O₃ would be found and the C1s and O1s peak intensities were gained as a result. This may have caused some displacement in C1s and O1s results. Secondly, exact peak binding energies varied slightly between measurements. In addition, according to (Süzer et al. 1999) even with the C1s peak as a reference at 285.0 eV referencing errors up to about 1 eV are not uncommon. Therefore interpretation of the C1s carbon compound as graphite includes some uncertainty.

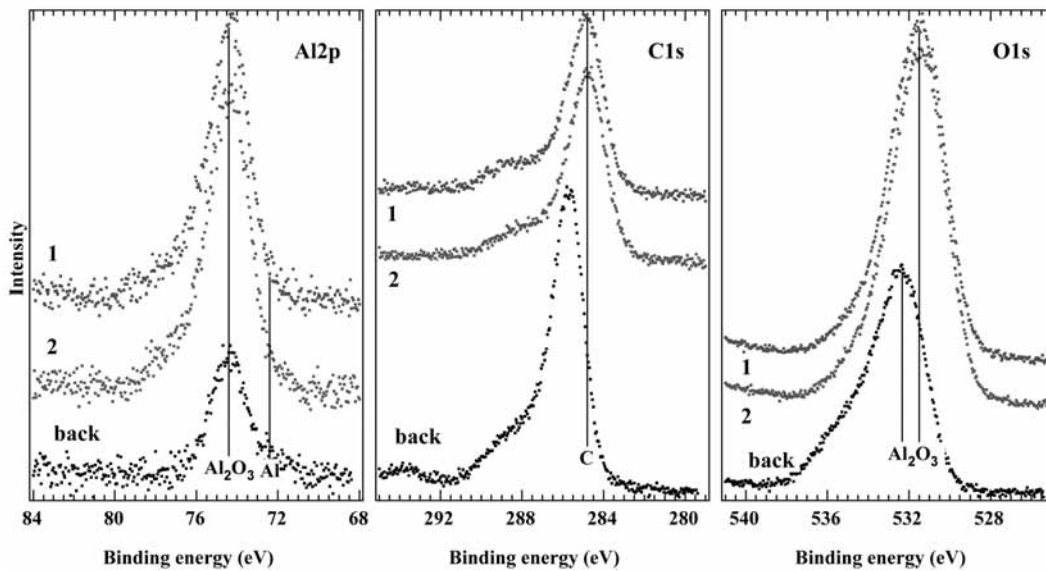


Figure 5.3. XPS analysis of two samples of a typical surface, denoted as 1 and 2, and backside of the surface, denoted as "back". Corresponding peak intensity binding energies of samples 1 and 2 are related to Al_2O_3 (74.35 eV and 531.52 eV) and C in graphite form (284.8 eV).

5.1.3 Optical microscopy analyses

Optical microscopy was utilized to analyse the form and distribution of the carbon layer of the surface (Publication B). Based on the optical microscopy analysis, it may be possible that the grinding process mechanically incorporates adsorbed and agglomerated graphite or a mixture of graphite-alumina into the surface. The carbon matrix structure in turn could be composed of agglomerated graphite or graphite-alumina clusters.

Assuming a graphite cluster interpretation, then the graphite thickness and coverage is likely to dominate the absorption of the surface, since no absorptance higher than 0.91 has been achieved so far. If the surface would be covered by a homogeneous sufficiently thick carbon layer, the solar absorptance would be up to 0.94 (Duffie and Beckman, 1991). In order to find the manufacturing parameters which would maximize α , 27 experimental samples were manufactured (Publication B). Most of these surfaces have α over 0.88 and ε higher than 0.25. Fig. 5.4 shows optical photographs of the samples with the smallest (sample number 25) and the highest (sample number 16) emittance. The photographs were taken with exactly the same microscope parameters (see Publication B for more details). The absorptance of samples 25 and 16 is 0.90 and 0.91 and the emittance is 0.22 and 0.46, respectively. As can be seen by comparing samples 25 and 26, the surface of sample 16 appears significantly darker than the surface of sample 25. In addition, the visible graphite coverage is larger for sample 16. It should be noted that the optical resolution of the optical microscope and CCD-camera used for obtaining Fig. 5.4 and other optical photographs in Publication B prohibits analyses of objects of size smaller than approximately 1-2 times the wavelength of incident light. For example, the observed contrast between topographic microgrooves and plateaus of the same size range might occur only because of light trapping in the grooves themselves irrespective of any absorbing carbon layer. However, analyses of larger areas together with measured optical properties indicate differences between the two surfaces.

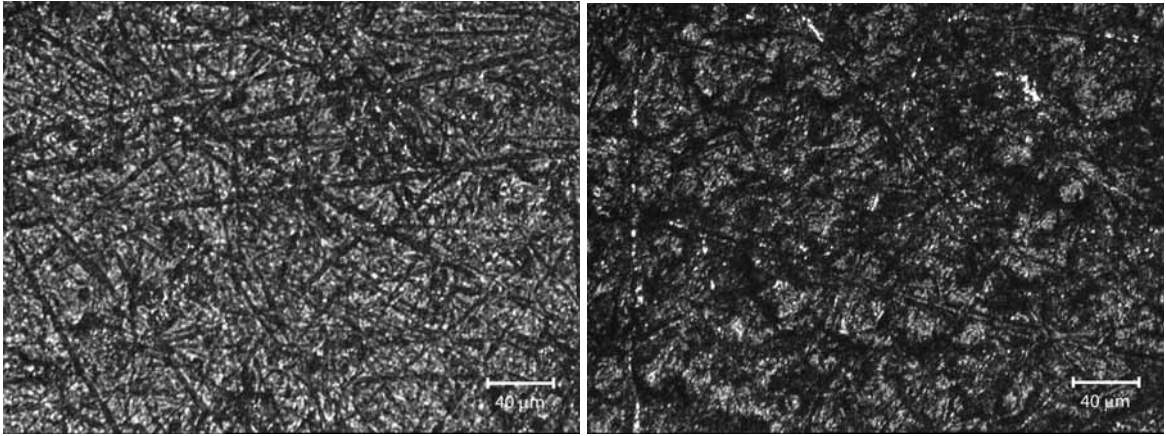


Figure 5.4. Optical photograph of the surface sample number 25 (left) and sample number 16 (right).

The author estimated the luminosity of samples 25 and 16 with the Adobe Photoshop 5.0 program (Publication B). The luminosity distribution of sample 16 is significantly more biased towards dark end of the scale. Although it is not possible to directly determine the thickness of the graphite layer from the luminosity analysis, it is likely that the assumed graphite layer of sample 16 is significantly thicker than sample 25. This results in more than doubling ε compared to sample 25. However, the estimated graphite coverage difference between samples 25 and 16 has almost no effect on α . The thicker graphite layer of sample 16 does not compensate for the estimated missing graphite coverage, and therefore α does not rise above 0.91 even for the samples with the highest ε .

5.1.4 AFM analyses

Atomic force microscopy (AFM) was used to determine the 3-dimensional structure of the optically best surface shown in Fig. 5.4 (left) in more detail. The maximum measuring area is $50 \times 50 \mu\text{m}$. Fig. 5.5 shows typical 3- and 2-dimensional AFM micrographs of the surface and Fig. 5.6 shows profiles of three cross sections denoted as 1-3 in Figs. 5.5 and 5.6.

Contrast from white to black in the AFM micrographs indicates the height of the measured point from top to bottom, respectively. The width of the three microgrooves visible within profiles 1 – 3 is approximately $0.7 - 1.2 \mu\text{m}$. Microgroove profiles are clearly distinguishable from cross section profiles 1 – 2: At the approximate height of 200 nm (80 nm from the groove bottom) both profiles becomes sharply broader on one side indicating the end of a clearly separate single microgroove. In contrast profile 3 has a knifelike sharp V-form having a height of 160 nm from the groove bottom. These results indicate that the surface has microgrooves with variable sharpness and a depth of approximately 80 – 160 nm. The total difference in elevation is approximately 400 nm, which is typical for this surface (based on all the AFM analyses conducted on this surface).

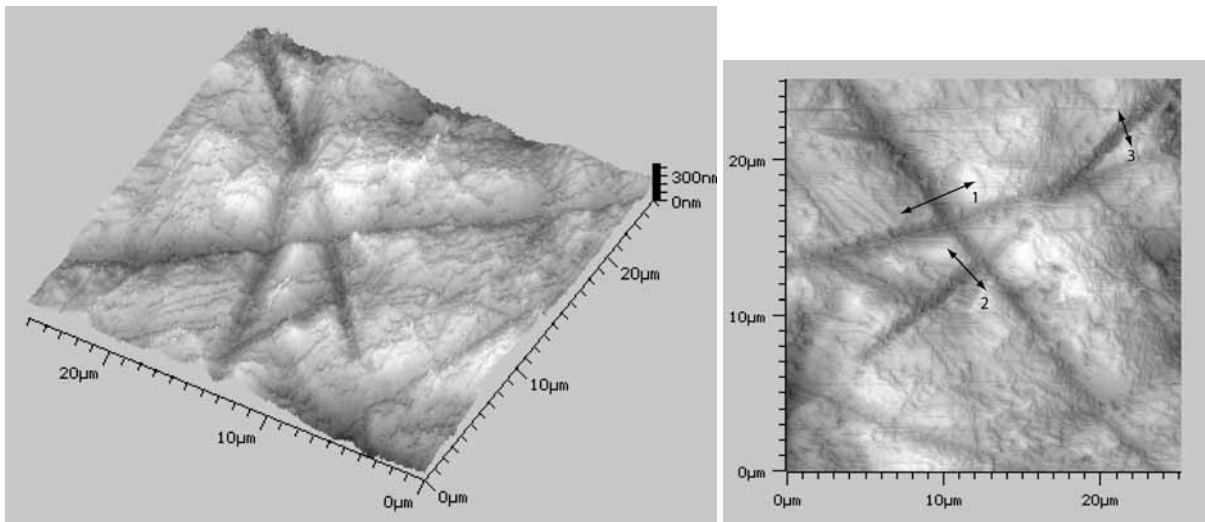


Figure 5.5. 3D (left) and 2D (right) AFM micrographs of the same area of an absorber sample having $\alpha = 0.90$ and $\varepsilon = 0.22$ (denoted as surface 25 in Publication B). Surface area is $25 \times 25 \mu\text{m}$. Optical photograph of different area of the same surface sample is shown in Fig. 5.4 (left). Cross section profiles of areas denoted as 1-3 are shown in Fig. 5.6.

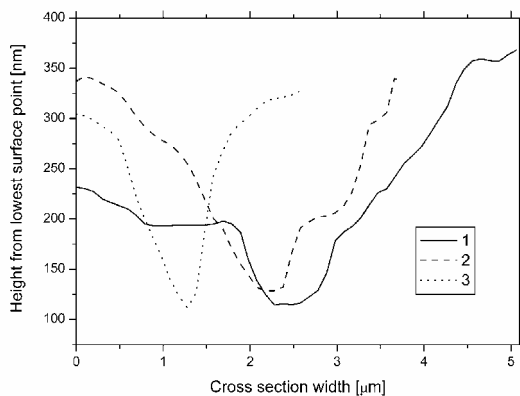


Figure 5.6. Cross section profiles of the three microgrooves denoted as 1-3 in Fig. 5.5 (right).

5.1.5 Crosscut sample SEM analyses

Fig. 5.7 shows a crosscut field emission SEM micrograph (FESEM type DSM 982 Gemini) of a typical absorber surface sample (Publication B). Visible in Fig. 5.7 (just below the surface borderline) are light colour areas (denoted as 3), which may be interpreted as clustered graphite adsorbed and agglomerated on the $\text{Al}_2\text{O}_3/\text{Al}$ surface. The estimated maximum visible graphite cluster thickness is approximately 300 nm. Another possibility is that the interface 3 in Fig. 5.7 consists of a mixture of graphite and alumina on Al substrate. Further FESEM and EDS analyses were conducted in order to verify the composition of the interface. The same crosscut sample as in Fig. 5.7 was carefully cleaned by a series of ultrasonic cleaning treatments, first four times in 99% pure ethanol, followed with acetone and the final ethanol treatments, three minutes each. After cleaning, the sample was analysed again with the same FESEM and EDS as before. Fig. 5.8 shows a FESEM micrograph and the corresponding elemental map of one area of the surface.

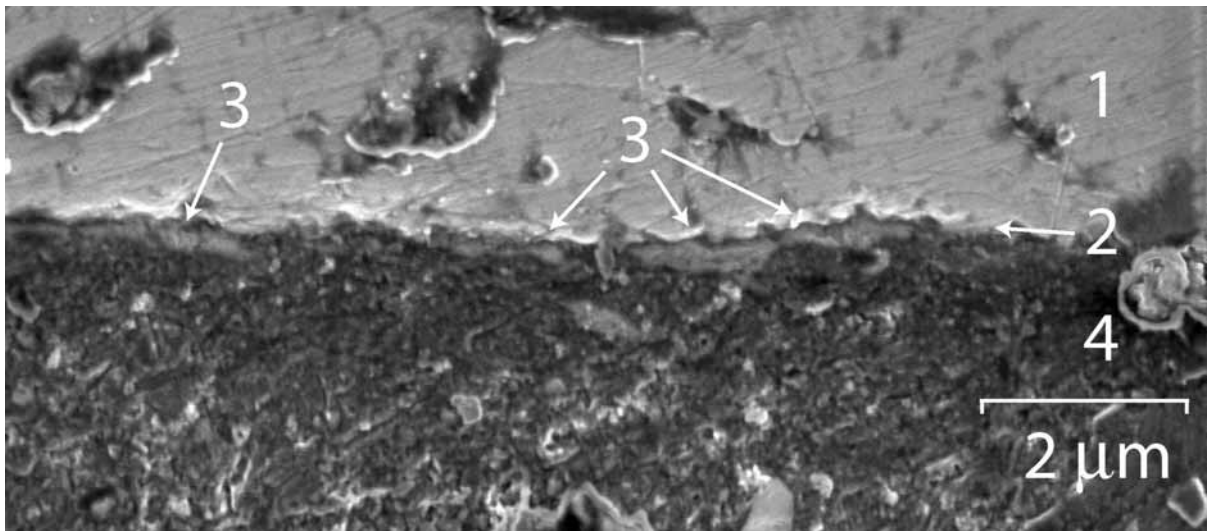


Figure 5.7. A crosscut FESEM micrograph of a typical surface sample, horizontal sample orientation. 1) stainless steel (SS) attached on top of the surface before crosscutting, 2) surface borderline between the SS and $\text{Al}_2\text{O}_3/\text{Al}$ layers, 3) areas that may be interpreted as graphite clusters (or mixture of graphite-alumina) agglomerated on the Al surface 4) Al substrate.

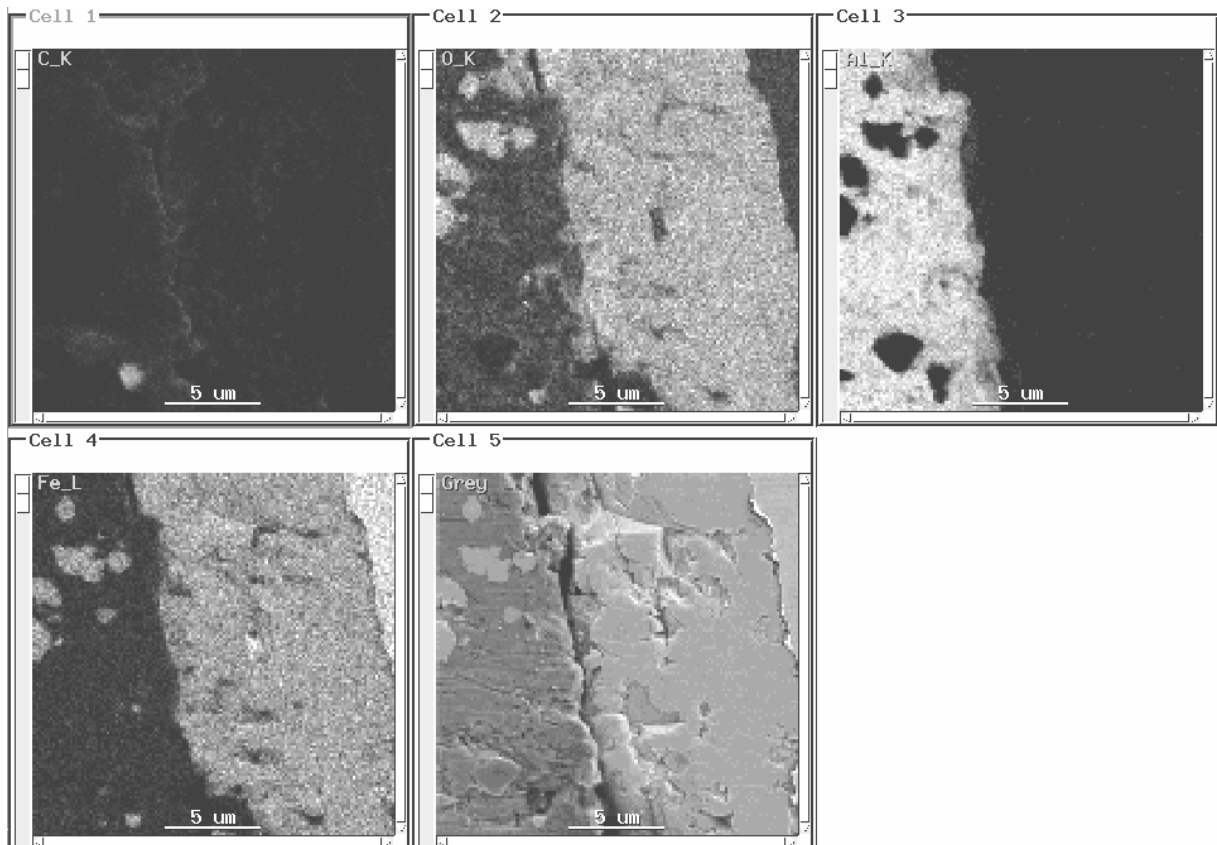


Figure 5.8. A crosscut FESEM micrograph (Cell 5) of another spot of the same sample as in Fig. 5.7 after a series of ultrasonic cleaning treatments. Vertical sample orientation, Al-substrate on the left, SS layer on the right, vertical borderline in between. Corresponding elemental mapping EDS analyses from K-shells of C, O, Al and Fe (Cell 1 to Cell 4, respectively).

It is very difficult to interpret the elemental composition of the interface layer from the elemental mapping EDS analyses in Fig. 5.8. The dominant Al-layer, with some Fe-contamination on it, can be clearly identified. Similarly the area on the upper right is clearly SS. However, the large area on the right contains both Fe and O thus indicating an oxidized steel layer of approximately 10 μm in thickness. It is unknown if this oxidized layer has been on the surface during the manufacturing, or if it has formed later. The most uncertain is the interpretation of the carbon-containing interface layer. In this as all the other EDS analyses topographic differences interfere with the EDS signals adding extra uncertainty for interface analyses. It has not been possible to positively determine the elemental composition of the absorber crosscut surface interface layer from this or other EDS analyses conducted (Publications B and C). The interface might contain separate graphite clusters, but there could be intermixed graphite-alumina layers as well, or even other carbon compounds.

The crosscut sample should be manufactured in a way that keeps the graphite or graphite-alumina layer intact, and that produces as flat as possible crosscut surface. The problem is that so far no better method than that used for the sample presented in Figs. 5.7 – 5.8 has been found for manufacturing and preparing such a carbon-containing crosscut sample. If the surface is coated with, e.g., gold, sharp and clear micrographs can be obtained, but no reliable elemental analyses are possible. Therefore the author refrains from presenting micrographs or EDS analyses taken from gold-coated crosscut samples due to the uncertainty of their analyses.

5.1.6 Summary of microstructural analyses

The optical properties and durability of the surface essentially depend on the microstructure of the absorber surface. Scanning electron microscopy, energy dispersive x-ray spectroscopy, x-ray photoelectron spectroscopy, optical microscopy, thermogravimetry and atomic force microscopy were used to study and analyse the microstructure of the C/Al₂O₃/Al surface from different points of view. As a result of all these analyses we have gained a relatively good understanding of the microstructure of the C/Al₂O₃/Al surface. However, some questions remain for further studies. The analyses show that carbon may be clustered in a graphite form on the surface as layers with thickness varying between 0 and 400 nm. The surface contains a thicker Al₂O₃ layer than what is naturally formed on aluminium. The Al₂O₃ layer may be separated under the graphite layer or intermixed with the graphite and possibly other carbon compounds.

If the C/Al₂O₃/Al absorber surface structure is still to be optically improved, more exact information of the surface composition is needed to enable modelling and calculation of the theoretically best C/Al₂O₃/Al surface composition. In addition, with a better theoretical understanding of the surface, absorber surface scanning electron microscopy and energy dispersive x-ray spectroscopy of both surface and cross-section may be sufficient as measurement approaches.

An interesting question is that whether the surface acts as an optical trapping device. Optical trapping occurs by reflective and resonant scattering. Reflective scattering is obtained purely by the geometry of the surface. According to Lampert (Lampert, 1979), for particulate coatings a resonant scattering deals with both the size and optical properties of the particles and the surrounding media. The Mie effect and Maxwell-Garnett theory predict high forward scattering from particles much less than 0.10 of the wavelength of the incident energy. The distance between microgrooves varies and is never exactly the same between any given spots on a surface. In any case the whole surface is not evenly and thoroughly covered with the microgrooves and graphite clusters. Taking into account the size of the microgrooves (Fig.

5.1) and graphite or graphite/alumina clusters and their coverage (Figs. 5.4 and 5.7), it is unlikely that optical trapping contributes to a large extent to the absorptance of the surface.

5.1.7 Comparison with the literature

After formulating the hypothesis that the C/Al₂O₃/Al surfaces may contain adsorbed and agglomerated graphite clusters we were able to make comparisons to the literature (Publications D and E). Botten and Ritchie (Botten and Ritchie, 1977) have theoretically calculated optimal parameters for a solar absorber surface based on diffraction gratings embodied in thin film interference systems. They studied single dimensional uniform sinusoidal profile graphite-copper interfaces by altering the mean thickness of the idealized graphite layer with a refractive index of $1.95 + 0.34i$, the period of the surface modulation, and the depth of the roughening. By using periodic surfaces they could utilize a grating absorption phenomenon known as surface plasmons for eliminating the deleterious absorption minimum of the graphite. Surface plasmons can be utilized in, e.g., optical transmission through subwavelength holes (Ebbesen et al. 1998; Ghaemi et al. 1998). Analysis of surface plasmons is out of the scope of this dissertation. Detailed introduction to surface plasmons on rough surfaces can be found in, e.g., (Raether, 1988).

Surface plasmons are excited on the long wavelength side of Wood anomalies (Wood, 1935) ($\lambda = D/n$; D is the grating period and n is an integer) and are determined by the shape of the roughened surfaces and the optical properties of the media surrounding the interface. Botten and Ritchie (1977) aimed to excite a surface plasmon centred on the absorption minimum at approximately $0.6 \mu\text{m}$ and therefore used a grating period of $0.5 \mu\text{m}$ in order to station a Wood anomaly at a wavelength of $0.5 \mu\text{m}$. They calculated that a surface with optimized diffraction gratings would have $\alpha = 0.884$ and $\varepsilon = 0.062$ (mean graphite thickness $0.12 \mu\text{m}$, the depth of roughening $0.15 \mu\text{m}$ and a roughness period $0.5 \mu\text{m}$). Based on the achieved results they predicted that random roughening to the scale of $0.5 \mu\text{m}$ would produce results similar to those for sinusoidal form.

For comparison to sinusoidal surfaces, Botten and Ritchie (1977) calculated optical values for uniform graphite film thicknesses (Table 5.2). An absorptance under 0.90 is typically too low for practical purposes. On the other hand, emittance rises rapidly as the graphite layer thickness and α increases. Therefore optimal uniform graphite film thickness can not be determined. The highest absorptances for unspecified air mass, $\alpha = 0.86$ and $\alpha = 0.84$, are achieved for a 400 nm and 300 nm thick layers, respectively. Thermal emittances at 700K for these surfaces are $\varepsilon = 0.41$ and $\varepsilon = 0.25$, respectively. Both emittances are too high for practical applications especially connected with relatively low absorptances.

Values of $0.81 \leq \alpha \leq 0.91$ (AM 1.5) and $0.22 \leq \varepsilon \leq 0.46$ (373K) have been measured for the mechanically manufactured C/Al₂O₃/Al samples (Publications A-C). Raising the emitter temperature from 373K to 700K raises the calculated ε of the C/Al₂O₃/Al samples some 0.15 units. The estimated graphite film of C/Al₂O₃/Al samples is not uniformly thick and homogeneous, nor does it form a sinusoidal profile (Fig. 5.7). Comparison of the values of optical properties of mainly uniform graphite thicknesses obtained by Botten and Ritchie (1977) to those reported in Publications A and B indicate that the C/Al₂O₃/Al surfaces may behave similarly, in an optical sense, despite the difference in profiles. Hence, the estimated maximum graphite layer thickness of 300 – 400 nm in Fig. 5.7 may be in the right neighborhood.

Table 5.2. Variation of absorptance and emittance values as a function of plane graphite film thickness (t) in graphite-copper system. Adapted from (Botten and Ritchie, 1977).

t (nm)	50	80	100	120	150	200	300	400
α	0.60	0.71	0.74	0.76	0.79	0.82	0.84	0.86
ε	0.017	0.023	0.030	0.038	0.061	0.110	0.248	0.410
α/ε	35	31	25	20	13	7.4	3.4	2.1

Botten and Ritchie (1977) also compared the performance of a roughened surface with that obtained by grading the refractive index of the absorber. They found that refractive index grading tends to smooth the entire absorption spectrum by removing any deep absorption minima coinciding with the peak of the solar spectrum for a sinusoidal graphite layer. However, this result is not directly applicable to rough surfaces. As there has not been measured any distinguished absorption minima for the C/Al₂O₃/Al surfaces (see Publication A), it is most likely that the surface roughness cancels out all thin film interference.

Golomb (Golomb, 1978) have experimentally studied interference films, silicon on aluminium and graphite on copper, which were deposited by electron beam evaporation on holographically produced diffraction gratings and meshes. Most of his study concentrates on silicon-on-aluminium systems. He noticed a strong plasmon effect in his experiments, for graphite-copper systems, raising α from 0.79 to 0.88 while leaving ε constant at 0.04. The parameters used were: roughness period of 0.642 μm , graphite thickness of 0.12 μm and groove depth of 0.17 μm . Compared to a plane interface with the same graphite thickness the solar reflectance was approximately halved while ε was increased by < 0.01 . Golomb found that biperiodic surfaces have slightly greater α than uniperiodic surfaces. This feature implied that a randomly roughened surface might be even more absorbing than the corresponding uniperiodic surface, which is in accordance with the results of Botten and Ritchie (1977).

McKenzie (McKenzie, 1978) studied the effect of substrate on graphite selective surfaces. He determined that at operation temperatures below 100°C, copper, silver and nickel are almost equally good candidates for metal substrates. However, the graphite layer thickness required to yield the most available power varied significantly from 0.317 μm for copper and silver to 0.163 μm for nickel. Based on these results it is uncertain if the thicknesses obtained by Botten and Ritchie (1977) and Golomb (1978) for graphite-copper interfaces are directly applicable to graphite-aluminium interfaces.

The manufacturing parameters of the C/Al₂O₃/Al surface should be altered to produce surfaces having surface layer thickness and periodicity close to that recommended by Botten and Ritchie (1977) and Golomb (1978). This would require optimization of the composition of the grinding pad and the grinding pattern, as the commercially available grinding pads tested so far do not seem to allow optimized surface topology to be formed (Publication B).

Further improvements in the absorber structure could include use of antireflection (AR) coating (Yoshida, 1979; Reddy et al. 1987; Zhang and Mills, 1992; Eisenhammer, 1995; Zhang et al. 1996; Chaudhuri et al. 1997; Granqvist and Wittwer, 1998; Nostell et al. 1998; Farooq et al. 1998; Eisenhammer et al. 1999; Farooq and Hutchins, 2002a).

A possible low-cost option could be colloidal silica dipped AR-coating (Tsfamichael and Roos, 1998; Nostell et al. 1999a; Gombert et al. 2000), or a sol-gel coating (Ozer, 1996; Varol and Hinsch, 1996; Granqvist, 1998; Ozer et al. 1999; Ghodsi and Tepehan, 1999; Nostell et al. 1999a; Chen, 2001; Kaluza et al. 2001; Ivanova et al. 2003). Some of the op-

tions are shown in Fig. 5.9. If an AR-coating could be enhanced to act as a moisture barrier layer as well, it would add moisture resistance for very humid climates. However, the antireflection/moisture barrier -coating needs to be inexpensive in order to keep the original C/Al₂O₃/Al absorber manufacturing concept simple and low-cost.

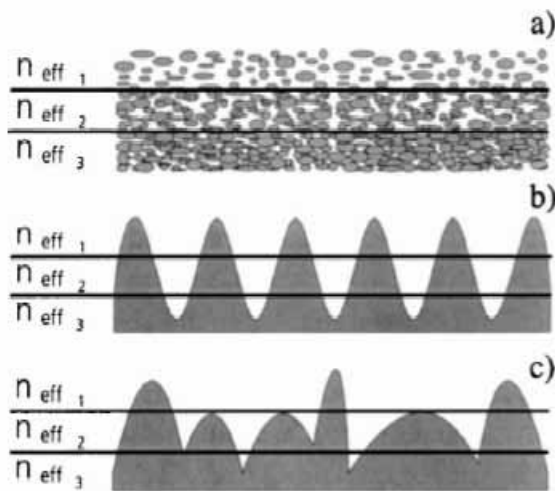


Figure 5.9. Approaches for subwavelength-structured AR surfaces according to Gombert et al. (2000): (a) porous sol-gel coatings, (b) periodic surface-relief structures and (c) stochastic surface-relief structures. Effective refractive indices, n_{eff} , are formed depending on the volume fraction of the subwavelength structured material in air.

5.2 Accelerated aging

5.2.1 Thermal stability

Thermal stability of C/Al₂O₃/Al absorber surfaces was studied according to the IEA SHC recommendations in ‘draft ISO/DIS 12592’ (Carlsson et al. 2000b) (Publication D). Spectral reflectance of the samples before and after aging is shown in Fig. 5.10. The peak between 8 and 10 μm in Figures 5.10 – 5.13 is discussed in Section ‘3.1.4 Error estimates of emittance measurement’. All the samples passed the adhesion tape test. The PC value for the samples was -0.004, which is well within the criterion ($PC \leq 0.015$). Therefore no further thermal stability tests were required for qualification.

In order to study the thermal stability of an aged surface, a solar collector was disassembled after four years of natural exposure at the HUT test site (in Espoo, Finland, 60°11' N, 24°49' E) and surface samples were studied similarly. All these samples passed the criteria as well (Publication D).

A conclusion is that the optical properties of the C/Al₂O₃/Al absorber surfaces should not deteriorate by the thermal stress alone during the first 25 years of normal operation. However, as it is pointed out by Czanderna (Czanderna, 2002) no statement can be made to indicate what the actual service lifetime will be after 25 years.

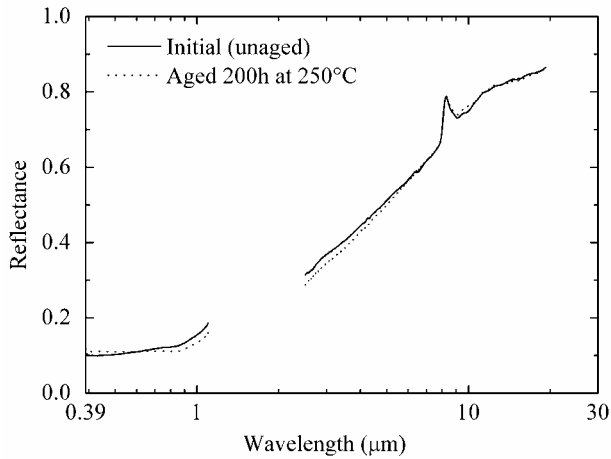


Figure 5.10. Changes of the spectral reflectance of a C/Al₂O₃/Al absorber surface samples (previously unaged) due to high temperature degradation. Wavelength ranges measured include 0.39 – 1.1 μm and 2.5 – 20 μm.

5.2.2 Moisture/condensation resistance

A series of condensing moisture measurements were conducted according to the IEA SHC recommendations (draft ISO/DIS 12592) (Carlsson et al. 2000b). The failure time required to reach $PC = 0.05$ was estimated to be 30h at 40°C (Publication D). Similar to thermal stability testing, naturally aged reference samples were tested and the failure time was estimated to be 50h at 40°C. Additional moisture tests were conducted at 30°C. The exposure time required to reach $PC = 0.05$ for unaged and naturally aged samples at 30°C was 400h and 300h, respectively.

Figure 5.11 shows mean spectral reflectance of samples before and after aging at 30°C. The peak between 8 and 10 μm was discussed in Section ‘3.1.4 Error estimates of emittance measurement’. Absorption bands in the IR spectrum are discussed a bit further. All samples passed the adhesion tape test. The C/Al₂O₃/Al absorber surfaces passed the IEA SHC recommendations for condensation tests (Carlsson et al. 2000b; Brunold et al. 2000b; Köhl, 2001).

Carlsson et al. (Carlsson et al. 1994; Carlsson et al. 2000a) have studied degradation of nickel-pigmented anodized aluminium absorber coating. They reported that one main degradation mechanism is hydration of aluminium oxide to pseudoboehmite (AlO · OH · XH₂O, X = 0.4 – 1) and to boehmite (γ-AlO · OH). They stated that this mechanism requires high humidity or condensed water on the surface of the absorber to be operative. According to Carlsson et al. (2000a), an indication of hydration is strong absorption bands that appear at 3 μm, between 6 and 7 μm and at around 9 μm, suggesting the formation of pseudoboehmite. Such absorption bands at these wavelengths are seen in Fig. 5.11B. It is likely that hydration of aluminium oxide to pseudoboehmite has occurred on the surface of C/Al₂O₃/Al samples. In Fig 5.11A, the absorption band between 6 and 7 μm is missing, thus suggesting the formation of boehmite and possible other aluminium oxide hydroxides as well, e.g. bayerite, gibbsite, forms of amorphous phases of hydrated aluminium oxide (Carlsson et al. 1994). These results indicate that a hydration mechanism similar to the one degrading the nickel-pigmented anodized aluminium absorber coating is affecting the mechanically manufactured C/Al₂O₃/Al absorber surfaces as well.

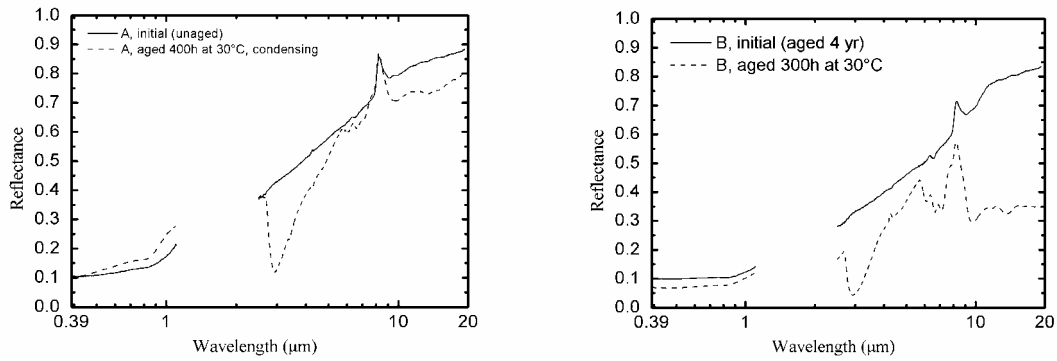


Figure 5.11. Changes of the spectral reflectance of C/Al₂O₃/Al absorber surface samples due to moisture condensation degradation at 30°C. A = unaged prior to the tests, B = four years naturally aged prior to the tests.

Non-condensing high humidity tests for unaged and naturally aged samples were conducted inside the climate chamber concurrently with the 30°C moisture tests (Publication D). After 1000h at a sample temperature of 35°C and chamber humidity of 95 per cent relative humidity (r.h.) the $PC = -0.015$. For naturally aged samples $PC = -0.01$. No sign of hydration was detected either by visual inspection of the samples or in the spectral reflectance (Fig. 5.12).

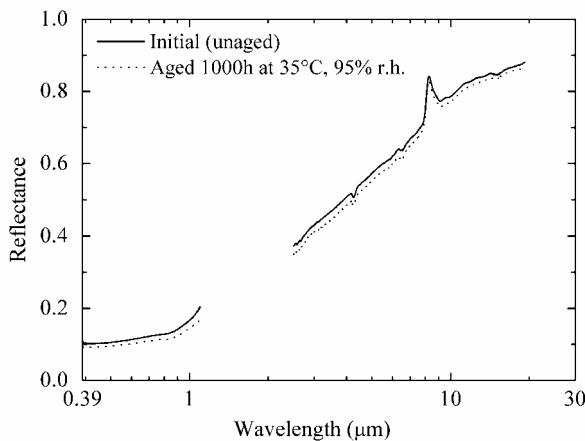


Figure 5.12. Changes of the spectral reflectance of a C/Al₂O₃/Al absorber surface samples (previously unaged) due to non-condensation moisture degradation at 35°C, 95% relative humidity.

5.2.3 Cyclic testing and UV-Vis.-IR exposure

Absorber surface samples were subjected to 383 days of combined temperature and irradiance cycling within the temperature range of -40°C...120°C and UV – Vis. – IR irradiance of 1000 – 7000 W m⁻² (Publication E). As a result α increased significantly, by an increment of 0.03 to 0.07, and ε remained unchanged within the measurement accuracy for the majority of the samples. The biggest change in α occurred after the first 50 days of aging with negligible UV levels. Constant temperature tests after a few hundred hours at 120°C and 180°C showed similar changes in α . Increasing the total and UV irradiance during the cyclic test changed α slightly without lowering α . Similar values of α and ε were measured for test site samples after four years of natural exposure and for samples after 383 days of cycling, thus indicating corresponding aging behaviour in both cases. A possible explanation for the changes in α is

thermally-induced relaxation of surface tension due to the mechanical manufacturing of the surface lattice structure. Changes in the spectral reflectance after cycling can be due to changes in the surface topology (graphite cluster thickness, etc.) as well.

5.2.4 Reference measurements after natural aging

A reference surface (Publications C and E) was disassembled from a solar collector, which has been at a AES laboratory solar test site in Espoo for four years (most of the time without fluid circulation inside). Unfortunately α and ε of the reference surface before natural aging are unknown. Most likely they were in the range of $0.82 < \alpha < 0.86$ and $\varepsilon \approx 0.29$ because these were typical values for other samples of the same manufacturing period. After four years of natural exposure the optical properties measured for this surface were: $\alpha = 0.89$, $\varepsilon = 0.31$. It should be noted that these samples represent earlier stage of production (Publication A) and therefore ε of the latest samples (being originally lower) does not probably rise to the same level after natural aging.

5.2.5 Simulated acid and neutral rain tests

At pH 3.5 the variation of $\Delta\alpha$ between samples was up to 3x smaller than at pH 5.5 in simulated acid and neutral rain total-immersion tests (Publication G). The variation in $\Delta\varepsilon$ was mainly the opposite, i.e. up to 3x bigger at lower pH values. The resulting PC values were almost in all cases within the acceptable limit ($PC \leq 0.05$) at pH 3.5, distributed on both sides of the limit at pH 4.5, and were generally above the limit at pH 5.5.

The majority of the samples exhibited neither specific temperature-dependent nor gasification type/rate-dependent behaviour. In previous condensation tests (Publication D) for similar samples with de-ionized water all the samples exhibited Arrhenius-type temperature- and time-dependent degradation. In addition, there is no clear difference in degradation between the O_2 , N_2 or non-aeration, or the rate of aeration at any pH level. It seems that the pH level is the major determinant of the degradation rate in these tests.

The complexity of the simulated acid rain test method, which includes multiple variables, makes it difficult to determine the reasons for non-Arrhenius type behaviour. The most likely reason is uncontrolled movement of the acid rain solution causing irregular chemical reactions. Furthermore, the primary assumption of the combined effect of gas feeding and natural convection being sufficient for moving the solution seems to be inadequate. The amount of reactants in the solution is quite small (Table 1 in Publication G). Therefore small variations in solution composition may have caused different results as well.

All of the aged samples studied with EDS ($PC \geq 0.05$) showed a clear increment in O and decrease in Al, thus indicating oxidation of aluminium and/or hydration of alumina. FTIR-spectroscopy was used for determining the hydration level of the absorber substrate. Detailed analyses of the results show that Al_2O_3 hydroxides, i.e. pseudoboehmite and/or boehmite, possible other forms of hydroxides are identified in all but one sample at pH 5.5. The most degraded samples ($PC > 0.18$) have absorption bands related to both pseudoboehmite and boehmite, whereas the rest of the hydrated samples do not have the characteristic absorption band of pseudoboehmite. At pH 4.5 most of the samples were hydrated as well, whereas at pH 3.5 only a few samples were hydrated. It is likely that pH 3.5 is too acidic for aluminium hydroxides to be formed, thus preventing further corrosion.

We used thermogravimetry (TG) analyses to determine the possible mass changes and the related water outgassing in a few of the samples (Publication G). The results show that only the

most degraded samples ($PC \geq 0.5$) exhibit clearly measurable mass changes between 230°C and 280°C. For samples degraded to $PC \leq 0.21$ no temperature-specific changes were detected within the measurement accuracy. The combined mass of carbon possibly reacted to CO_2 and outgassed water may be too small to be measured with the TG equipment used.

In our studies we observed similar degradation for another type of commercial aluminium substrate-based selective absorber surface as well. All these results indicate that unglazed solar absorber surfaces based on aluminium substrate need to be well protected against rain diffusion onto the substrate in order to prevent degradation caused by hydration of aluminium oxide.

5.2.6 Lifetime estimates of C/Al₂O₃/Al absorber surfaces

We calculated service lifetime estimates for C/Al₂O₃/Al absorber surfaces inside glazed collectors based on the assumption that the hydration process is the main significant active degradation process during the lifetime of the collector (Publication D), as no other major degradation process has been found so far. Carlsson et al. (1994) reported electrochemical oxidation of metallic nickel to nickel oxide and nickel sulphate decreasing the absorptance of nickel-pigmented anodized aluminium absorbers. These mechanisms cannot occur for the C/Al₂O₃/Al absorbers due to absence of nickel, although similar Al₂O₃ hydration degradation mechanisms seem to take place for both types of absorber surfaces.

The frequency distribution of the C/Al₂O₃/Al absorber temperature or collector microclimate humidity was not measured. Instead we used reference data from literature sources in order to estimate activation energies and calculate the corresponding acceptable service lifetime for the collector. Reference data included measured time of wetness of collector nickel-pigmented anodized aluminium absorbers microclimate during one year in: 1) Rapperswil, Switzerland by Carlsson et al. (1994) and 2) Zurich, Switzerland by Köhl (2001). Both data are shown in Fig. 5.13.

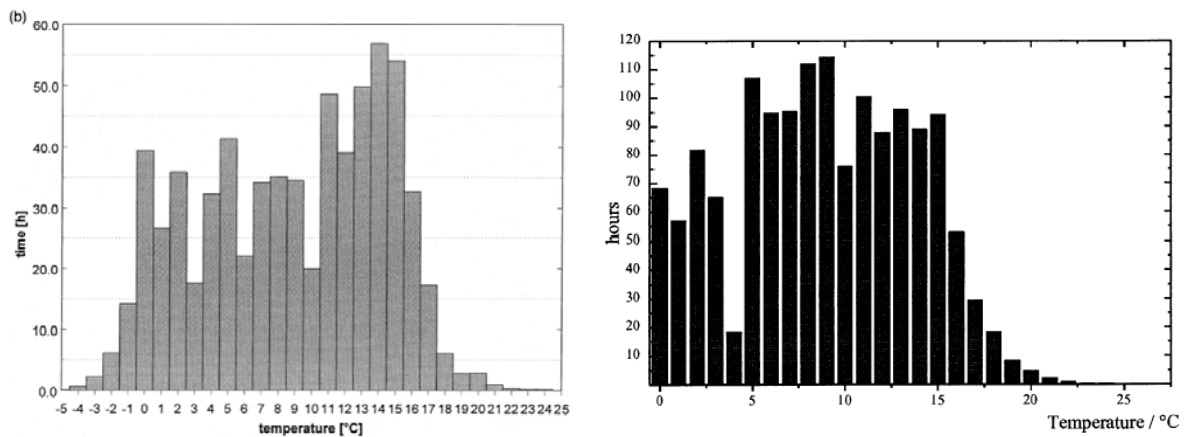


Figure 5.13. Time of wetness frequency distribution during one year by Brunold et al. (2000b) (left, identical data in Carlsson et al. (1994)) and Köhl (2001) (right).

The temperature dependence of the degradation process was assumed to follow the Arrhenius relationship (Köhl, 2001):

$$a_n = \exp \left[\frac{E_T}{R} \left(\frac{1}{T_{ref}} - \frac{1}{T_n} \right) \right] \quad (4-1)$$

where a_n is the Arrhenius acceleration factor, T_{ref} is the reference absorber temperature measured in normal use, T_n is the constant temperature samples are exposed to in the laboratory test, E_T is the Arrhenius activation energy and R is the ideal gas constant. E_T was estimated from the nomograms by Brunold et al. (2000b) (originally published by Carlsson et al. (1994)) and Köhl (2001) shown in Fig. 5.14.

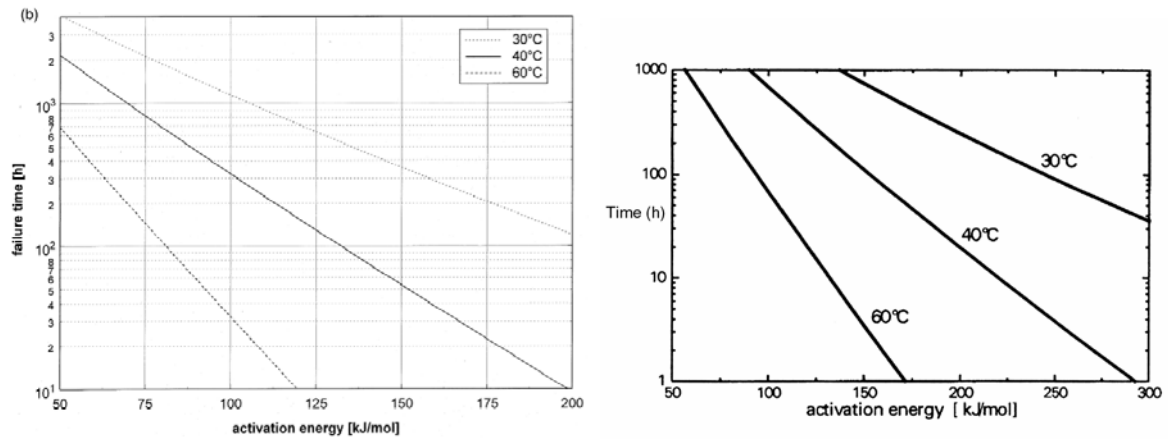


Figure 5.14. Arrhenius activation energy E_T as a function of shortest acceptable ‘failure time’ in hours for an absorber coating in different temperature condensation tests. Measured data for nickel-pigmented anodized aluminium absorbers according to Brunold et al. (2000b) (left) and Köhl (2001) (right). The failure time in each case corresponds to a service lifetime of 25 years.

Subsequently the Arrhenius acceleration factor a_n was calculated for T_{ref} between 0°C and 27°C by using a temperature step of 1°C. The time of wetness during 1 year load profiles (Fig. 5.13) were normalized to the 25 year service life time, weighted with the calculated a_n (for each T_{ref} , T_n and E_T separately) and integrated over the T_{ref} temperature range. The results were compared to the experimental shortest measured failure times for C/Al₂O₃/Al absorber surfaces (i.e., 300h and 400h at 30°C and 30h and 50h at 40°C) in order to determine the estimated service lifetime for the absorber surface.

The estimated Arrhenius activation energy E_T based on reference data (Carlsson et al. 1994; Brunold et al. 2000b) is 145 – 165 kJ mol⁻¹ for unaged absorber samples and 153 – 158 kJ mol⁻¹ for four year aged absorber samples. Service lifetime can be estimated to be 19 – 23 years in both cases (Fig. 5.15). The estimated E_T and service lifetime based on data from (Köhl, 2001) is 173 – 190 kJ mol⁻¹ and 23 – 26 years, respectively. The average service lifetime estimate based on (Carlsson et al. 1994; Brunold et al. 2000b) and (Köhl, 2001) is 20 and 25 years, respectively (Fig. 5.15). The main cause in the variation in service lifetime estimates is the divergence between the time of wetness frequency distribution in (Carlsson et al. 1994; Brunold et al. 2000b) and (Köhl, 2001) (see Fig. 5.13). The estimated 25 years service lifetime based on (Köhl, 2001) is sufficient for a commercial product and is in the same range as other commercially available aluminium-based absorber surfaces (Carlsson et al. 1994; Carlsson et al. 2000a; Brunold et al. 2000b; Köhl, 2001).

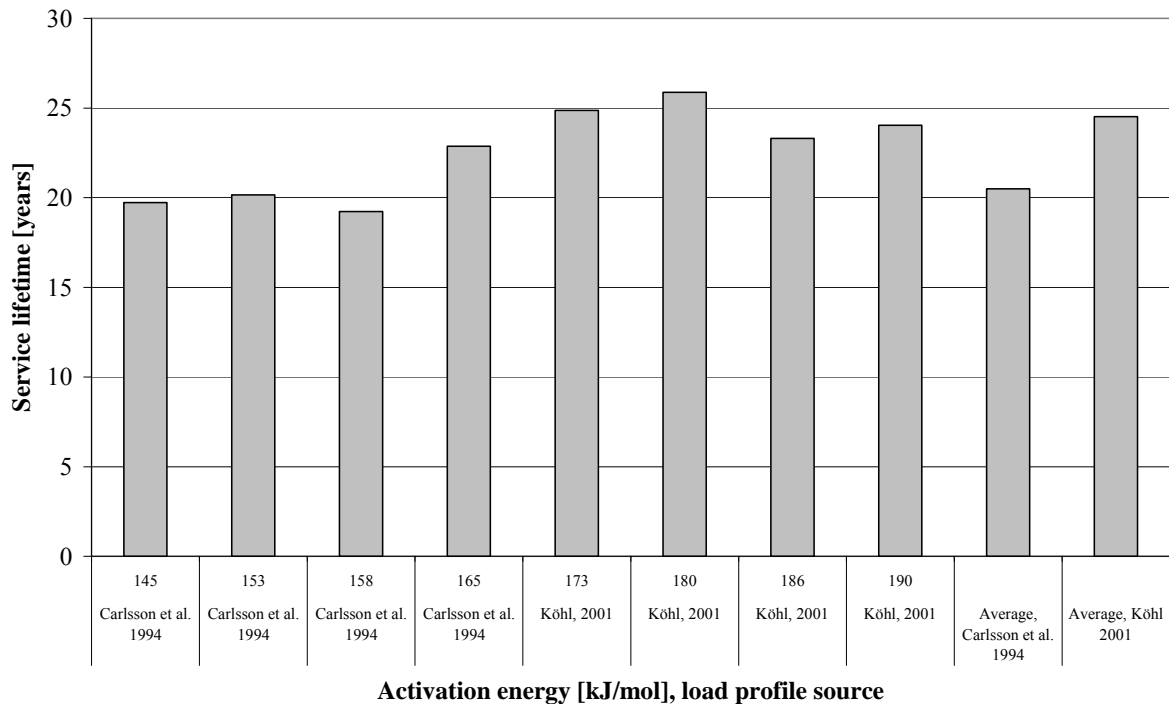


Figure 5.15. Estimated service lifetime of a single-glazed flat plate solar collector with $C/Al_2O_3/Al$ absorber surface. Based on calculated Arrhenius activation energies and measured time of wetness load profiles by Carlsson et al. (1994) (identical data in (Brunold et al. 2000b)) and Köhl (Köhl, 2001) weighted with corresponding accelerated factors.

5.2.7 Source of errors in lifetime estimates

The reference collector with nickel-pigmented aluminium oxide absorber surface used in Rapperswil, Switzerland (Carlsson et al. 1994; Brunold et al. 2000b) had a non-airtight back-side. The wind and rain loads may have had a stronger impact than usual on the microclimate of the collector. This is the likely reason for shorter service lifetime estimates for the $C/Al_2O_3/Al$ surfaces, i.e. 19 – 23 years compared to the 23 – 26 years obtained with the reference data from Zurich, Switzerland (Köhl, 2001).

The real expected service lifetime of $C/Al_2O_3/Al$ absorber surfaces depends on the actual time of wetness frequency distribution of the collector microclimate during the years of operation at any given location. Additionally, the collector service lifetime depends very much on the control strategy of the microclimate inside the collector. With an airtight collector and controlled ventilation longer lifetime can be reached due to less condensation compared to a non-airtight collector and uncontrolled air ventilation. The missing wavelength range between 1.1 μm and 2.5 μm caused some error in the optical measurements (see Section 3.1). Some divergence in results may have been caused by small fluctuations in the climate chamber temperature and sample temperature during the testing period (Publication D) combined with the heterogeneous microstructure of the samples (Publications A-C).

5.2.8 Discussion and conclusions on aging test results

Single-glazed flat plate solar collectors utilizing $C/Al_2O_3/Al$ absorber plates have been used in several countries including Finland and Spain for some six years now. Any visual changes of the surface resembling the changes seen in any accelerated tests where $PC \geq 0.05$ (e.g. Fig. 4 in Publication D) have not been reported so far by any of the owners (Hanslin, 2003).

Cycling the sample temperatures between the -40°C and 120°C combined with irradiance deepened the understanding of the aging response of mechanically manufactured selective $\text{C}/\text{Al}_2\text{O}_3/\text{Al}$ absorber samples, especially regarding improvement of the solar absorptance. The standard IEA SHC tests (200h at 250°C) do not provide any information about the UV induced degradation, or – in this case – the conditions needed for the improvement of α . The cycling method simulates natural exposure of elements to some extent, and here supplements the standard tests suggested by the IEA SHC.

It is possible that during the hydration process, the thin graphite layer on the surface is partly or completely oxidised through chemical reactions forming CO , CO_2 and other compounds (Hihara and Latanision, 1994). The revealed Al_2O_3 layer may subsequently follow the typical alumina-aluminium corrosion mechanisms.

Exposure tests at high temperature and moisture following the IEA SHC recommendations showed that the mechanically manufactured $\text{C}/\text{Al}_2\text{O}_3/\text{Al}$ absorber surfaces mainly degrade through moisture-based hydration of aluminium oxide to pseudoboehmite and boehmite. The hydration process accelerates at higher temperatures with the presence of condensed water on the surface. High humidity alone without condensation at the same temperature is significantly less harmful. High operating temperatures at dry conditions alone do not deteriorate the surface.

Based on measured time of wetness of collector microclimate reference data we estimated the service lifetime of the collector to be 20 – 25 years in normal use before the performance degrades 5 per cent of its initial value. The collector lifetime depends significantly in practice on the time of wetness frequency distribution and control strategy of the microclimate inside the collector. With an airtight collector and controlled ventilation the lifetime can be prolonged. Failures leading to increased humidity on the absorber surface present severe risk to absorber lifetime.

5.3 Optical performance and collector energy yield

The efficiency and energy production of a flat plate solar collector containing $\text{C}/\text{Al}_2\text{O}_3/\text{Al}$ absorber has been estimated by dynamic collector testing and computer simulations. Short term efficiency measurements indicate up to 5% lower η_0 and U_L –values compared to a nickel-pigmented selective anodized aluminium absorber collector in Espoo, Finland (Publication F; Konttinen, 2000). Computer simulations indicate 17% lower annual energy yield and 11% lower annual solar fraction against a commercial collector containing sputtered surface on a copper substrate for a typical Central European climate (Publication A). The results are indicative as they have not been verified against long-term controlled measurements of reference collectors. The values of the optical parameters used for the $\text{C}/\text{Al}_2\text{O}_3/\text{Al}$ absorber simulations were: $\alpha = 0.90$, $\varepsilon = 0.25$.

A rough comparison of absorber investment cost and annual energy yield between different absorbers gives an advantage to the $\text{C}/\text{Al}_2\text{O}_3/\text{Al}$ absorber if the annual net energy yield difference is below 15 – 20 kWh m^{-2} . Therefore the $\text{C}/\text{Al}_2\text{O}_3/\text{Al}$ absorber may be economically competitive against selective absorbers mainly in low-temperature applications such as pool heating or preheating applications. In high temperature applications it is more economical to use an absorber with a higher efficiency. On the other hand, the $\text{C}/\text{Al}_2\text{O}_3/\text{Al}$ absorber combined with cheaper glass, insulation and capsulation may offer a viable alternative to other middle-quality flat-plate collectors used e.g. in Greece.

6 Discussion and conclusions

As a result of this thesis the interrelationship between the C/Al₂O₃/Al solar absorber surface microstructure and its optical performance are now better understood. Significant improvements in optical properties and production methods have been obtained. The solar absorptance (α) of the C/Al₂O₃/Al solar absorber has been increased from ~0.6 to 0.90, and the thermal emittance (ϵ) has decreased from ~0.4 to 0.22.

The solar absorptance and the thermal emittance of absorber samples can be measured with reasonable accuracy and good repeatability after calibration of the UV-Vis.-NIR spectroradiometer and the IR spectrometer used for this work. Typical accuracy of the equipment is within $\pm 1 - 2$ percentage points compared to reference measurements of C/Al₂O₃/Al absorber samples.

The optical properties of the absorber surface essentially depend on the microstructure of the surface. Scanning electron microscopy, energy dispersive x-ray spectroscopy, x-ray photoelectron spectroscopy, optical microscopy, thermogravimetry and atomic force microscopy were used to study and analyse the microstructure of the C/Al₂O₃/Al surface. The analyses show that carbon may be unhomogeneously clustered in a graphite form on the surface as layers with thickness varying between 0 and 400 nm. The surface contains a thicker Al₂O₃ layer than what is naturally formed on aluminium. The Al₂O₃ layer may be separated under the graphite layer or intermixed with the graphite and possibly other carbon compounds. If the absorber surface structure is to be further improved optically more exact information of the surface composition will be needed to enable modelling and calculation of theoretically best C/Al₂O₃/Al surface composition. Up to now all the microstructural methods used have been necessary. With a better theoretical understanding of the absorber microstructure, scanning electron microscopy and energy dispersive x-ray spectroscopy of both the top surface and the absorber cross-section may be sufficient.

To fully capture the improvements in optical properties suggested in this study, the manufacturing process of the C/Al₂O₃/Al absorbers should incorporate customized grinding pads. An optimized pad combined with optimal grinding pattern might allow more homogeneous graphite coverage to approach the theoretical maximum of 0.94 for carbon absorptance. In addition, the solar absorptance might be slightly improved with an antireflection (AR) layer. The AR layer could be implemented either in the current surface manufacturing process or it could be a part of the further process development together with customized grinding pad optimization. If sufficiently dense, the AR layer could additionally act as a moisture barrier for collectors to be used in very humid climates.

The theoretical minimum emittance depends on the thickness of the layers on the surface and on the surface roughness. Thermal emittance could theoretically be reduced with utilization of optimal graphite thickness and groove structure (Botten and Ritchie, 1977; Golomb, 1978). For smooth aluminium the emittance is 0.04...0.05. The emittance of ground rough aluminium is higher, depending on the surface roughness. Additional Al₂O₃ and graphite layers also contribute to the emittance. Considering all these factors, the theoretical lower limit for the emittance of optimized C/Al₂O₃/Al absorber is difficult to estimate accurately, but most likely it will remain above 0.10.

Degradation mechanisms and the corresponding estimates of C/Al₂O₃/Al absorber lifetime were also studied in this work. Different operating conditions for glazed and non-glazed collectors containing these absorbers were studied as well. The absorber is estimated to have a

service lifetime between 20 and 25 years in normal use inside a ventilated glazed solar collector. The estimated service lifetime of 25 years is based on humidity and temperature load measurements of properly insulated reference collectors. The surface withstands dry temperatures up to at least 250°C without any observed degradation. The main degradation mechanism is found to be hydration of alumina to pseudoboehmite, boehmite and other hydrated forms. The hydration is found to occur on surfaces where water has condensed at elevated temperature for a long period of time.

Four years of natural exposure in Finnish climatic conditions of which most was in stagnation did not degrade the surface inside a glazed flat plate collector despite repeated cycles of dew formation and drying. There has not been any reported failures under normal operating conditions in any of the countries where the absorber is in use inside glazed collectors, at latitudes ranging from Finland to Spain. Based on accelerated and outdoor aging test results the C/Al₂O₃/Al absorber surface is estimated to be suitable for glazed applications in normal operational conditions excluding extremely humid climates, and is expected to have a service lifetime in the same range as other commercial absorbers. However, at the present stage of development the surface is not suitable for low cost unglazed collectors without an additional moisture barrier layer, due to rain-induced degradation of optical properties.

The manufacturing of the C/Al₂O₃/Al absorber takes approximately 15 minutes in a single phase mechanical grinding. The manufacturing method is the only one based on solely mechanical treatment known to the author. The absorber surface is easy to manufacture provided that the manufacturing parameters, i.e. grinding speed, pressure, temperature, grinding pattern, structure of the grinding pad, etc. are correct. The manufacturing can be done in any country irrespective of the local technical level. The price of the manufacturing infrastructure is very low – it is nearly zero for a manual method which requires only labour, a flat grinding worktable, grinding pads and substrate aluminium sheets. A more sophisticated mechanical workshop could cost some tens of thousands euros. The number of absorber sheets manufactured simultaneously can be scaled up inexpensively.

Computer simulations of a solar collector containing C/Al₂O₃/Al absorbers indicate 17% lower annual energy yield and 11% lower annual solar fraction against a commercial collector containing a sputtered surface for a typical Central European climate. The results are indicative as they have not been verified against long-term measurements of reference collectors. Values of the optical parameters used for the C/Al₂O₃/Al absorber simulations were: $\alpha = 0.90$, $\varepsilon = 0.25$.

Due to its inferior optical performance the C/Al₂O₃/Al absorber cannot economically compete with high quality (e.g. sputtered) absorbers in high temperature applications if the annual energy yield loss is over 15 – 20 kWh m⁻². On the other hand, a lower performance collector may be considerably cheaper due to utilization of a low cost absorber, such as C/Al₂O₃/Al, selective paint or non-selective black paint, and normal window glass, cheaper insulation and capsulation. High performance absorbers and collectors compete predominantly among themselves within their market sector. Lower performance absorbers and collectors address a different market.

The optical performance of the mechanically manufactured C/Al₂O₃/Al absorber surface is comparable to that of commercial selective paints. Both C/Al₂O₃/Al absorber and selective paint absorbers offer viable alternatives to non-selective black paint in cases where their better overall performance is preferred to the moderately lower cost of non-selective black paint.

REFERENCE LIST

- Agnihotri, O.P. and Gupta, B.K. (1981) Solar selective surfaces. New York: Wiley-Interscience.
- Andersson, L., Hunderi, O. and Granqvist, C.G. (1980) Nickel pigmented anodic aluminum oxide for selective absorption of solar energy. *J. Appl. Phys.* **1**, 754-764.
- Arancibia-Bulnes, C.A. and Ruiz-Suarez, J.C. (1998) Scaling analysis of the optical properties of cermets at oblique incidence. *Sol. Energy Mater. Sol. Cells* **52**, 199-206.
- Assmann, W., Reichelt, T., Eisenhammer, T., Huber, H., Mahr, A., Schellinger, H. and Wohlgemuth, R. (1996) ERDA of solar selective absorbers: Proceedings of the 1995 4th European Conference on Accelerators in Applied Research and Technology, ECAART-4. *Nucl. Instrum. Methods Phys. Res., Sect. B* **113**, 303-307.
- Bachman, B.J. and Vasile, M.J. (1989) Bombardment of polyimide films. *J. Vac. Sci. Technology A* **7**, 2709-2716.
- Binnig, G., Quate, C.F. and Gerber, C. (1986) Atomic Force microscope. *Phys. Rev. Lett.* **56**, 930-933.
- Boström, T., Wäckelgård, E. and Westin, G. (2003a) Solution-chemical derived nickel-alumina coatings for thermal solar absorbers. *Solar Energy* **74**, 497-503.
- Boström, T.K., Wäckelgård, E. and Westin, G. (2003b) Anti reflection coatings for solar absorbers. *ISES Solar World Congress 2003*, Göteborg, Sweden, June 14 – 19, 2003.
- Botten, L.C. and Ritchie, I.T. (1977) Improvements in the design of solar selective thin film absorbers. *Opt. Commun.* **23**, 421-426.
- Boyle, G. (1998) Renewable Energy Power for a sustainable future. Oxford: Oxford University Press.
- Brunold, S., Frei, U., Carlsson, B., Moller, K. and Kohl, M. (2000a) Round robin on accelerated life testing of solar absorber surface durability. *Sol. Energy Mater. Sol. Cells* **61**, 239-253.
- Brunold, S., Frei, U., Carlsson, B., Möller, K. and Köhl, M. (2000b) Accelerated life testing of solar absorber coatings: Testing procedure and results. *Sol. Energy* **68**, 313-323.
- Buhrman, R.A. (1986) Physics of solar selective surfaces. In *Advances in Solar Energy*, Vol 3. Boer, K.W. (ed). pp. 264-276. ASES Plenum Press, New York.
- Cao, A., Zhang, X., Xu, C., Wei, B. and Wu, D. (2002) Tandem structure of aligned carbon nanotubes on Au and its solar thermal absorption. *Sol. Energy Mater. Sol. Cells* **70**, 481-486.
- Carlsson, B., Frei, U., Köhl, M. and Möller, K. (1994) Accelerated life testing of solar energy materials - Case study of some selective materials for DHW-systems. IEA SHCP Task X.
- Carlsson, B., Moller, K., Frei, U., Brunold, S. and Kohl, M. (2000a) Comparison between predicted and actually observed in-service degradation of a nickel pigmented anodized

- aluminium absorber coating for solar DHW systems. *Sol. Energy Mater. Sol. Cells* **61**, 223-238.
- Carlsson, B., Moller, K., Kohl, M., Frei, U. and Brunold, S. (2000b) Qualification test procedure for solar absorber surface durability. *Sol. Energy Mater. Sol. Cells* **61**, 255-275.
- Chaudhuri, S., Bhattacharyya, D., Maity, A.B. and Pal, A.K. (1997) Surface coatings for solar application. *Mater. Sci. Forum* **246**, 181-206.
- Chen, D. (2001) Anti-reflection (AR) coatings made by sol-gel processes: A review. *Sol. Energy Mater. Sol. Cells* **68**, 313-336.
- Christie, A.B. (1989) X-ray photoelectron spectroscopy. In *Methods of surface analysis - Techniques and applications*. Walls, J.M. (ed.). pp. 127-168. Cambridge: Cambridge University Press.
- Czanderna, A. W. (ed.) (2002) Performance and durability assessment of optical materials for solar thermal systems. Manuscript, dated 18.10.2002.
- Duffie, J.A. and Beckman, W.A. (1991) *Solar engineering of thermal processes*, 2nd ed. New York: Wiley-Interscience.
- Ebbesen, T.W., Lezec, H.J., Ghaemi, H.F., Thio, T. and Wolff, P.A. (1998) Extraordinary optical transmission through sub-wavelength hole arrays. *Nature* **391**, 667-669.
- Eisenhammer, T. (1995) Quasicrystal films: Numerical optimization as a solar selective absorber. *Thin Solid Films* **270**, 1-5.
- Eisenhammer, T., Haugeneder, A. and Mahr, A. (1998) High-temperature optical properties and stability of selective absorbers based on quasicrystalline AlCuFe. *Sol. Energy Mater. Sol. Cells* **54**, 379-386.
- Eisenhammer, T., Nolte, H., Assmann, W. and Dubois, J.M. (1999) Preparation and properties of solar selective absorbers based on AlCuFe and AlCuFeCr thin films: industrial aspects: Proceedings of the 1998 MRS Fall Meeting - Symposium LL on 'Quasicrystals'. *Mater. Res. Soc. Symp. - Proc.* **553**, 435-446.
- ESTIF (2003a) Sun in Action II – A Solar Thermal Strategy for Europe, Volume 1, Market Overview, Perspectives and Strategy for Growth. European Solar Thermal Industry Federation. <http://www.estif.org/11.0.html>, 15.12.2003.
- ESTIF (2003b) Sun in Action II – A Solar Thermal Strategy for Europe, Volume 2, The Solar Thermal Sector Country by Country, 21 National Reports. European Solar Thermal Industry Federation. <http://www.estif.org/11.0.html>, 15.12.2003.
- European Commission (1997) Communication from the Commission - ENERGY FOR THE FUTURE: RENEWABLE SOURCES OF ENERGY - White Paper for a Community Strategy and Action Plan COM(97)599 final (26/11/1997).
- Farooq, M. and Hutchins, M.G. (2002a) Optical properties of higher and lower refractive index composites in solar selective coatings. *Sol. Energy Mater. Sol. Cells* **71**, 73-83.
- Farooq, M. and Hutchins, M.G. (2002b) A novel design in composites of various materials

- for solar selective coatings. *Sol. Energy Mater. Sol. Cells* **71**, 523-535.
- Farooq, M. and Lee, Z.H. (2003) Computations of the optical properties of metal/insulator-composites for solar selective absorbers. *Renewable Energy* **28**, 1421-1431.
- Farooq, M.O., Green, A.A. and Hutchins, M.G. (1998) High performance sputtered Ni : SiO₂ composite solar absorber surfaces. *Sol. Energy Mater. Sol. Cells* **54**, 67-73.
- Gampp, R., Gantenbein, P., Kuster, Y., Reimann, P.P., Steiner, R., Oelhafen, P., Brunold, S., Frei, U., Gombert, A., Joerger, R., Graf, W. and Koehl, M. (1994) Characterization of a-C:H/W and a-C:H/Cr solar selective absorber coatings: Optical Materials Technology for Energy Efficiency and Solar Energy Conversion XIII. *Proc. of SPIE* **2255**, 92-106.
- Gampp, R., Oelhafen, P., Gantenbein, P., Brunold, S. and Frei, U. (1998) Accelerated aging tests of chromium containing amorphous hydrogenated carbon coatings for solar collectors. *Sol. Energy Mater. Sol. Cells* **54**, 369-377.
- Ghaemi, H.F., Tineke, T., Grupp, D.E., Ebbesen, T.W. and Lezec, H.J. (1998) Surface plasmons enhance optical transmission through subwavelength holes. *Phys. Rev. B* **58**, 6779-6782.
- Ghodsi, F.E., Tepehan, F.Z. and Tepehan, G.G. (2001) Study of time effect on the optical properties of spin-coated CeO₂-TiO₂ thin films. *Sol. Energy Mater. Sol. Cells* **68**, 355-364.
- Ghodsi, F.E. and Tepehan, F.Z. (1999) Heat treatment effects on the optical properties of Sol-gel Ta₂ O₅ thin films. *Sol. Energy Mater. Sol. Cells* **59**, 367-375.
- Gier, J.T. and Dunkle, R.V. (1955) Selective spectral characteristics as an important factor in the efficiency of solar collectors. *Transactions of the Conference on the Use of Solar Energy* **2**, 41-55.
- Gindele, K., Köhl, M. and Mast, M. (1985) Spectral reflectance measurements using an integrating sphere in the infrared. *Appl. Opt.* **24**, 1757-1760.
- Goldstein, J.I., Newbury, D.E., Echlin, P., Joy, D.C., Romig, A.D.Jr., Lyman, C.E., Fiori, C. and Lifshin, E. (1992) Scanning electron microscopy and X-ray microanalysis. New York: Plenum Press.
- Golomb, M. (1978) Diffraction gratings and solar selective thin film absorbers: An experimental study. *Opt. Commun.* **27**, 177-180.
- Gombert, A., Glaubitt, W., Rose, K., Dreiholz, J., Blasi, B., Heinzl, A., Sporn, D., Doll, W. and Wittwer, V. (2000) Antireflective transparent covers for solar devices. *Solar Energy* **68**, 357-360.
- Gordo, P.R., Cabaco, J.M.C., Nunes, Y., Paixao, V.M.B. and Maneira, M.J.P. (2002) Cylindrical hollow magnetron cathode. Al-N selective coatings for solar collector absorbers. *Vacuum* **64**, 315-319.
- Gordon, J. (2001) Solar Energy The state of the art - ISES position papers. London: James & James.
- Granqvist, C.G. (1998) Progress in solar energy materials: examples of work at Uppsala

University: Proceedings of the 1998 World Renewable Energy Congress V. Part 1 (of 2). *Renewable Energy* **15**, 243-250.

Granqvist, C.G. and Wittwer, V. (1998) Materials for solar energy conversion: An overview. *Sol. Energy Mater. Sol. Cells* **54**, 39-48.

Graseby Specac Ltd (2000) P/N 3610 spectroscopic grade KBr powder.

Gunde, M.K., Logar, J.K., Orel, Z.C. and Orel, B. (1996) Optimum thickness determination to maximise the spectral selectivity of black pigmented coatings for solar collectors. *Thin Solid Films* **277**, 185-191.

Haitjema, H. (1989) Spectrally selective tin oxide and indium oxide coatings. Doctoral Dissertation Thesis, Technische Universiteit Delft, The Netherlands.

Halme, J. (2000) Reflectance measurement of solar selective surfaces with FTIR spectrometer and a DRIFT accessory (in Finnish). Espoo: Helsinki University of Technology, Finland.

Hanslin, R. (2003) Private communication.

Hihara, L.H. and Latanision, R.M. (1994) Corrosion of metal matrix composites. *Int. Mater. Rev.* **39**, 245-264.

Hollands, K.G.T., Karagiozis, A. and Shipley, D. (1990) Histograms of Temperature and Humidity of Solar Collector Plate: Phase II and III. IEA SHCP Task X.

Inal, O.T. and Scherer, A. (1986) Optimization and microstructural analysis of electrochemically deposited selective solar absorber coatings. *J. Mater. Sci.* **21**, 729-736.

Iqbal, M. (1983) An introduction to solar radiation. Academic Press, Ontario, Canada.

ISO (1992) Solar energy. Reference solar spectral irradiance at the ground at different receiving conditions. Part 1: Direct normal and hemispherical solar irradiance for air mass 1,5. Report No. ISO 9845-1.

Ivanova, T., Harizanova, A., Surtchev, M. and Nenova, Z. (2003) Investigation of sol-gel derived thin films of titanium dioxide doped with vanadium oxide. *Sol. Energy Mater. Sol. Cells* **76**, 591-598.

Jeol Ltd. JEOL JSM-820 Scanning Microscope, Instructions.

Kaltenbach, T., Graf, W. and Koehl, M. (1998) Assessment of diffusion processes in thin films. *Sol. Energy Mater. Sol. Cells* **54**, 363-368.

Kaluza, L., Orel, B., Drazic, G. and Kohl, M. (2001) Sol-gel derived CuCoMnO_x spinel coatings for solar absorbers: Structural and optical properties. *Sol. Energy Mater. Sol. Cells* **70**, 187-201.

Kilpi, R.J. (2003) Private communication.

Köhl, M. (2001) Durability of solar energy materials. *Renewable Energy* **24**, 597 – 607

Köhl, M., Gindele, K., Freij, U. and Haeuselmann, T. (1989) Accelerated ageing test

procedures for selective absorber coatings including lifetime estimation and comparison with outdoor test results. *Sol. Energy Mater.* **19**, 257-313.

Koltun, M.M. (1981) Selective optical surfaces for solar energy converters. New York: Allerton Press.

Konttinen, P. (2000) Accelerated aging and optical characterization of absorber surfaces for solar collectors. Espoo: Licentiate Thesis, Helsinki University of Technology, Finland.

Kudryashova, M.D. (1969) Mechanical treatment of collector surfaces in solar installations leading to improved selectivity of optical properties. *Appl. Solar Energy* **5**, 24-25.

Lampert, C.M. (1979) Coatings for enhanced photothermal energy collection I. Selective absorbers. *Sol. Energy Mater.* **1**, 319-341.

Lampert, C.M. (ed.) (1989) Failure and degradation modes in selected solar materials: A review. IEA SHCP Task 10.

Lee, T.K., Kim, D.H. and Auh, P.C. (1993) Optical characteristics of black chrome solar selective films coated by the pulse current electrolysis method. *Sol. Energy Mater. Sol. Cells* **29**, 149-161.

Mabon, J.C. and Inal, O.T. (1984) Optimization and evaluation of black zinc selective solar absorber surfaces. *Thin Solid Films* **115**, 51-73.

Mastai, Y., Polarz, S. and Antonietti, M. (2002) Silica-carbon nanocomposites - A new concept for the design of solar absorbers. *Adv. Funct. Mater.* **12**, 197-202.

McDonald, G.E. (1975) Spectral reflectance properties of black chrome for use as a solar selective coating. *Solar Energy* **17**, 119-122.

McKenzie, D.R. (1978) Effect of substrate on graphite and other solar selective surfaces. *Appl. Opt.* **17**, 1884-1888.

Moore, S.W. (1986) Exposure testing of solar absorber surfaces. *Sol. Energy Mater.* **16**, 453-466.

Myers, D. R. Licor Spectrometer Uncertainty. Electronic mail dated 30 April 2003.

Nefedov, V.I. (1982) A comparison of results of and esca study of nonconducting solids using spectrometers of different constructions. *J. Electron Spectrosc. Relat. Phenom.* **25**, 29-47.

Niklasson, G.A. and Granqvist, C.G. (1983) Surfaces for selective absorption of solar energy: an annotated bibliography 1955-1981. *J. Mater. Sci.* **18**, 3475

Nishimura, M. and Ishiguro, T. (2002) Solar light absorption property of nano-structured silver layer and application to photo-thermal energy conversion coating. *Mater. Trans., JIM* **43**, 2073-2079.

Nitz, P., Ferber, J., Stangl, R., Rose Wilson, H. and Wittwer, V. (1998) Simulation of multiply scattering media. *Sol. Energy Mater. Sol. Cells* **54**, 297-307.

- Nostell, P., Roos, A. and Karlsson, B. (1998) Antireflection of glazings for solar energy applications. *Sol. Energy Mater. Sol. Cells* **54**,223-233.
- Nostell, P., Roos, A. and Karlsson, B. (1999a) Optical and mechanical properties of sol-gel antireflective films for solar energy applications. *Thin Solid Films* **351**, 170-175.
- Nostell, P., Roos, A. and Rönnöw, D. (1999b) Single-beam integrating sphere spectrophotometer for reflectance and transmittance measurements versus angle of incidence in the solar wavelength range on diffuse and specular samples. *Rev. Sci. Instrum.* **70**, 2481-2494.
- Orel, C., Orel, B. and Gunde, M.K. (1992) Spectrally selective SnO₂ : F film on glass and black enamelled steel substrates: spray pyrolytical deposition and optical properties. *Sol. Energy Mater. Sol. Cells* **26**, 105-116.
- Orel, Z.C. (1999) Characterization of high-temperature-resistant spectrally selective paints for solar absorbers. *Sol. Energy Mater. Sol. Cells* **57**, 291-301.
- Orel, Z.C. and Gunde, M.K. (2000) Spectral selectivity of black and green painted surfaces. *Sol. Energy Mater. Sol. Cells* **61**, 445-450.
- Orel, Z.C. and Gunde, M.K. (2001) Spectrally selective paint coatings: Preparation and characterization. *Sol. Energy Mater. Sol. Cells* **68**, 337-353.
- Orel, Z.C., Gunde, M.K., Lencek, A. and Benz, N. (2001) The preparation and testing of spectrally selective paints on different substrates for solar absorbers. *Sol. Energy* **69**, 131-135.
- Orel, Z.C., Gunde, M.K. and Orel, B. (1997) Application of the Kubelka-Munk theory for the determination of the optical properties of solar absorbing paints. *Prog. Org. Coat.* **30**, 59-66.
- Orel, Z.C. and Orel, B. (1995) Thermal stability and cross-linking studies of diisocyanate cured solar absorptance low-emittance paint coatings prepared via coil-coating process. *Sol. Energy Mater. Sol. Cells* **36**, 11-27.
- Orel, Z.C., Orel, B., Leskovsek, N. and Hutchins, M.G. (1996) Spectrally selective silicon paint coatings: Influence of pigment volume concentration ratio on their optical properties. *Sol. Energy Mater. Sol. Cells* **40**, 197-204.
- Ozer, N. (1996) Sol-Gel Optics: Processing and Applications, Lisa C. Klein (Ed.), Kluwer Academic Publishers, Boston, 1994. 592 pages. ISBN: 0-7923-9424-0. *Sol. Energy Mater. Sol. Cells* **43**, 319-320.
- Ozer, N., Cronin, J.P., Yao, Y.-J. and Tomsia, A.P. (1999) Optical properties of sol-gel deposited Al₂O₃ films. *Sol. Energy Mater. Sol. Cells* **59**, 355-366.
- Paparazzo, E. (1988) XPS analysis of oxides. *Surf. Interface Anal.* **12**, 115-118.
- Pavlovic, T. and Ignatiev, A. (1987) Optical properties of spectrally-selective, anodically-coated, electrolytically-colored aluminium surfaces. *Sol. Energy Mater.* **16**, 319-331.
- Perers, B. (1995) Optical modelling of solar collectors and booster reflectors under non stationary conditions. Doctoral Dissertation Thesis, Uppsala University, Sweden.

- Pettit, R.B. (1983) Accelerated temperature aging of black chrome solar selective coatings. *Sol. Energy Mater.* **8**, 349-361.
- Raether, H. (1988) Surface plasmons on smooth and rough surfaces and on gratings. Berlin, Germany: Springer-Verlag.
- Rayleigh, L. (1871) On the light from the sky, its polarization and colour. *Philos. Mag.* **41**, 107-120,274-279.
- Reddy, G.B., Pandya, D.K. and Chopra, K.L. (1987) Chemically deposited PbS-antireflection layer selective absorbers. *Sol. Energy Mater.* **15**, 153-162.
- Richtmyer, F.K. and Kennard, E.H. (1947) Introduction to modern physics. New York: McGraw-Hill.
- Roos, A. (1991) Interpretation of integrating sphere signal output for nonideal transmitting samples. *Appl. Opt.* **30**, 468-474.
- Roos, A. (1993) Use of an integrating sphere in solar energy research. *Sol. Energy Mater. Sol. Cells* **30**, 77-94.
- Roos, A. and Georgeson, M. (1991) Tin-oxide-coated anodized aluminium selective absorber surfaces. II. Aging and durability. *Sol. Energy Mater.* **22**, 29-41.
- Roos, A. and Ribbing, C.G. (1988) Interpretation of integrating sphere signal output for non-Lambertian samples. *Appl. Opt.* **27**, 3833-3837.
- Roos, A., Ribbing, C.G. and Bergkvist (1988) Anomalies in integrating sphere measurements on structured samples. *Appl. Opt.* **27**, 3828-3832.
- Roos, A., van Nijnatten, P. and Upstone, S. (2000) Optical measurements of reflectance and transmittance (mini-symposium). Uppsala, Sweden: Uppsala University.
- Sai, H., Yugami, H., Kanamori, Y. and Hane, K. (2003) Solar selective absorbers based on two-dimensional W surface gratings with submicron periods for high-temperature photothermal conversion. *Sol. Energy Mater. Sol. Cells* **79**, 35-49.
- Schreiber, G. Selective layer for thermal solar collectors to improve absorption of sunlight and minimise emission of collectors. Enquiry, dated 18 February 2002.
- Schuler, A., Geng, J., Oelhafen, P., Brunold, S., Gantenbein, P. and Frei, U. (2000) Application of titanium containing amorphous hydrogenated carbon films (a-C:H/Ti) as optical selective solar absorber coatings. *Sol. Energy Mater. Sol. Cells* **60**, 295-307.
- Schuler, A. and Oelhafen, P. (2001) Photoelectron spectroscopic characterization of titanium-containing amorphous hydrogenated silicon-carbon films (a-Si_{1-x}C_x:H/Ti). *Appl. Phys. A* **73**, 237-245.
- Schuler, A., Videnovic, I.R., Oelhafen, P. and Brunold, S. (2001) Titanium-containing amorphous hydrogenated silicon carbon films (a-Si:C:H/Ti) for durable solar absorber coatings. *Sol. Energy Mater. Sol. Cells* **69**, 271-284.
- Schön, J.H., Binder, G. and Bucher, E. (1994) Performance and stability of some new high-

- temperature selective absorber systems based on metal/dielectric multilayers. *Sol. Energy Mater. Sol. Cells* **33**, 403-416.
- Shanker, K. and Holloway, P.H. (1985) Electrodeposition of black chrome selective solar absorber coatings with improved thermal stability. *Thin Solid Films* **127**, 181-189.
- Smith, G.B., Gentle, A., Swift, P.D., Earp, A. and Mronga, N. (2003) Coloured paints based on iron oxide and silicon oxide coated flakes of aluminium as the pigment, for energy efficient paint: optical and thermal experiments. *Sol. Energy Mater. Sol. Cells* **79**, 163-177.
- Süzer, S., Kadirgan, F. and Sohmen, H.M. (1999) XPS characterization of Co and Cr pigmented copper solar absorbers. *Sol. Energy Mater. Sol. Cells* **56**, 183-189.
- Süzer, S., Kadirgan, F., Sohmen, H.M., Wetherilt, A.J. and Ture, I.E. (1998) Spectroscopic characterization of Al₂O₃-Ni selective absorbers for solar collectors. *Sol. Energy Mater. Sol. Cells* **52**, 55-60.
- Tabor, H. (1955a) Selective radiation. I. Wavelength discrimination. *Bull. Res. Council. Israel* **5A**, 119-128.
- Tabor, H. (1955b) Selective radiation. II. Wavefront discrimination. *Bull. Res. Council. Israel* **5A**, 129-134.
- Tabor, H.Z. (1999) Selected reprints of papers by Harry Zvi Tabor Solar Energy Pioneer. Israel: Balaban publishers and International Solar Energy Society (ISES).
- Taixin, W., Qinhu, Z. and Xiaoxi, C. (1993) Preparation process and property analysis of a solar selective absorbing surface on milled steel. *Sol. Energy Mater. Sol. Cells* **30**, 285-290.
- Teixeira, V., Sousa, E., Costa, M.F., Nunes, C., Rosa, L., Carvalho, M.J., Collares-Pereira, M., Roman, E. and Gago, J. (2001) Spectrally selective composite coatings of Cr-Cr₂O₃ and Mo-Al₂O₃ for solar energy applications. *Thin Solid Films* **392**, 320-326.
- Teixeira, V., Sousa, E., Costa, M.F., Nunes, C., Rosa, L., Carvalho, M.J., Collares-Pereira, M., Roman, E. and Gago, J. (2002) Chromium-based thin sputtered composite coatings for solar thermal collectors. *Vacuum* **64**, 299-305.
- Tesfamichael, T. (2000) Characterization of selective solar absorbers Experimental and theoretical modeling. Doctoral Dissertation Thesis, Uppsala University, Sweden.
- Tesfamichael, T. and Roos, A. (1998) Treatment of antireflection on tin oxide coated anodized aluminum selective absorber surface. *Sol. Energy Mater. Sol. Cells* **54**, 213-221.
- Tesfamichael, T., Vargas, W.E., Wäckelgård, E. and Niklasson, G.A. (1998) Feasibility study of integrally colored Al-Si as a solar selective absorber. *Sol. Energy Mater. Sol. Cells* **55**, 251-265.
- Varol, H.S. and Hinsch, A. (1996) SnO₂:Sb dip coated films on anodized aluminum selective absorber plates. *Sol. Energy Mater. Sol. Cells* **40**, 273-283.
- Vince, J., Surca Vuk, A., Opara Krasovec, U., Orel, B., Köhl, M. and Heck, M. (2003) Solar absorber coatings based on CoCuMnO_x spinels prepared via the sol-gel process: structural and optical properties. *Sol. Energy Mater. Sol. Cells* **79**, 313-330.

- Vuletin, J., Lampert, C.M., Kulisic, P., Bosanac, M. and Mastelic, J. (1989) Chemical and optical properties of a black copper absorber for flat plate collectors. *Sol. Energy Mater.* **19**, 249-256.
- Wagner, C.D., Passoja, D.E., Hillary, H.F., Kinisky, T.G.S.H.A., Jansen, W.T. and Taylor, J.A. (1982) Auger and photoelectron line energy relationships on aluminium-oxygen and silicon-oxygen compounds. *J. Vac. Sci. Technol.* **21**, 933-944.
- Weiss, W. and Faninger, G. (2002) Solar thermal collector market in IEA-member countries. IEA SHCP.
- Wernick, S., Pinner, R. and Sheasby, P.G. (1987) The surface treatment and finishing of aluminium and its alloys. 5th edn. 729-772. ASM International, Ohio, USA.
- Wood, R.W. (1935) Anomalous diffraction gratings. *Phys. Rev.* **48**, 928-936.
- Yin Zhiqiang (2003) Developments of solar thermal systems in China. ISES Solar World Congress 2003, Göteborg, June 14-19 .
- Yoshida, S. (1979) Antireflection coatings on metals for selective solar absorbers. *Thin Solid Films* **56**, 321-329.
- Yue, S., Yueyan, S. and Fengchun, W. (2003) High-temperature optical properties and stability of $\text{Al}_x\text{O}_y\text{-AlN}_x\text{-Al}$ solar selective absorbing surface prepared by DC magnetron reactive sputtering. *Sol. Energy Mater. Sol. Cells* **77**, 393-403.
- Zhang, Q.-C. and Mills, D.R. (1992) High solar performance selective surface using bi-sublayer cermet film structures. *Sol. Energy Mater. Sol. Cells* **27**, 273-290.
- Zhang, Q.-C., Yin, Y. and Mills, D.R. (1996) High efficiency $\text{Mo-Al}_2\text{O}_3$ cermet selective surfaces for high-temperature application. *Sol. Energy Mater. Sol. Cells* **40**, 43-53.